DIGITAL IMAGE PROCESSING FOR PROGNOSTIC AND DIAGNOSTIC CLINICAL PATHOLOGY

A THESIS SUBMITTED IN PARTIAL FULFILMENT OF THE REQUIREMENTS FOR THE DEGREE OF DOCTOR OF PHILOSOPHY

JOHN MADDISON

AWARDED BY THE UNIVERSITY OF HUDDERSFIELD

AUGUST 2005

Rikshospitalet – Radiumhospitalet HF

THESIS CONTAINS

CD

Abstract

When digital imaging and image processing methods are applied to clinical diagnostic and prognostic needs, the methods can be seen to increase human understanding and provide objective measurements. Most current clinical applications are limited to providing subjective information to healthcare professionals rather than providing objective measures. This Thesis provides detail of methods and systems that have been developed both for objective and subjective microscopy applications. A system framework is presented that provides a base for the development of microscopy imaging systems. This practical framework is based on currently available hardware and developed with standard software development tools. Image processing methods are applied to counter optical limitations of the bright field microscope, automating the system and allowing for unsupervised image capture and analysis.

Current literature provides evidence that 3D visualisation has provided increased insight and application in many clinical areas. There have been recent advancements in the use of 3D visualisation for the study of soft tissue structures, but its clinical application within histology remains limited. Methods and applications have been researched and further developed which allow for the 3D reconstruction and visualisation of soft tissue structures using microtomed serial histological sections specimens. A system has been developed suitable for this need is presented giving considerations to image capture, data registration and 3D visualisation, requirements. The developed system has been used to explore and increase 3D insight on clinical samples.

The area of automated objective image quantification of microscope slides presents the allure of providing objective methods replacing existing objective and subjective methods, increasing accuracy and reducing manual burden. One such existing objective test is DNA Image Ploidy which seeks to characterise cancer by the measurement of DNA content within individual cell nuclei, an accepted but manually burdensome method. The main novelty of the work completed lies in the development of an automated system for DNA Image Ploidy measurement, combining methods for automatic specimen focus, segmentation, parametric extraction and the implementation of an automated cell type classification system.

A consideration for any clinical image processing system is the correct sampling of the tissue under study. While the image capture requirements for both objective systems and subjective systems are similar there is also an important link between the 3D structures of the tissue. 3D understanding can aid in decisions regarding the sampling criteria of objective tests for as although many tests are completed in the 2D

realm the clinical samples are 3D objects. Cancers such as Prostate and Breast cancer are known to be multi-focal, with areas of seeming physically, independent areas of disease within a single site. It is not possible to understand the true 3D nature of the samples using 2D micro-tomed sections in isolation from each other. The 3D systems described in this report provide a platform of the exploration of the true multi focal nature of disease soft tissue structures allowing for the sampling criteria of objective tests such as DNA Image Ploidy to be correctly set.

For the Automated DNA Image Ploidy and the 3D reconstruction and visualisation systems, clinical review has been completed to test the increased insights provided. Datasets which have been reconstructed from microtomed serial sections and visualised with the developed 3D system area presented. For the automated DNA Image Ploidy system, the developed system is compared with the existing manual method to qualify the quality of data capture, operational speed and correctness of nuclei classification.

Conclusions are presented for the work that has been completed and discussion given as to future areas of research that could be undertaken, extending the areas of study, increasing both clinical insight and practical application.

Acknowledgements

Table of Contents

List of Figures

List of Tables

List of Equations

Glossary

Term	Definition
AFM	Atomic force microscope
Antibody	A Special type of protein that is synthesizes in the response to the presence of a particular antigen
Antigen	Any substance that may be specifically bound by an antibody molecule
CCD	Charge coupled device
Chromosome	One of the threadlike structures in a cell nucleus that carry the genetic information in form of genes. It is composed of a DNA coiled in to a helix with associated proteins.
Cytology	Study of cells
Cytoplasm	Part of a biological cell, a gel like fluid which provides a platform in which organic operation takes place such as cell growth and replication. Located between the nucleus and the cell membrane.
DCIS	Ductal Carcinoma In Situ. Early stage of breast cancer.
Diagnosis	The process of determining the nature of a disorder by considering the patient's signs and symptoms
DNA	Deoxyribonucleic acid. The genetic material of nearly all living organisms, located in the cell nucleus.
DNA Ploidy	Relative amount of DNA contained in a cell or tissue
Drosophila	A family within a genus of fly. Commonly called fruit flies
Epithelial cell	Structural cell
Feulgen stain	A stoichiometric stain for demonstrating the presence of DNA in cell nuclei
Fibroblast	Cell from connective tissue
Ganglion	Group of nerve cells
Histology	Study of tissue structure and organisation
Hydatidiform mole	An abnormality during pregnancy; a tissue mass or growth that forms within the uterus as a result of a genetic errors during the fertilisation process
Immunofluorescence	A method of locating antigens in tissue, or of identifying an antigen by fluorescence resulting when the antigenic material is exposed to a specific antibody coupled fluorescent dye
Immunohistochemistry	The use of antibodies for identifying patterns of antigen distribution within a tissue or an organism
Isosurface	A surface of constant value
Köhler illumination	A microscopy method to ensure correct setup of the optical planes within the microscope
Lymph Node	One of the a number of small swellings found at intervals along the lymphatic system
Lymphatic system	A network of vessels that conveys electrolytes, waters proteins from the tissue fluids to the bloodstream
Lymphocyte	White blood cells
Membrane (cell)	Part of a biological cell, the Boundary structure between the structures outside the cell
Metastasis	The distant spread of malignant tumour from its site or origin
Metastatic	A tumour spreading from one location to another
Microtome	A device used for cutting sections from embedded tissue
Nomarski optics	Differential interference contrast lens used to enhance contrast

	in a biological specimen
Nucleus	The part of the cell that contains the genetic material (DNA)
Pixel	The basic unit of a digital image
Plasma cell	A mature Lymphocyte
Ploidy	The condition of having multiple the normal number of chromosomes for the species
Prognosis (medical)	An assessment of the future course and outcome of a patient's disease
SEM	Scanning Electron Microscope
Stereo anaglyphs	A moving or still picture consisting of two slightly different perspectives of the same subject in contrasting colours that are superimposed on each other, producing a three-dimensional effect when viewed through two correspondingly colour filters
Stoichiometric	Quantitative stain where the relationship between the intensity and area of the stain and the biological areas it represents which can be accurately reproduced, such as the Feulgen stain
TEM	Transmission Electron Microscope
Voxel	Volume pixel. A three-dimensional pixel

Chapter 1 Introduction

1.1 Research Background

The requirement for prognostic and diagnostic systems in healthcare is of prime importance for the successful treatment of disease; currently the vast majority of systems are manual and centre on subjective human review. This situation is particularly the case within pathology disciplines where tissue is studied to determine the presence of disease (diagnosis) and for determination of expected outcome of disease (prognosis). Histological review is a practice within the field of pathology where the structure and organisation of tissue is visually studied and is the most common method of determining a diagnosis of cancer. For histological review an extracted biopsy is embedded in wax, sectioned using a microtome to obtain a thin 2D slice of the material, the specimen is then placed on to a glass slide and then stained using chemical methods to highlight different tissue structures. The slide is then placed on a bright field microscope and visually reviewed by a pathologist. While histological review is relatively accurate in the detection of disease in most cases, it is subject to human error and limited as to the quantitative measurements that can be obtained. The existing limitations of this practice can been seen to be use of a 2D sections to try to understand an inherent 3D object and attempting to use the human visual system complete accurate quantitative measurements to which it is ill suited.

The application of existing scientific methods may provide the solutions for further improvement in the efficiency and accuracy of prognostic and diagnostic healthcare services; but without suitable applications designed for use by healthcare professionals, such advances will not find practical application and will remain subject only to academic study. This report describes systems that have been developed using proven image analysis methods as applied in other disciplines. These methods have been applied to the development of a 3D registration and visualisation system for use in histology and for the development of a system for the attempted automation of DNA Ploidy. Where DNA Ploidy is an existing method used to quantitatively determine the content of DNA within single cell nuclei (central functional component of a cell) and has been shown to be able to determine both the existence and provide information on the progression of cancer.

Computational prognostic models are increasingly used in medicine to predict the natural course of disease, or the expected outcome after treatment, based on human interpretation of visual review of samples. The application of computer systems using software developed with current software design tools may provide systems that combine

the scientific advances made in medical science with that of the application of computing and imaging technology. With the implementation and application of novel and well researched and validated systems, it is possible that new approaches and knowledge will also be found in this combined area, contributing to the clinical science and understanding of problems that are elusive using current methods of research.

To enable efficient design and implementation of such systems for this study area, an framework is required, addressing both the hardware and software needs. The framework provides the starting blocks required for future systems, addressing the generic needs of clinical imaging systems and providing the potential for future expansion.

Systems that are required for prognostic and diagnostic review can be seen to be categorised into two areas. Qualitative systems, allowing for presentation of new or improved information to healthcare professionals, where manipulated data can enable increased insight. Quantitative systems can be used to provide numeric or objective results which can then in turn be used as diagnostic or prognostic indicators. Systems for use in the quantification of biological samples require sampling methods to be employed to make quantification methods practical for clinical use due to time and resource constraints. It is known that some cancers are multi focal having seeming different and independent areas of disease. The 3D tools developed and explained within the report provide the mechanism to explore the structure of these cancers and to determine the sampling schemes that should be used for quantitative tests such as DNA Ploidy. The hardware and software development requirement for imaging of samples for both 3D imaging and DNA Image Ploidy can be seen to have commonality.

1.2   Outline Of Report

Chapter 2 Literature review. - A comprehensive review of the literature related to image capture from microscopes has been completed where the use of different types of microscopes for imaging different types of specimens and for differing purposes is reviewed. The current works and state of research for the use of computer vision for image understanding in medical application are detailed, considering both state-of-the-art of current research, both for disciplines outside that of microscopy and those that relate directly to it.

Medical applications using computer vision are detailed, exploring the important requirements of analysis within imaging systems and the considerations required including, colour, intensity, texture and shape. The current state-of-the-art and applications of 3D reconstruction in medical imaging are reviewed, reflecting on current systems that have

been implemented within the main study area. The background research relating to DNA Image Ploidy and the use of DNA Ploidy as a prognostic and diagnostic test is provided.

Chapter 3 The bright field microscopy system: - The functional and optical aspects of the bright field microscope are detailed. The illumination light source of the microscope is discussed, explaining the considerations that must be given to achieve consistent and reliable results for both qualitative and quantitative systems. A basic review is given as to the consideration of the selection of specimen stains required. The physical characteristics of the microscope which have an important impact on the suitability of attachment of imaging equipment are discussed. The imaging system which has been developed is presented, detailing the automation equipment used and the software considerations for the capture system. This chapter provides a background for the work detailed in Chapters 4, 5 and 6.

Chapter 4 Software Framework For Clinical Imaging: - The software environment for the development of medical imaging and characterisation software is described. The block diagrams of the developed system are presented, detailing the general rational of the software development approach.

Chapter 5 The 3D Reconstruction And Visualisation System: - The system is presented as an application that has been developed within the framework. Considerations are given as to the user interface. Algorithms that have been used and developed are introduced.

Chapter 6 Automated DNA Image Ploidy System: - Presentation is given explaining system design and improvements over the manual method. The new methods and systems that have been used to automate DNA Image Ploidy are also presented. These include novel methods for automatic focus, segmentation, parametric extraction and automatic object classification.

Chapter 7 Experimental Test Results: - This chapter has three main sections, the presentation of results obtained for 3D reconstruction, those comparing the Automated DNA Image Ploidy system with existing manual systems and the clinical studies that have been completed using the automated DNA Image Ploidy system.

Chapter 8 Conclusions And Further Work: - The completed work is concluded upon with reference to aims set out. Conclusions are given for results that have been obtained on the designed systems. Further work is discussed that would extend the research completed, discussion is given as to the work that could be completed in the areas of clinical study; advances image processing and real-time applications and the use of telemedicine for distributed healthcare solutions.

1.3   Aims and Objectives

In the following defined aims the development of the image capture system is required enabling infrastructure. The work completed for the development of the automated DNA Image Ploidy system and subsequent validation work represents the primary area of application and development novelty as the culmination of the doctoral programme of supervised research. The aims and objectives of the completed research are summarised as follows.

1.3.1   Development Of An Image Capture System.

To allow for images to be captured both for medical prognostic, diagnostic and research use, a robust and reliable system is to be developed. The system designed is to take account of the optical characteristics of the bright field microscope, and image processing of the resultant images for optimum results. The automation requirements for the system are to be addressed using third party automation hardware, controlled by the software system developed. The development of a software environment is to form part of the aims for this study and provide a framework for future systems. The software environment developed has to address the issues of usability, scalability and future expansion of methods and inclusion of new algorithms. The usability of the system is of prime importance, and to this end the software will be developed for the Microsoft Windows platform, allowing for maximum user penetration and acceptance. This aim is addressed in Chapter 4.

1.3.2   Development Of Medical Image Algorithms For 3D Reconstruction And Visualisation

A system is to be designed and developed for the purpose of exploration of histological exploration of micro-tomed serial sectioned datasets. The algorithms used for the serial section registration and 3D visualisation are to be presented and discussed with regard to the suitability of the algorithms for the study of the specimens under consideration. New methods that have been developed are to be presented. This aim is addressed in Chapter 5.

1.3.3   Development Of An Automated Image DNA Ploidy Analysis System

An aim of the research is to develop a system that allows automation of DNA Image Ploidy, an accepted manual method which has a high labour burden. The developments are to attempt to reduce the manual burden of completing the test, one of the reasons why it is suffering limited clinical uptake. It is the development of the automated DNA Ploidy system

where the main novelty of work presented in this Thesis lies. This aim is addressed in Chapter 6.

1.3.4 Evaluation Of Completed Work Using Clinical Tests.

Study is to be completed to review the objective and subjective results of the systems that have been researched and developed. For the development completed on the 3D reconstruction system the results are to be presented in subjective form. Objective presentation is to be given for the results of the Automatic DNA Image Ploidy system, comparing the existing manual method and determining the system's suitability for clinical use. This aim is addressed in Chapter 7.

The following chapter contains a comprehensive literature survey on the use of microscopes for prognostic and diagnostic imaging. The literature is reviewed and limitations and short fallings in the current methods are detailed. The current applications for image analysis and computer vision are reviewed. The important elements for image analysis systems in medicine in the literature are explained. The various options for the implementation of imaging systems are detailed, and the limitations discussed.

Chapter 2 Literature Survey

The literature survey includes the review of the state-of-the art and application of various microscopes and related optical and physical characteristics, advantages and disadvantages for implementation of medical imaging systems. Applications of image processing and understanding in computer vision have been reviewed. Methods of medical imaging analysis and computer vision have been considered. The use of 3D image reconstruction for medical and research use has been detailed. Current research related to DNA Image Ploidy is presented. The final section presents a review of image analysis and rendering software for medical applications. For the areas presented problems or merits of current approaches have been identified and outlined in relation to the specific application areas considered in this Thesis.

2.1 Microscopes For Image Capturing

A range of microscope systems are available, fluorescence, confocal, dark field, bright field and electro-scanning. In previous work reviews have been given as to the application of the different types of microscopy systems, describing issues and applications of imaging and its advantages as applied to medical informatics [1;2]. Atomic Force Microscope (AFM), Transmission Electron Microscope (TEM) and Scanning Electron Microscope (SEM) can be used for high resolution imaging of biological specimens with lateral resolutions up to 2nm compared to 0.2μm for the bright field microscope. The AFM, TEM and SEM require specialised specimen preparation and attract high capital costs (> £100,000). A major disadvantage is that imaging systems using electrostatic transfer or surface based imaging systems cannot be used to produce colour images representative of the specimen, so biological markers cannot be used to aid identification of specific structures. This is a core requirement for the examination of pathology specimens.

There are three classes of light based microscopes; confocal, dissection or stereo microscope, and the compound or bright field microscope, these are now considered in more detail.

2.1.1 Confocal Microscope

The confocal microscope uses a focused laser to scan the specimen to produce a point sampled image. The scanning laser passes back and forth over the specimen in a raster pattern focused at a specific optical depth, the light emitted from the specimen is collected by a detector with out of focus light being rejected by a pinhole, through which light passes before reaching the collector [3;4]. The confocal microscope allows for a single plane to be more efficiently isolated in the specimen than when using a bright field

microscope. Immunofluorescence can be used to enable the use of bio-markers highlighting defined biological areas. Making the confocal suitable for the generation of 3D datasets and other imaging requirements where accurate resolution of detail in the Z axis of the microscope is required. The confocal microscope again attracts a high capital cost (£20,000 - £100,000). Confocal systems can be used for the accurate imaging of clinical specimens but have limitations. The use of the single point scanning laser/emitter combination requires that the specimen has a fluorescence dye applied so that when illuminated with a specific excitation wavelength a known emitted wavelength will be emitted and can be measured [3]. Fluorescent dyes suffer from photo bleaching creating imaging problems as the intensity of the emitted signal degrades with even the most minimal exposure time making quantification of the emitted signal difficult. In consideration of 3D imaging requirements the optical penetration of the scanning laser is limited and cannot be used for the imaging of thick specimens.

2.1.2 Dissection Microscope

The Dissection, Stereo Microscope or Stereoscope allows for the visualisation of specimens in original form, illuminated either by ambient light or by a local external light source. The stereoscope has a limitation in that by not using a condenser to focus illuminating light final resolution is limited, and it is not possible to accurately resolve separate optical planes, a maximum optical resolution of approximately $2\mu m$ can be achieved. For imaging requirements where a limited magnification and resolution is required the stereoscope provides a cheap solution [5;6], however its limited resolution is a restrictive factor for objective and 3D reconstruction applications.

2.1.3 Compound Or Bright Field Microscope

The compound or bright field microscope is the most commonly used microscope for microscopic review in healthcare and research applications [7]. The bright field microscope allows for the preservation of original colour, allowing application of bio-markers or stains, increasing the visual contrast between different tissue type and cellular structures. The differing uses of stains and markers are explained in Chapter 3. The use of focused illumination and compound lenses provide a good compromise in terms of the capital cost of the equipment and that of the resolving power compared to expensive and complicated atomic force microscopes and simple but limited standard stereo microscopes. The resolving power provided is suitable for many clinical applications ranging from haematopathology (study of blood and the organs and tissues that use blood cells to perform functions within the body), through to cytology (study of cell structures) and

histology (study of tissue). With the development of imaging instrumentation and digital signal processing, more and more bright field microscopes have been linked with imaging equipment and used for research applications. Previous work includes research and clinical work in many areas [8;9].

As discussed the bright field microscope offers many advantages in consideration of the economics and practicality as a platform for the completion of qualitative and quantitative microscopy medical imaging not least the ability to use bio-markers to identify clear areas of biological interest. It also presents many challenges, these issues include the normalisation of the illumination, automation concerns and resolution, these are described in the next chapter and addressed in Chapters 4, 5 and 6.

2.2 Computer Vision For Image Understanding

Computer vision is a consideration of the provision of algorithms within systems with that typical of human vision [10], such as morphologic object and pattern recognition. This study area has produced applications that are common place in industrial automation, robotics, space exploration and biomedicine [11-13]. Complex algorithms allowing the use of imaging systems to move from the simple representation of images, to using complex and sophisticated algorithms has been marred by the complexity required in consideration of the economic availability of computing platforms and has been the subject of other studies [14-16]. For many applications the processing power required is now provided by common, economically viable, powerful and affordable computing systems such as processing units based on the Pentium class (Intel Corporation, USA) Central Processor Units (CPU), as described in previous work [14;15;17].

2.3 Medical Applications Of Computer Vision

The integration of image features; colour, texture and shape, has been used for content-based image retrieval [18]. Integrative low level visual features can be used for image understanding and interpretation.

There are many examples of computerised imaging techniques in varied disciplines of medical services, applications range from primary care including dermatology, radiology, ultrasound imaging, Magnetic resonance Imaging (MRI) and Computerised Tomography (CT) [19-27], to more research based applications for drug development, exploration and study of bio-mechanisms [28-31]. Previous work describes the use of texture analysis of nuclei [32-39], One of the prime concerns for image analysis is efficient segmentation systems which are required to identify the object of interest from the background [40;41].

The development of systems that provide defined prognostic and diagnostic information is possible and requires increased validation and clinical studies. Completed work on the development and validation of the automated DNA Ploidy system that has been detailed within this report is once such system.

2.3.1 Colour

For microscopy applications the resultant image colour can be false or a direct representation of the imaged subject after application of specific stains or markers (more detail is provided in Section 3.6.5). There are many instances where the resultant colour is used purely for visualisation and descriptive purposes only, such as for the interpretation of visualisations arising from complex datasets, where false colouring can be used to highlight or provide interpretable minor differences in graduations in the original image or calculated information such as edge or textual features [42;43]. The use of false colouring is particularly useful in complex visualisation situations in 3D visualisation, where Volume pixels (Voxels), the 3D equivalent 2D pixels (picture elements) are used for the visualisation of the dataset as described in Section 2.4, highlighting what can be subtle differences in the original dataset. An indiscrete colour map can be applied to a greyscale dataset illustrating minor differences [44;45], which would otherwise be all but lost in the visualisation process. 3D visualisation systems have used colour to aid in the provision of depth perspective of 3D visualised datasets. Methods include the use of red and green glasses to produce stereo anaglyphs where an object is rendered from two slightly different perspectives overlaid on each other where the user sees the object as a single 3D object [46]. For practical reasons auto-stereoscopic viewing is more acceptable as the viewer is not required to wear filter glasses, methods enabling this include the use of colour to achieve depth perspective of a 3D object, where along with other depth cues the object colour can be used provide perspective, for example blue appears more distant than red [46]. Random dot stereogram can also be used to where darker areas are used to give the perception of distance compared to lighter areas.

It is possible to use colour to visually identify specific areas of concern, applications of this can be seen in many non bright field microscopy situations [47;48]. In some cases colour of the specimen can be usefully controlled in microscopy by the selection of specific markers or dyes. There are many instances where the use of colour can be carefully controlled and specific chromagens can be bound to bio-markers providing a visual representation of a significant biological area or event [49;50].

As well as the importance for colour representation in the visual display of imaged specimens, colour can be used for object recognition, segmentation and quantification [51-

54]. Colour spaces such as HSV (Hue, Saturation and Value) , HLS (Hue, Luminance and Saturation), LAB (Luminance, A, B) separate chromaticity and intensity information, rather than the RGB (Red, Green, Blue) colour space traditionally used for the storage of images and capture from imaging devices (and viewing in the human eye), as such provide more suitable models for machine vision. HSV and HLS colour spaces allow for the single independent parametric specification of colour for analysis and visualisation. LAB can be used to more closely mimic the logarithmic response of the human eye but requires two variables to specify colour. The logarithmic response of the human eye has been explained physiologically as being caused by excited light receptors within the eye inhibiting its neighbours and through the chemical process resulting changes occurring within the eye at different intensity levels [55]. Also through the process of evolution as for most human activities the visual determination of image gradients is more important than of absolute determination of intensities, previous studies have shown the logarithmic relationship [56]. Many applications outside that of microscopy use colour spaces other than RGB, including where the use of HSV and LAB colour spaces have been used to discriminate between different food preparations and plant types [57-59], while the use of these colour spaces is not common place within microscopy applications, this could be due to the primary use of medical imaging for subjective review, where the RGB colour space is suitable. For microscopy quantification systems the colour spaces used in other areas can be applied and used within quantification systems.

The resultant image seen with a microscope is a convolution of the illumination conditions, the specimen and optical track (also display system eye and brain for human vision) the final image colour data is highly susceptible to illumination conditions. In order to effectively extract colour and intensity information as a reliable descriptor of an object or field, colour reflectance/absorbance intrinsic to the specimen must be extracted [45].

Variations of colour appearance due to object shape, viewing and illumination pose, as well as illumination colour need to be discounted to allow for accurate measurements. In serial sectioning techniques the specimen thickness can vary affecting the colour and intensity characteristics of the specimen, this again needs to be controlled external to the image capture system if accurate measurements are be obtained. Colour constancy or colour invariant normalisation can be used to achieve colour invariant representation [45]. Recent advances in colour based object recognition may have application in medical object recognition [60-62]. Existing works provide a mechanism to remove illumination artefacts from an image [62]; however in a well controlled microscopy system it is possible to obtain a reliable reference image for background correction and this the approach taken in the development of the systems detailed in this report.

Using specific illumination and detection wavelengths can aid in the specificity of analysis, reducing susceptibilities of external environmental effects to influence imaging systems. Existing works have considered the advantages of using specific wavelength independent of local environmental change to achieve this for other machine vision applications [63]. A medical imaging example where illumination is carefully controlled is the quantitative imaging of the Feulgen stain, used within DNA Image Ploidy. A filter is used with a central transmission wavelength of 546 nm, 560nm or 590nm (dependent on the stain) with a narrow band pass, eliminating the effects that spectral illumination variations has on measurements [64].

2.3.2 Texture

Although the precise definition of texture has been elusive, the notion of texture generally refers to the presence of a spatial pattern that has some properties of homogeneity [65]. Texture features have been used to identify contents of aerial imagery such as bodies of water, crop fields and mountains [66]. Texture may be used to describe content of many real-world images: for example, clouds, trees, bricks, wood, hair, fabric all have individual textural characteristics [67].

Metrics used to describe texture include Entropy, Energy, Homogeneity, Coarseness, Auto-correlation, Anisotropy, and Granularity [1,2]. Entropy can be used to describe the randomness of an image; Energy the orderliness; Homogeneity uniformity of the image; Auto-correlation can provide a measure of the repeating pattern within the image; Anisotropy characterises directional differences; Granularity the level of componentization or minimum detail of structures within the image [68]. Within medical imaging applications granularity has previously been used to quantify noise spectrums in Computerised Tomography (CT) scanners and auto-correlation has also been shown to be a useful measure of repeatability or the detection of any non random noise introduced in the system by the image reconstruction filters used in such systems [69].

The major attempts at modelling texture include but are not limited to the following approaches: random field modelling, fractal geometry, Grey Level Co-occurrence Matrices (GLCM) and spatial-frequency techniques which include in particular Wavelet analysis and Gabor filters [70;71] for coarseness, contrast and directionality texture features.

The use of texture analysis in medical systems offers both increased objective possibilities, replacing existing manual methods, and the ability to produce results based on information that is not visible by the human observer [72]. If these methods are to be introduced to microscopy it is essential that robust image capture systems are introduced

and validated using less abstract analysis functions that can be proved to have a foundation in biological science.

Texture is an important consideration in the analysis of any image and has been used previously to provide diagnostic information [35;62;73]. Texture measurements calculated can be of low or high order, where low order characteristics can be seen with the human eye high order characteristics may only be detectable with the use of machine vision and associated algorithms [74]. Texture can also be used for the classification of different objects in medical imaging and for the use in the determination of prognostic and diagnostic features [34]. In addition to object recognition and content-based image retrieval. Textural features can include 2D and 3D parameters which can also be used for image visualisation, in particular image based realistic rendering and image synthesis [75;76] as applied outside medical areas.

The methods of texture extraction can offer increased amounts of image information and range in complexity and processing requirements. If it possible to achieve the good results by the application of basic pixel statistic based texture measures such as standard deviation or variance of pixel areas rather than more complex analysis methods such wavelet or GLCM, greater systems speeds can result.

2.3.3   Local And Global Image Characteristics

Independent consideration has to be given to the differing methods required to calculate local and global image parameters [1]. The global characteristics (that of the whole field) can by the most part be calculated without human interaction or complex segmentation, however measurements and quantification made on local portions or individual objects within the field of the image present issues requiring either manual selection or the development of complex automatic methods for segmentation of the relevant area.   Segmentation in image processing applications is probably the most important image processing consideration, as unless an image can be effectively segmented then any further analysis of specific structures of interest is not possible, much previous work has been completed in the area of segmentation [62;77-81]. The basic methods available for segmentation are pixel intensity or spatial and frequency dependent segmentation.

The intensity or colour histogram of an image may be used for segmentation, dependent on the intensity separation between the objects and background under analysis [82]. Histogram segmentation can be quick to complete and can reduce the introduction of human subjectivity if automatic methods are used [77-81]. Histogram based segmentation can be found to be ineffective in situations where intensities between complex structures

are subtle as is often the case in biology where other methods have to be explored and developed.

Textual segmentation can use a variety of different calculation methods as above acting on the whole image or window regions [83]. Textual classification methods can also be used to perform automatic textual segmentation based on colour properties [84;85]. The use of textual segmentation presents clear advantages in addressing the segmentation problem, particularly in consideration that it may be the intensity information that is providing the quantifiable of subjective information, but it can be time consuming to perform.

2.4   3D Image Reconstruction And Visualisation For Medical Images

3D reconstruction has different meanings dependant on the technology to which it refers; for Computerised Tomography (CT) and Magnetic Resonance Imaging (MRI) based systems it refers to the algorithms used to reconstruct back projected image data to form a contiguous interpretable 3D data set; for serial section reconstruction within histology samples as explained later in this chapter it refers to the methods used to reconstruct a 3D dataset from unaligned adjacent micro-tomed serial sections. The term 3D visualisation is used to describe a method that allows the display of a 3D dataset so that it can be viewed and interpreted by a user. Typical 3D visualisation approaches include the use of auto-stereoscopic methods, structural light based vision systems and motion based approaches where the visualisation of a 3D dataset is aided by the presentation of an animated image sequence. The data acquisition methods used to acquire data to be visualised is dependant on the sample under study and the exploratory requirements.

2.4.1   3D Visualisation

3D visualisation methods employed fall into two primary classes. Surface (or geometric) and volumetric reconstructions [86]. Surface rendering is concerned with the visualisation of a simplified geometric (or polygon) representation of the dataset, in this method an isosurface is generated using a meshing algorithm such as the marching cubes algorithm to represent a surface between defined intensity values within a dataset with polygons [87]. In Volumetric (or Voxel) reconstruction the visualisation of the original collected data is obtained using algorithms that simulate accumulation of light projected through specimen either from behind the specimen normal to the axis of the users view port or the reverse [88].

There are a diverse range of study areas where 3D visualisation techniques have been used to increase understanding and found subsequent clinical application. MRI, CT imaging and subsequent visualisation methods have been previously been used to increase

13

clinical understanding in many different areas, including heart disease [101], lung disease [102, 111], and diseases of the head and neck [107]. These studies and others present methods that have been used to provide increased information for subjective review and in some cases have provided objective measurements [89]. The CT and MRI imaging technologies used for these studies have previously proved ineffective for the study of soft tissue structures as reported in previous studies [89;90] due to maximum system resolutions and suitability for measuring subtle gradients within soft tissue. Techniques using CT micro-tomography have been used for the study of small biological samples where µm resolution is required, existing studies have shown application for the study of mineral deposits in bones and teeth [91] and small areas of biological tissue [92] the methods have again been used to image mainly solid tissue structures within specimens.

In previous studies results have been completed comparing the interpretation of the results obtained using both surface and Voxel rendering techniques [93;94], finding that Voxel rendering can present information more useful for diagnosis as finer tissue structure within the data set is not removed as is the case with surface rendering. Previous research shows that geometric reconstruction methodology is a suitable method for the reconstruction of objects where a polygon grid can be fitted to represent a solid surface such as bone or other solid structures [95]. These structures have definite separation in terms of intensity from the adjacent tissue and the surface that is generated is representative of that within the original sample [117,123, 126], however there is an issue in presenting what is essentially a simplification of a surface structure on an object that does not have a clear boundary [111] as found in histological samples.

The use of volumetric rendering is found to be more suitable for studies where a clear threshold cannot be defined, as it allows for each Voxel to retain much of its original intensity characteristics and allows the visualisation of Voxels with differing opacity values. Voxel rendering has been used for the visualisation of medical datasets in previous work including where it has been used to visualise head and neck data from data acquired with MRI systems [131] and serial section datasets as described in Section 2.4.2.

If the use of 3D histology is to be used clinically or to increase clinical understanding then 3D visualisation systems are required that can be used by biomedical scientists to produce meaningful visualisations, as the samples under analysis are to be soft tissue structures a Voxel rendering system is most appropriate. The development of the 3D reconstruction system detailed in Chapter 4 aims to achieve this.

2.4.2 Serial section Reconstruction

Serial section registration or reconstruction of data from serial sections has been previously described [96]. The basic approach is to image specimen slices that have been cut from the specimen, appropriately prepared to show the relevant biological structures, placed on a microscope and imaged, the captured images are then registered with respect to each other. Voxel rendering has previously been used in combination of serial sectioning for the visualisation of tissue structures using electron microscopy including the study of hair cells [137], blood vessels [140], and other cellular structures [37].

An alternative to the normal serial sectioning technique is provided by Denk et al. [97], for the study of neural structures in 3D using the Scanning Electron Microscope (SEM). In this method the block face is imaged within the SEM vacuum chamber, sequentially deeper sections of the tissue block are removed and the surface of the block is imaged. This method removes the requirement for the registration of serial sections as the block from which the images are obtained remains static.

Existing serial section registration methods include the use fiducial markers and the use of imaged structures within the dataset. Alignment of the data using fiducial markers is achieved by pushing/drilling a solid object in to the paraffin block and can produce good results as there is a reference point for which to complete dataset registration after sectioning [98]. However the use of fiducial markers has limitations in that the insertion of solid fiducial point may cause damage and distortion to the data set. There is also a risk of sample damage as since only the top of the object can be seen when the markers are inserted in to the block the fiducial point may be inserted through what later turns out to be the most relevant part of the dataset. Fiducial markers may damage the microtome (sectioning equipment) used to cut the serial sections or cause cutting aberrations within the sectioned tissue as since the requirement of the fiducial marker is that it is rigid enough to insert through the tissue without the marker being distorted it is liable to be harder than the tissue that comprises the biological sample causing issues during the cutting of the sections.

As images collected from serial sections are from adjacent areas of the same tissue block the images captured have similar characteristics. The similarity between the images can be used to register the dataset, as described in existing methods [99;100] relying on the overall object shape or border for alignment, these methods can be in-effective when considering histological structures where low frequency detail is known to change section to section as the anatomical features vary, such as a duct passing diagonally through the specimen or where there are limited definable contours within the dataset.

The serial sectioning technique does not have a maximum depth limitation as with the confocal microscope, allows for the use of specific robust staining methods to highlight biological instances within the individual serial section prior to reconstruction and visualisation which it is not possible with transmission imaging systems or the Electron Microscopes. For example serial sectioned tissue may be stained to detect a specific protein such as Human Epidermal Growth Factor Receptor 2 (HER2) which is used to in a non 3D applications to determine breast cancer treatment by highlighting specific biological instances within tissue [101]. If 3D visualisation is completed on serial sections stained with such specific stains then increased understanding may be possible not only in the visible tissue structures of the specimen but also the bio-mechanisms within the tissue.

As has been described fiducial point alignment method is problematic and can cause sectioning problems and aberrations, methods that use the image similarity between image slices are advantageous but if there is reliance on low frequency information the methods may not work for datasets where large macro changes occur within the sample. Previous work has described cross-correlation as a measure to describe the correctness fit between two sections when completing block face imaging [102]. It follows that conversely cross-correlation could be able to provide a mechanism for the alignment of two adjacent serial sections; however as performing cross correlation on two large images is a computationally expensive technique. Methods of reducing the compute time have to be found to make the use of cross correlation using whole slide alignment a practical option.

Histological samples are routinely embedded in wax blocks and as the thin sections (2-6μm) cut from these blocks are delicate, regularly suffering structural degradation therefore a semi-automated system is required so there can be manual intervention where these section are damaged. The development of a system containing medical image algorithms for 3D reconstruction is an aim for this study as detailed in Section 1.3.2.

2.5   DNA Image Ploidy

Ploidy is a cytogenetic term for the number of single sets of chromosomes in a cell or an organism. Diploid cells contain one pair of chromosomes, as found in normal cells. If the DNA duplicates without a following cell division, the cell will contain two pairs of chromosomes and will be called tetraploid. Tetraploid cells are not necessarily abnormal. Aneuploid cells contain a number of chromosomes that is not an exact multiple of the normal, diploid number. In humans, aneuploid cells are considered abnormal [103].

Aneuploidy is a sign of malignancy in cancer, and is often related to a poor prognosis for the patient [103-109].   It is therefore of great interest to develop the most

16

accurate method for measuring DNA Ploidy, regarding sensitivity, specificity and quality of results.

DNA Ploidy refers to the statistical distribution of Integrated Optical Density (IOD) for a group of cells within a sample. The data required can be measured by image cytometry or flow cytometry. Image cytometry is based on the Feulgen technique, a well-known cytohistochemical staining method that enables specific staining of DNA in situ. The colour intensity of the reagent is proportional with the DNA concentration. The amount of DNA in the nuclei is expressed as the amount of light absorbed by the Feulgen stain over the nuclei. Optical Density (OD) is, for a given wavelength, an expression of the transmittance of an optical element. DNA Ploidy is set by calculations of Integrated Optical Density (IOD), the sum of all grey levels for all the optical elements in a cell nucleus. Flow cytometry is performed on cells that have been stained with DNA specific fluorochromes . In flow cytometry the emitted light is measured optically with a photo-detector. The relative fluorescence intensity of the cells indicates the amount of DNA in the nuclei. Flow cytometry enables fast measurement of large numbers of nuclei. However, the method gives no morphological control of the analyzed nuclei and there tends to be some background debris. Image cytometry has the advantages in that the morphology of nuclei can be verified prior to analysis so it is possible to ensure that not debris is included in the measurements. The images can also be stored for later analysis. Traditionally, image cytometry has been time consuming and the numbers of nuclei have been fewer than that collected with flow cytometry. However, studies have shown that sensitivity, specificity in the part of conclusive analysis are significantly higher for image cytometry than for flow cytometry [110;111]. A review and detailed descriptions on diagnostic DNA image cytometry are given in Haroske *et al.*, [64]

Existing DNA Ploidy systems using manual methods have presented results that have been shown to be significant; however the manual operation of the system limits the number of cell nuclei that can be included in analysis and the statistical relevance of minor populations. The development of an automated DNA Ploidy system is an aim for this study as described in Section 1.3.3

2.6 Image Analysis And Rendering Software For Medical Applications

The applications available for microscopic image analysis, reconstruction and visualisation can be seen to vary in scope from those aimed at the end user, through technical tools to development libraries. As each of these categories is considered it can be seen that as the technical knowledge required to use the tools increases so does flexibility and ability to develop a targeted specific application.

Specific 3D reconstruction tools aimed at the bio-scientist that are currently available include Voxblast (Vaytek, USA), Imaris (Bitplane, Switzerland), Amira (TGS, USA) and Vitrea (Vital Images Inc, USA). Voxblast offers a fairly technical environment that can perform both Voxel and surface reconstruction [112]. Imaris offers a high quality primarily surface rendering system for research use and concentrates mainly on confocal imaging requirements [113;114]. Amira of the three offers the easiest to use from an end user point, but again concentrates on surface rendering for generic visualisation requirements [115]. Vitrea has been used in clinical applications on CT and MRI collected datasets [116;117]

A selection of generic image analysis tools aimed at the end user are available that can be used for the analysis of medical images. These packages include generic image analysis functions with graphical user interfaces such as Image Pro Plus (Media Cybernetics, USA), NIH Image (National Institute of health, USA), PAX-it! (MIS, USA), the software systems allow for generic image processing methods to be developed. Both Image Pro Plus and Pax-it allow for the integration of generic machine vision cameras and for specialised microscopy cameras. Simple applications can be developed using the supported macro languages and can be used to proto-type image processing methods efficiently. It is difficult to see these applications being used in a clinical setting, due to the inability to integrate the work flow pipeline effectively for specific needs for non technical use. However these system have been used for the evaluation of methods in previous research applications [118-120].

Moving on from generic applications with graphical interfaces, software packages are available that provide toolsets for both image analysis and visualisation. Using these 4G development tools the generation of prototype systems and for the development of new algorithms is efficient. Such tools include Matlab (Mathworks Inc, USA), Octave (Free software foundation, USA), VTK (Kitware Inc, USA) and IDL (Research system Inc). For the technical user the added flexibility that is provided can offer an environment suitable for researching new ideas [121], but for the non technical user the possibilities for using these applications is limited.

The penultimate option requiring greater technical knowledge than the use of the 4GLs above is the use of Open source and commercial image processing and visualisation libraries within a custom application. The use of custom libraries provides isolated reconstruction and processing functions both from specialist providers such as Lead Technologies Inc (Lead tools) and companies providing low level software support for the hardware products provided such as the performance libraries developed and distributed by Intel Corp. The use of these libraries offers the flexibility to design dedicated applications,

that while using core image processing functionality from pre-developed functions, the user interface can be customised and total flexibility is maintained.

The final option is to develop image software functions in a low level application development language such as C or C++, this offers the ultimate flexibility but requires the most technical implementation, it is a most time consuming method and requires the greatest amount of validation and testing. Development of applications at this low level has advantages in that specific functionality can be developed that rely on efficient and dedicated code.

There is often a trade off between the speed of application development and execution speed, this should be considered when assessing and selecting the implementation method. There can also be financial considerations if third party tools are to be used there may be licensing considerations.

These applications, toolkits and development options are generally aimed at the computer scientists, engineers or researchers (with the exception of Vitrea). In reality, the use of these systems requires complex understanding of the image processing methods, and the understanding of the key concerns of application development. It is considered that increased acceptance can be achieved if applications area developed for a specific purpose. Clinical systems have to be developed so that the systems can be ultimately used by bio-medical scientists and healthcare professionals. A major consideration is the ease of use of new systems as detailed in subsequent chapters, however commercial considerations will also dictate the long term successes of any project, clinical application and continued research.

With the advance of the computing power, image analysis has great potential to be applied in clinical applications. Based on the literature survey, this Thesis presents applied advanced image processing techniques in computer vision for medical applications and diagnosis. Two main systems have been developed that consider medical visualisation and computer systems, these being subjective imaging tools and that of computer vision based objective analysis.

Specifically, the work includes, design and implementation of a system for serial section alignment with ability to interactively semi-automatically align serial section datasets, fiducial point alignment and geometric warping methods. A Voxel rendering application is presented, suitable for visualisation of serial section datasets, within histology. In the implementation of the 3D reconstruction system novel methods for visualisation specifically appropriate for histological datasets will be explored. An objective system has been designed and implemented for automated DNA image Ploidy measurement. There is

presentation of the automation concerns, parametric extraction and clinical studying completed in order to verify and validate the systems operation.

The following chapter explains the bright field microscope for medical imaging, providing the background theory of the optical system and hardware constraints. The design for an optical capture system is introduced which incorporates the use of third party automation hardware.

Chapter 3 Fundamentals Of The Bright Field Microscope

The literature review finds that the bright field microscope is the most appropriate and commonly used apparatus for the imaging of specimens for both qualitative review and quantitative analysis within Pathology. It is the bright field microscope that will be used as an imaging base for histological 3D serial section reconstruction and the automated DNA Image Ploidy system both of which are described in this Thesis. The following chapter details the fundamental optical considerations and elements of its physical construction that can be automated to increase the usefulness of the system as an automated image capture platform. As required to meet the aim of developing an image capture systems for use in microscopy and subsequently the development of an automated DNA Ploidy analysis system as described as aims in Sections 1.3.1 and 1.3.3 respectively.

3.1   The Bright Field Microscope And Its Control

This review considers the microscope operating in transmission mode, the mode used most commonly for review of histological and cytology specimens. A cross section of the microscope is shown **Figure 3.1** [122], which shows both bright field (transmitted light) and dark field (reflected light) illumination and optical systems. The three main components for consideration are shown, the illuminating light source, optical track and manual physical control devices.

3.2   Light Source

Consideration of the light source is important as the final image is a convolution of the optical track, illumination and transmission characteristics of the specimen. There are two main considerations when selecting or assessing the light source to be used, stability and the spectral illumination it provides. Light source stability is determined by the choice of power supply, primarily if it is regulated or unregulated. The unregulated power supply provides a sinusoidal AC supply to the lamp, where with the regulated supply a smoothed DC output is provided. Both types of supply units are suitable for human vision, as the flicker from the unregulated supply is not perceivable. However an unregulated supply results in unusable images when captured digitally. The effect of this can be seen in **Figure 3.2** where two sequentially captured images using an unregulated power supply are shown and can be seen to have different intensities caused by the variation of the light intensity.
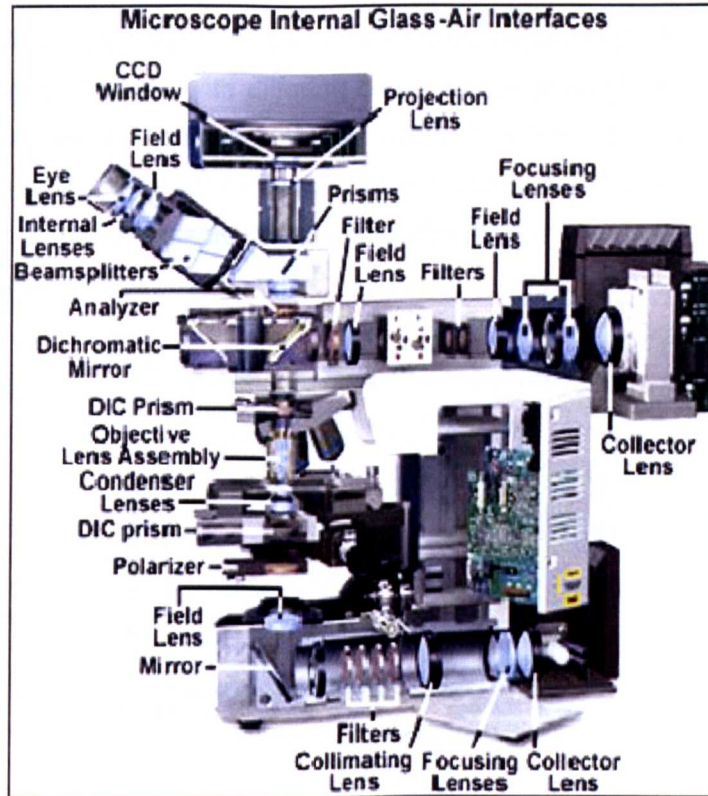
Figure 3.1 Microscope cross section

[Source: Olympus Corporation, Japan]
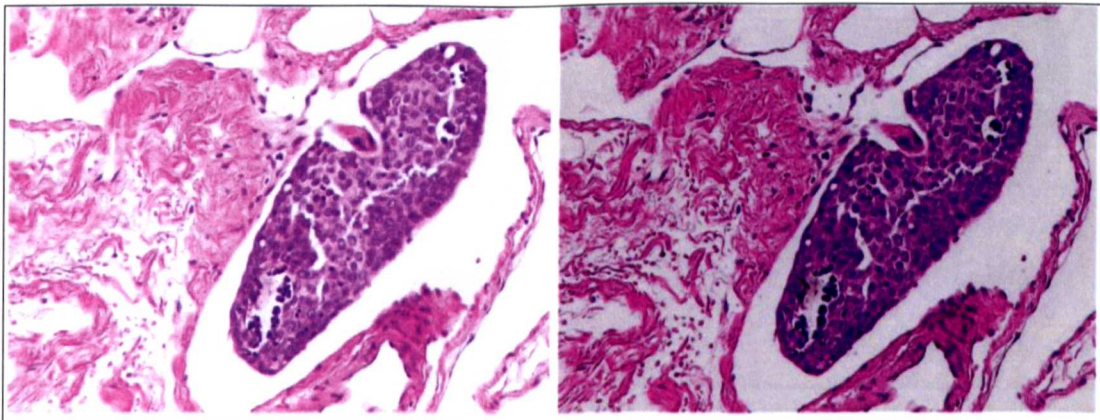
Figure 3.2 Sequentially captured frames from an un-regulated light source

An important consideration of the light source is its spectral characteristics as this varies between systems and is also dependent on selected illumination levels. Bright field microscope lamp housings are fitted with tungsten halogen lamps. The brightness is controlled by varying the applied voltage from the power supply and as shown in **Figure 3.3**

the illumination spectrum changes are dependent on the level setting of the lamp, from warm (higher red component) to cooler (higher blue component). **Figure 3.4** shows the difference in images obtained with differing colour temperature illumination. There are two common power ratings for the lamp 30W and 100W. The 100W light box is able to produce spectra which while still unbalanced toward the infrared end of the spectrum contains more blue light, which is more suitable for imaging due to the frequency response of digital camera equipment.

Tungsten Lamp Emission Spectrum
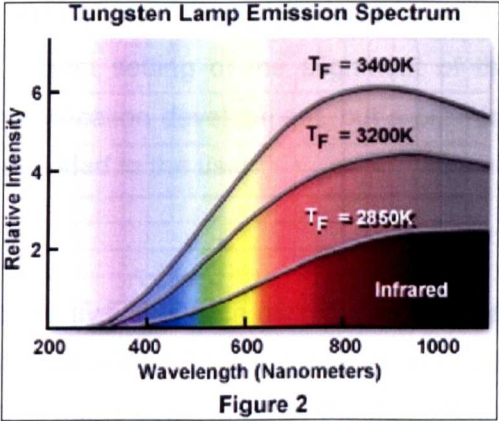
Figure 2

Figure 3.3 Tungsten lamp emission spectrum
[Source: Olympus Corporation, Japan]
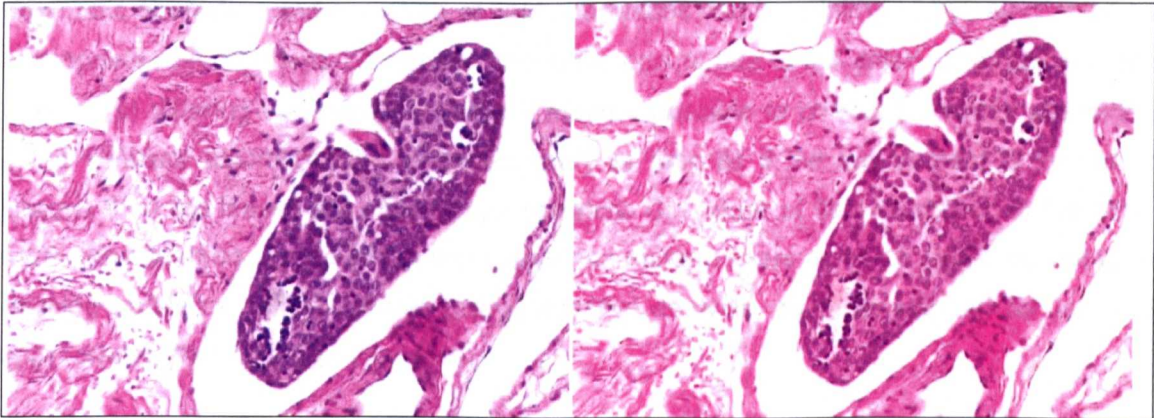
Figure 3.4 Images captured using different bulb colour temperatures
The image to the left shows was captured with high intensity setting the image on the right a low intensity setting.

Computer controlled voltage regulators are available that offer control of the light source. As these devices are voltage regulators only and do not directly measure light reaching the camera, or the effect of the changing colour balance has, these devices offer

only course adjustment. Both colour and intensity correction should be provided within the software to enable reliable and consistent results to be obtained.

3.3 Microscope Optics

The optics in a bright field microscope are complex, consisting of two sets of conjugate focal planes. There are four sets for the image-forming conjugate set and four aperture planes for the illumination conjugate set [123]. The alignment of the optical planes are adjusted to achieve Köhler illumination which is a common microscopy term, ensuring that the conjugate optical planes are correctly aligned through following defined sequence of operations [122]. The correct setting of the alignment of the optical planes is not a concern for automation or application development, but a pre-requisite for system use and correct training should be provided to the user.

3.3.1 Objective Lenses

A wide selection of lenses are available from microscope manufactures, specifications and selection has two primary considerations, resolving power and correction for common aberrations. The resolving power is determined by the numerical aperture of the lens or NA as described later in this section and aberration corrections which include: astigmatism, chromatic aberration, curvature of field, geometrical distortion and spherical aberration.

The most common aberrations that cause problems for digital imaging which are chromatic aberration and curvature of field aberrations can be minimised by selection of an appropriate objective lens. Chromatic aberration occurs due to the differing refractive index of glass at differing wavelengths. While it may be possible to correct for colour aberration using software algorithms this is unnecessary so long as if the requirement is for colour images then the lenses are chosen appropriately. Curvature of field correction is the other main consideration, as this effect can cause non-uniform focus across a single field of view causing problems both for visual and quantitative analysis, again lenses can be selected appropriately that minimise this issue.

3.3.2 Condenser Lenses

The condenser forms part of the optical track and has similar optical selection considerations to that of the objective lenses in terms of correction of optical aberrations. Common recommendations are that the Numerical Aperture (NA) of the condenser should be equal or greater to the NA of the objective lens used.

3.4 Resolution

One of the ultimate concerns for imaging systems is the achievable spatial resolution. Resolution has to be considered for both vertical and lateral directions. A common way to explain what is meant by resolution is the use of airy patterns as shown in **Figure 3.5**. The maximum resolution according to the Rayleigh criterion is where two points are resolved when the first minimum (zero crossing) of one Airy disk is aligned with the central maximum of the second Airy disk [122]. The theoretical equations used to calculate the resolution are shown in **Equations 3.1-3.3**.
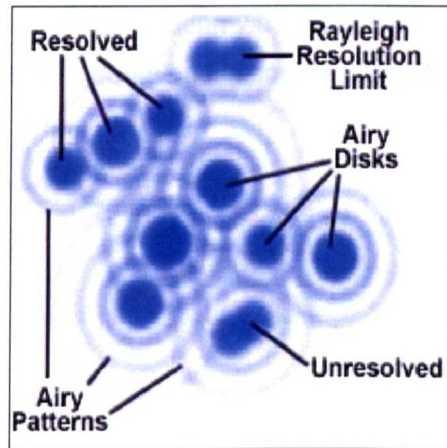
Figure 3.5 Airy Patterns
[Source: Olympus, Japan]

$R = \lambda / 2NA_{Objective}$	..(3.1)
$R = 0.61.\lambda / NA_{Objective}$	..(3.2)
$R = 1.22.\lambda /(NA_{Objective} + NA_{Condenser})$	..(3.3)

Where R the Rayleigh Resolution Limit is defined as the smallest distance that can be resolved between two objects, where two objects can be seen to be separated from each other. NA the numerical aperture. λ the wavelength of light in Nanometers.

The reasons for differences in the equations is the consideration of differing theoretical phenomenon by optical physicists, and the fact the ultimate resolution may also be effected by the specimen contrast and other characteristics. An of example typical resolving resolutions for a selected range of Nikon lenses is shown in Table 3.1.

The theoretical equations given for calculation of the optical resolution of the microscope do not account for internal misalignment of optical lenses within the microscope or aberrations as described in Section 3.3.1. The Modulation Transfer Function (MTF) is a practical measure that can be used to express the microscopes ability to transfer image contrast from the specimen to the imaging plane as a single parameter [123]. For microscopy systems the MTF can be measured using an optical line grating etched on to a glass slide. The resultant image will not be a direct representation of the grating with sharp edges but contain transitional areas between dark and light areas. The MTF of a microscope can be measured for a given frequency using the original image and the image that is captured. The frequency of the grating where the MTF reduces to zero this is termed the first resolution point. The MTF equation is shown in **Equation 3.4.**

$$MTF = \frac{Modulation_{Image}}{Modulation_{Object}}$$

..(3.4)

Where

$$Modulation = \frac{I_{max} - I_{min}}{I_{max} + I_{min}}$$

..(3.5)

Where I_{max} and I_{min} are the maximum and minimum observed intensities of the observed image and object.

The Optical Transfer Function (OTF) represents the ratio of contrast in the object to that of that of the image and takes into account the phase shift between the observed image and the actual image. The imaginary term of the OTF is known as the Phase Transfer Function (PTF) and the modulus the MTF. The OTF equation is shown in **Equation 3.6.**

$$OTF = MTF.e^{i\phi(f)}$$

..(3.6)

Where ϕ is the phase shift for a given and spatial frequency f.

If the PTF is linear in terms of frequency then the result in the observed image is a simple lateral shift, however if the PTF is non linear then distortion in the image will occur. In the most adverse case of 180 degree phase shift, the intensities of dark and light patterns are inverted.

The resolving power of the lens is a consideration in the choice of the digital camera used within in the imaging system as explained later in Section 3.6.4 of this chapter. In considering the maximum theoretical resolution of the microscope it can be seen that the available pixel sizes within imaging devices allow optimum sampling particularly for higher NA lenses, where it is possible to fulfil Nyquist sampling requirements. As the magnification of the lens reduces and assuming that high quality lenses are used, it is not possible to correctly sample all the image data from the microscope. There is a very large cost difference increase between objective lenses dependant on quality, where an Apochromat lens may cost in the order of £6,000 each and the next objective down in quality will only cost half this price, as such unless the image data can be fully resolved with the selected camera, combined with economic considerations there are good reasons to select a lesser lens.

To allow consideration of the imaging equipment in relation to the resolution of available lenses examples are now given for the high power 40x objective lens and the low power 4x objective lens.

The Plan Apochromat 40x high power objective. As shown in Table 3.1, the lateral resolution is given as 0.29μm. Common Charged Coupled Device (CCD) element sizes of cameras range from 4-10μm which at a 40x magnification relates to a microscope resolution of 0.1μm to 0.25μm (pixel size/objective magnification). Nyquist sampling criteria can be meet with imaging devices with pixel sizes of less than 5.8μm.

Considering the Plan Apochromat 4x low power objective, again given data in Table 3.1 the lateral resolution is given as 1.375μm and again given the same range of CCD pixel sizes (4-10μm) at 4x magnification the CCD resolution translates to a microscope resolution of between 1μm and 2.5μm. The image from this lens cannot be sampled according to the Nyquist criteria unless the size of the CCD pixels is 2.75μm which much smaller than available in common scientific cameras.

For the developed systems the scanning method used to capture images for subsequent 3D alignment and visualisation of serial uses a 10x objective lens, where the image can be adequately resolved with available scientific cameras and produces a far superior image to that possible using a lower magnification lens as would be required to capture the whole specimen in a single image. The DNA Ploidy system uses the 40x Zeiss Neofluor (Carl Zeiss, Germany) equivalent to the 40x Plan Fluorite shown in Table 3.1, while this lens does not have a resolving power as high as the Apochromat lens it is more adequately matched to the selected camera the C4742 (Hamamatsu, Japan) which has a 6.7μm pixel size which is below the minimum pixel size required to achieve Nyquist sampling which is 7.4μm for this lens.

As shown in **Figure 3.5** an object can be said to be resolved even when there is a blurring of boundaries. The blurring can is caused both by diffraction within the optical system and maximum optical separation possible between two objects on a given system. This blurring can cause problems in automatic object recognition systems for tasks such as object counting or analysis of objects where the independent size of an object is critical.

Magnification	Objective Type					
	Plan Achromat		Plan Fluorite		Plan Apochromat	
	N.A.	Resolution (µm)	N.A.	Resolution (µm)	N.A.	Resolution (µm)
4x	0.1	2.75	0.13	2.12	0.2	1.375
10x	0.25	1.1	0.3	0.92	0.45	0.61
20x	0.4	0.69	0.5	0.55	0.75	0.37
40x	0.65	0.42	0.75	0.37	0.95	0.29
60x	0.75	0.37	0.85	0.32	0.95	0.29
100x	1.25	0.22	1.3	0.21	1.4	0.2

N.A. = Numerical Aperture

Table 3.1 Optical resolutions from a selection of lenses

[Source: Nikon Corporation, Japan]

3.5 Depth Of Field

The depth of field of an objective is an important consideration in the design of imaging systems, as it effects the amount of specimen that is resolved for any given focus position, as such limits the resolution obtainable vertically. For some situations it may be an advantage to have a short depth of field such, as that of optical sectioning as used in 3D visualisation so individual optical plans may be resolved distinctly from each other. For other applications such as the human review of histological section a longer depth of field may be advantageous as the more of the sections falls within the depth of focus of cut section. The depth of field for any objective can be calculated from the equation given in **Equation 3.7**. **Figure 3.6** shows the effect that the NA has on this range.

$$d_{tot} = \frac{\lambda_0 n}{NA^2} + \frac{n}{M.NA} e$$

..(3.7)

Where d_{tot} represents the depth of field, λ_0 is the wavelength of illuminating light, n is the refractive index of the medium (usually air (1.000) or immersion oil (1.515)) between the cover slip and the objective front lens element, and NA equals the objective numerical aperture. The variable e is the smallest distance that can be resolved by a detector that is

placed in the image plane of the microscope objective, whose lateral magnification is M. Using this equation, depth of field d_{tot} and wavelength λ_0 must be expressed in similar units. **Table 3.2** shows example depth of fields for given objective lenses.

Depth of Field Ranges
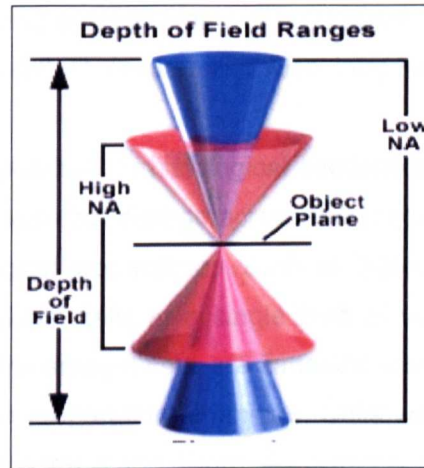
Figure 3.6 Depth of field

[Source: Nikon Corporation, Japan]

Magnification	Numerical Aperture	Depth of Field (µm)	Image Depth (µm)
4x	0.1	55.5	0.13
10x	0.25	8.5	0.8
20x	0.4	5.8	3.8
40x	0.65	1	12.8
60x	0.85	0.4	29.8
100x	0.95	0.19	80

Table 3.2 Depth of field examples

[Source: Nikon Corporation, Japan]

There is a requirement to re-focus the microscope both each time a new slide is placed on the microscope and when looking at different locations of the specimen. Variations of the thickness of the glass slide, specimen and physical construction of the microscope cause variations outside the depth of field range of the objective as shown in **Table 3.2**. As the depth of field falls with increasing NA, focus is particularly a concern for applications requiring high magnification objectives and greater resolutions.

Due to physical tolerance in the manufacture of the microscopes specimen stages it is common to have a ±5µm linear gradient across the stage surface from one end of the specimen to another [124]. The glass slide thickness can vary for example by ±127µm

within a single batch and ±51μm along a single slide [125]. Inexact alignment of the stage with respect Z axis of the lens can also cause of variations within a single field of view in extreme cases, but it is normal to see a 30μm gradient across the whole specimen as a result of this misalignment. The thickness of a histological section is typically 4-10μm. A histological section is cut using a microtome from a paraffin block and the cutting process can cause ripples in the resultant section and also introduce a gradient across the cut section.

The optimum focus position for histological sections can be seen to largely remain constant for a single field of view but change across the specimen due to concerns external to the specimen. For cytological preparations, such as that used in DNA Ploidy there is a difference of focus for individual cells in a single field of view. The differing viscosity of individual cell nuclei affects the amount cells are flattened when transferred to the slide from the centrifuge as used in the preparation technique. Cells within a single field of view can have focus differences of between 4 and 10μm. As cytology is concerned with the study of cell structure, high magnifications are required and a 40x objective or higher is required to view the relevant detail, as such accurate and rapid focus for cytology specimens represents a significant challenge for automated imaging systems as is addressed in Chapter 6.

Imaging processing algorithms are available and in development that can be used to effectively increase the resolution or more correctly, clarify of captured data. The algorithms cannot retrieve data that has been lost completely, but can be used to increase the clarity and separation between distinct objects and structures. In general there are two types of algorithms. Blind algorithms that apply a general approximated Point Spread Function (PSF) to the image [126] and system specific algorithms that require the PSF of the equipment to be measured or calculated which is then de-convolved with the resultant image to provide an estimation of the original image [127]. The OTF of the optical system used will define the how successfully deconvolution will be able to restore the image, the MTF defines the detail present in the source image and restricts much true detail can be extracted by deconvolution, the linearity of the PTF will affect the ability for the deconvolution algorithm to correctly estimate the original image in the presence of any phase distortions. Deconvolution has not been used for the studies presented in this report, as the automated the results from DNA Ploidy would be adversely affected by inaccuracies deconvolution would cause on captured data also, the size of the objects captured are far greater than the maximum optical resolution of the selected lens so the image processing challenge of separating individual objects would not be reduced by employing deconvolution

algorithms. The work that has been completed using serial section reconstruction for histology does not require deconvolution as the images that are required for visual review do not rely on frequencies close to the optical resolution of the selected lenses. If however studies had concentrated on the use of optical sectioning deconvolution methods would have had to be employed to remove out of focus blur from the captured image stack.

3.6   Hardware, Software Environment And Algorithmic Considerations

The bright field microscope as detailed above provides a robust platform for image analysis systems. However the microscope was originally designed for human operation and not for machine or automated image processing. As such, some of the system characteristics are not ideal for machine vision and can be improved by both image analysis techniques and automation. It can be considered that the current microscope is a manual system that by automation can be modified to make it suitable for automated tasks. At the time of writing new hardware developments are in progresses that are set to provide systems that are designed solely for machine and automated imaging. These new systems have a modified optical track and do not provide an optical human interface. The following section provides a review of the automation used within the design of the systems detailed in this Thesis.

3.6.1   Microscope Stage Automation

The field of view of the microscope is somewhat limited in consideration of the size of an average specimen when using anything but the lowest power objective lens. The microscope XY (or specimen) stage presents one area where automation can be applied to great effect, increasing the flexibility of the system for automated analysis, replacing the existing coaxial manual controllers which allows the user to move the stage in either the X or Y, direction and course and fine focus control Z or focus position of the system. Fitting automated devices allows the field of view to be increased and controlled automatically, such automated stage devices such as that shown in **Figure 3.7**. These stage control systems allow for the specimen to be positioned with an accuracy of up to ±0.3μm and with settle times in the order of 100-500ms dependent on the distance of the movements [124]. Slide inserts are available that can hold between 1 and 8 specimens simultaneously, again further increasing the automation possibilities.

31
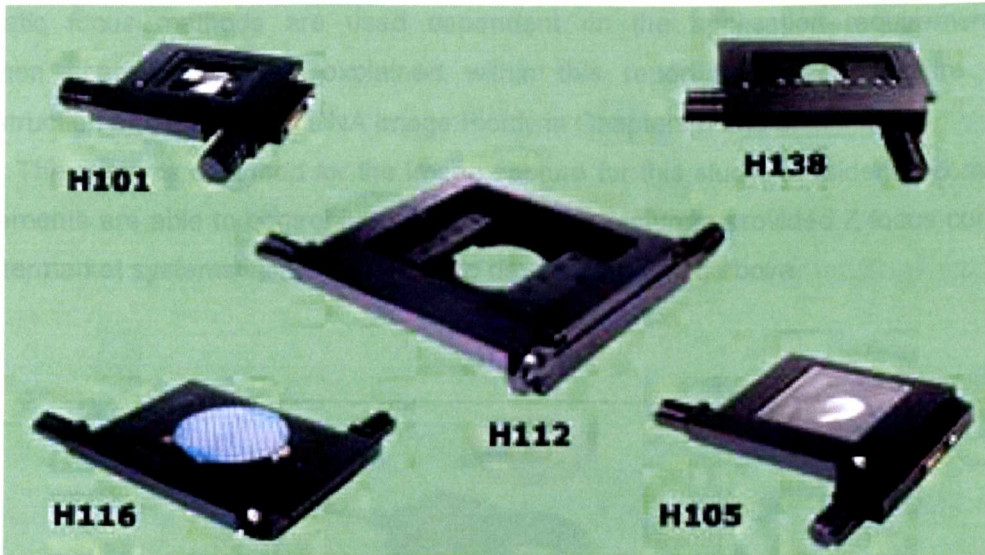
Figure 3.7 Robotic Stages.

[Source: Prior Scientific Ltd, UK]

H101, H138 are robotic stage units for use on a upright bright field microscopes holding 1 and 8 slides respectively. H112, H116 and H105 are robotic stage units used for examination of larger specimens such as semiconductor wafers.

The control of the Z focus has two primary considerations, speed and accuracy (resolution and repeatability).   Most modern microscopes can be fitted with a motor controlled focus device either as an option from the manufacturer or from a third party supplier.   These controllers replicate the control of the Z Focus of the microscope as it would be operated manually by the user, and act directly on the focus mechanism.   These motorised devices are suitable for slow and control of the focus position to approximately ±0.5µm where the inaccuracy is caused mainly by the coupling of the motorised focus controller to the focus mechanism of the microscope. For some applications such as optical sectioning, using high Numerical Aperture (NA) oil emersion lenses where there is a requirement to capture multiple successive optical sections with inter-section differences down to 100µm for the highest NA lenses, it can be advantageous to attach high precision focusing devices for fine and rapid movement. Such a device is the Pifoc-Piezo focus unit (PI, Germany), as shown **Figure 3.8**.   This device is fitted between the objective and the turret as illustrated in **Figure 3.1**. On certain microscopes the limited clearance between the lens turret and the stage present a physical opposition in doing this. The successful attachment provides the system with a focus control accurate to ±20nm with a settle time of approximately 30ms.   The primary reason for fitting a microscope with an automated Z stage (except when required for optical sectioning) is to provide an auto-focus mechanism. The automatic focus system used must be suited to the specimen under review. Different

32

automatic focus methods are used dependent on the application requirements and specimen characteristics as explained within this report for image capture for 3D reconstruction and automated DNA image Ploidy in Chapters 5 and 6.

The systems designed for the image capture for this study, considering commercial requirements are able to control both traditional manufacturers provided Z focus controllers and aftermarket systems including the Piezo device mentioned above.

Figure 3.8 Pifoc Piezo unit

[Source: Physik Instrumente, (Germany)]

3.6.2 Other Modes Of Automation

The four main microscope manufacturers Zeiss, Leica, Nikon and Olympus all offer fully robotic bright field microscopes with automation of condenser assembly, filter arrangement and lens turret. For bright field microscopy applications with the exception of dynamic telepathology, the user and automated systems benefit very little from automation outside of the two mechanisms mentioned here of X-Y and Z control. Increased automation is required for applications requiring specialised light source arrangements such as fluorescence.

3.6.3 Imaging Constraints When Using Automation

The resolution provided by robotic stages is typically slightly lower than the optical resolution of the objective lens used, this results in a tiling effect being visible if the image is reviewed at the original resolution and if images are places adjacent to each other. Algorithms can be considered that improve this and automatically re-align data the captured images, the need for this is dependent on the final use for the captured images.

As discussed in 3.1.1 the illumination source is a consideration in both human and automated systems. Both the intensity and illumination spectrum provided by the light source changes from manufacture to manufacture and from microscope to microscope. Any automated system requires that this change is counteracted in order not to introduce noise into any quantitative measurement. Systems designed as part of this study compensate for this characteristic by the use of basic background subtraction, algorithms as detailed in Chapter 5.

3.6.4 Camera Selection

As the end point of all work in this Thesis is to use microscopy images either in qualitative systems or to use analysis methods to turn images into numeric results, consideration of some of the basic concerns of camera selection and digitisation of the image is required.

Analogue or digital, both classes of cameras have approximately the same price for comparable features, however there are significant advantages in the use of digital cameras. The advantages include digitisation of the images at the camera head, reducing noise pickup on the signal wires on the way to the host PC, and hence a reduction in noise. Analogue cameras in general tend to have a lower resolution, adhering to general video transmission standards and offer resolution following these standards (NTSC(525x480) /PAL (625x576)). Whereas digital cameras do not have this limitation are available with pixel numbers from 1 to 8 million pixels. For high resolution colour imaging, choices of 3 Charge Coupled Device (CCD) based Red Green Blue (RGB) digital cameras is limited and many systems are offered with a 3 colour mask (Bayer) which through a method of CCD masking and interpolation is used to produce colour images from a single CCD, effectively reducing the resolution of the final image. There is a range of the data output specifications. The selection of digital outputs includes USB2, IEEE1394, camera link or LVDS RS644. The camera link standard at time of writing is the highest performance and most accepted standard for scientific cameras, although many existing cameras still use LVDS RS644. The Universal Serial Bus 2 (USB2) due to the ease of interfacing is increasingly becoming popular.

Speed, for most microscopy applications a speed of between 10 and 30 frames per second is acceptable, for subjective systems the speed that each frame can be captured effects the usability of the system as if this is too slow then processes such as colour setup, location of view port on the specimen and focusing can become cumbersome. For automatic systems the speed of the image capture will effect overall speed of the system, not primarily for the image capture used in the analysis but as auto-focus as this is a

requirement for nearly all microscopy applications. The multitude of images required for auto-focus algorithms can have a bigger impact.

Mono/Colour, the requirements and the use of a mono or colour camera is dependent on both the final application and the stain that has been applied to the specimen. For qualitative systems a colour camera is almost always required, where as for quantitative measurement system it is dependent on the application. As algorithmic development and image processing is less complex and greyscale cameras are cheaper, colour cameras should only be used if required. There are two methods of producing colour images, to use the Bayer filter arrangement as described above or to use 3 CCD and a chromatic separation filter which can dramatically increase the system cost. The 3 CCD colour cameras provide the best quality image and would be considered a requirement for system requiring colour analysis.

Resolution, pixel size and transfer lenses. Firstly the transfer lens. It is possible to place a transfer lens before the camera as shown in **Figure 3.1** however it is not desirable to do this as it can affect the final image quality achieved, given the range of cameras available it is not often required. As objective lenses do not provide planar focus for the whole field of view increasing the view port into these areas provides a disadvantage. Pixels should ideally be square (1:1 width/height aspect ratio), this makes analysis easier and for visual review does not distort the shape of the objects. Camera elements also have a parameter called fill ratio, this is the representation of the active CCD area to that of the total CCD area, most cameras have small gaps between pixel elements information that fall on these areas is lost, as such it is best to select cameras with a fill ratio as close to 100% as possible.

The pixel size is the size of each pixel element within the camera, the smaller this is the higher level of detail that can be resolved in each image, typical sizes range from 4 to 10μm. Taking these considerations of pixel number and size of pixels, it is the number of pixels that determine the size of the field of view of the camera not the resolution. It is the size of the pixels that determines the resolution of the image (unless a transfer lens is used). For example, using a camera with 1024x1024 pixel and 6.5μm square pixel elements, will give a field of view of 6.7 mm at the microscope camera port and with a 40x lens a field of view of 0.167 mm and a resolution of 0.16μm on the specimen.

Sensitivity and cooling, the sensitivity of the camera is defined by the number of photons that must be recorded in order to distinguish a change in the signal. The sensitivity is effected by the well size of the camera, dark current and the substrate efficiently used for the CCD fabrication (Quantum Efficiency). Some cameras have peltier cooling systems fitted which remove head from the camera detector, since thermal noise falls by a factor of 2

for every 8°C drop in temperature the dark current is reduced and sensitivity can be seen to increase.

Bit depth and dynamic range. In isolation it is not useful to consider the bit depth of the camera as the quality of the system is dependent on both the well capacity for each pixel element within the CCD and the noise within the system. The available signal differences (in photons) that can be measured from the scene is defined by the capacity (well capacity/$2^{BitDepth}$). The important consideration for image quality is the dynamic range or signal to noise ratio of the camera ($2^{BitDepth}$/noise level).

3.6.5   Selection Of Stains For Qualitative And Quantitative Imaging

In original normal form, most tissue structures would appear transparent under the microscope.   For the specimen to be imaged the specimen has to be stained so that required structures are shown and can be identified optically, different types of stains which can be applied are to histology are listed below [128].

Basic dyes: Basic dyes carry a positively charged chromophore group which is attracted to the negatively charged components of cells. Positive stain: cells are stained and background remains unstained Negative stain: cells are unstained, but the background takes on colour Simple stains: only one dye used during staining process.

Trichrome Stains: Differential stains, two acid dyes area used, use is made of dye competition, certain dyes will stain different types of tissue more readily than others. So certain tissue structures are stained with one dye and other structures with the other.

Neutral stains: Compounds of an acid dye and basic dye. The tissue stained with such a solution may show affinity to the acid dye, the basic dye or both.

Hematoxyl and Eosin (H&E): Commonly   used   for   the   subjective   review   of histological sections. Hematoxylin-metal complex acts as a basic dye, staining nucleic acids in the nucleus and cytoplasm blue, brown on black. Eosin is an acid aniline dye which stains the more basic proteins within cells (cytoplasm) and extra cellular spaces (collagen) pink to red.

Enzyme-histochemical stains: Use is made of the enzyme activity within the tissue. The enzyme is made to react with a specific substrate, this reaction may be directly viewed in the microscope or have a secondary reaction used to form a visible object or area. In this study the use of histological stains are used for the identification of specific areas for 3D reconstruction.

Periodic Acid Schiff (PAS):   Mild hydrolysis with HCL free the aldehyde group of dexyribose, which then is reacted with the Schiff's reagent. The reaction is highly specific for DNA and may also be used with a counter stain for the cytoplasm. It is the Feulgen

stain that has been used for the work that has been completed on DNA Ploidy described in this Thesis.

The next chapter details the design of a user friendly software environment for clinical image processing systems, detailing the design methods that have been undertaken, the software implementation approach and the functionality that has been included within the framework.

Chapter 4 Software Framework For Clinical Imaging

This chapter details work completed in the design and implementation of a software environment for the development of clinical software visualisation systems. The information given in this chapter provides generic information and considerations with more detailed descriptions of specific applications provided in later chapters, explanation of the 3D reconstruction system and algorithms are provided in Chapter 5 and of the Automated DNA Image Ploidy system in Chapter 6. The work detailed in this chapter represents work towards the aim of developing an image capture system as set out in Section 1.3.4.

4.1   Development Environment

Current software tools provide robust and highly developed platforms for the development and evaluation of new systems.   As described in Chapter 2, these development tools fall into two basic categories, traditional application development tools such as low level generic tools such as Microsoft Visual basic, Visual C++ and .Net languages. Fourth Generation Languages (4GL) such as Matlab and the Visualisation Tool Kit (VTK). The generic tools give the developer ultimate flexibility as the type of application to be developed and are free from the distribution and design constraints imposed by 4 GL providers. C++ is more suited to implementation of fast image processing algorithms, where Visual Basic provides a good development environment for producing good quality and functional Graphical User Interface (GUI).   The Microsoft .Net development environment introduced more recently allows for development to take place using the C# (C sharp) programming language, C# provides a good compromise allowing development in an object oriented environment, and the GUI development tools and interface opportunities that were previously only realistically available in the Visual Basic development environment.

4GL application development systems offer the ability to develop algorithms and to prototype ideas very quickly but do not offer the development or distribution flexibility of applications developed using generic development tools.   Limited 4GL user interface generation tools can be seen to act as an obstacle for producing a fully featured application that will gain clinical acceptance.

For the development of the image capture systems low-level access to the frame cards is required, in most cases the Software Development Kit (SDK) provided by the frame card vendors are delivered in the form of C/C++ libraries or Dynamic Linkable Libraries (DLL), and while access to the SDK is possible using both 4GL and other application development environments it is certainly much easier and efficient to integrate manufactures SDKs using C or C++ based code.

The systems that have been designed for this study have an overriding consideration that the systems must be usable by bio-technicians and medical scientists and also require easy access to the SDKs provided by frame cards manufacturers. Application development has steered clear of using 4GLs. The applications have been developed using Visual Basic to develop the GUI and Visual C++ for the functional backend code and to interface with the frame cards and other SDKs. Matlab and VTK have been used for exploratory work in the area of volume reconstruction as described in Chapter 5.

4.2   Addressing The Specific Imaging And Application Design Requirements

The literature finds that there are core algorithmic considerations in the design of any image based system these include: - Colour, intensity, texture, local and global characteristics, segmentation. As discussed in Section 3.2 the light source in terms of the intensity and colour temperature within the microscope cannot be precisely controlled and is subject variation, algorithmic development and application required to overcome these issues is detailed in Chapter 5. The colour and intensity correction are a core concern for any microscope based system independent of the application area. Local and global segmentation concerns are considered in Chapters 5 and 6, where the local and global segmentation methods are seen to differ and present separate and independent challenges dependent on the specimen under review. It can be seen that the texture of the image can effect the approach taken to segmentation of images, and also can be seen to provide parametric information. As discussed in Sections 3.4 and 3.5 the resolution provided by the microscope is dependent upon both the NA and the optical aberration corrections of both objective and condenser lenses. From **Equations 3.1-3.3** it can be seen that even with standard configurations the bright field microscope is able to resolve a high level of detail, and should prove a good apparatus in which to capture data for exploration and application of existing algorithms. The selection of the optical characteristics and the processing required for these images is again dependent on the specimens to be imaged.

4.3   Algorithmic And System Validation And Verification

During the course of this study existing algorithms have been coded and applied to the area of microscopy, new algorithms have also been developed. Existing algorithms include; solid body transformation using a geometric transform matrix; colour and gray shade image correction; merging of adjacent images into red and green colour channels of an RGB image to show alignment of the two image; transformation of an RGB image to a grey scale representation; normalised cross correlation coefficient for comparing adjacent serial sections in the alignment process; parametric extraction of morphological and grey

level characteristics of cell nuclei as detailed in Section 6.7.1; rule based decision tree for classification of cell nuclei; calculation of statistical measures for statistical determination of histogram; medically oriented analytic measures to express DNA Ploidy characteristics. Newly developed methods include; Fibonacci search method for translational and rotational alignment of adjacent serial sections; true colour 3 channel rendering using Back to Front Rendering (BTF) extending the pre-existing algorithm; opacity animation of the alpha bending curves used in BTF rendering; auto-focus of mono-layer cytology sections using object based focus and multiple linear regression and hybrid textual segmentation of cell nuclei in mono-layers.

Assessment is required as to the results that have been obtained from the systems that employ these methods. The criteria for the assessment of the methods can be seen to fall into two areas, qualitative and quantitative review. Qualitative review is required for algorithms where the output is of a visual nature, in these cases it is not possible to quantify the results, for example it is not possible to measure the increased insight that can be obtained from a 3D visualisation. Quantitative review is more suitable on numeric data. This report deals with qualitative system and quantitative systems, the most appropriate review has taken place in each case.

For the 3D reconstruction systems where the implemented system allows for registration of serial section datasets and subsequent reconstruction, the results obtained are evaluated to review if information is gained on the structure of the specimen that could not be previously determined. The automatic DNA Image Ploidy system presented provided quantitative results so it has been possible to statistically compare the results to that obtained to that from the existing manual system.

In review of the commercial applications available, there was concern of the complexity in that the intended users of these systems were not biologists but computer scientists and engineers. Systems are required that are usable by medical researchers and healthcare professionals who while tending to be moderately proficient in the use of PC software this is not the main proficiency of the users. If the systems developed are to be ultimately used by these researchers and healthcare professionals, it is important to consider how well the systems have been accepted, co-authored papers that have been produced show the application of the systems for practical use [129-131].

It would not have been possible to implement many of the methods reviewed and produce acceptable performance as little as 5 years ago without the use of specialist hardware and software. Now with the increase of the speed of affordable PCs, complex algorithms can now be efficiently implemented without the use of specialised hardware or computing platforms.

4.4 Software Design

A block diagram of the software environment is shown in **Figure 4.1**. With the generic component un-shaded and the specific elements shaded. The generic elements are the considered required for the systems in this Thesis and for future systems. The data acquisition system allows for communication and control of the hardware components of the system, including camera, stage and focus unit control, providing a generic automation base. The image processing sub system provides for functionality as required to process and to clean captured data from the acquisition sub-system, employing methods such as shade correction and colour normalisation. The image display subsystem provides generic functionality allowing for the efficient display of images to the user. Application specific modules provide user interfaces for the systems as well as application specific functionality. This model does not overly pre-suppose requirements for future systems and does not impose limitations for the future.
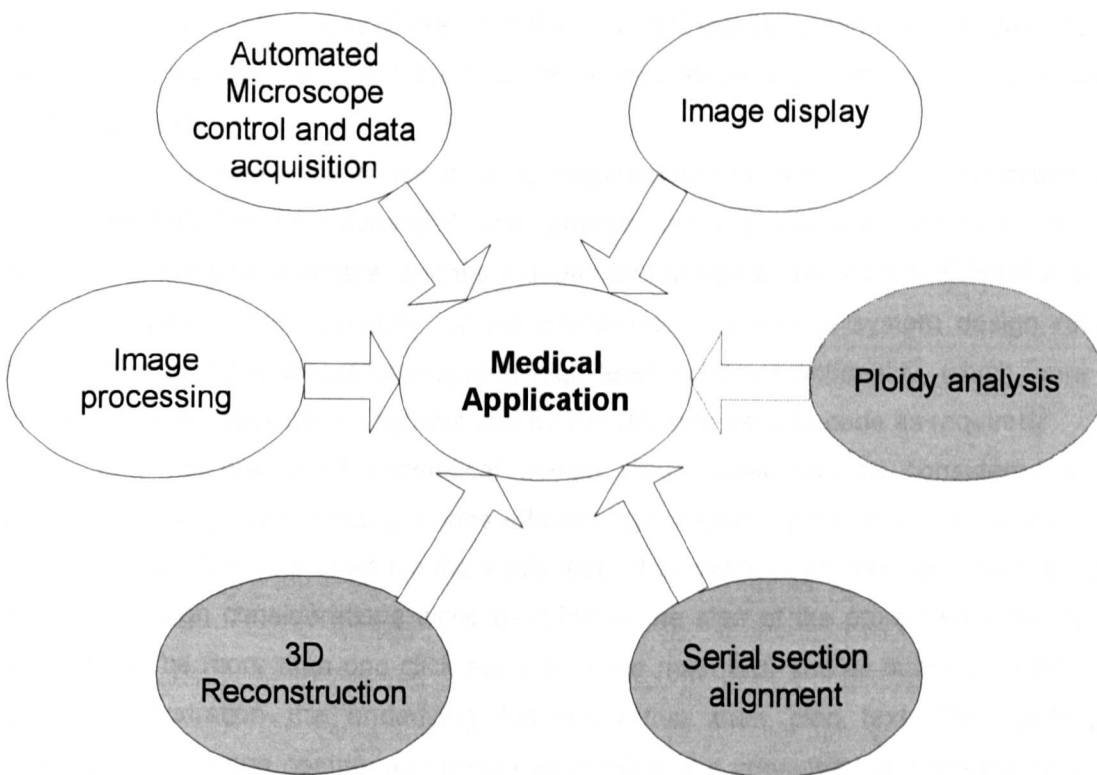
Figure 4.1 Software environment

Software design environments change every couple of years, particularly in respect to graphical user design tools, whereas in reality low level functional code development environments such as C++ change very little. To allow for this phenomena to be exploited there are two code bases within the code. Low level image processing and control functions are developed in Microsoft VC++, with high level or Graphical user interfaces being developed using Microsoft VB. This allows for the interface standards to change such as from Visual Basic to C#.Net and this will not require that the low level functions and algorithms are re-written. The method of separating the code into two levels also allows for aesthetical changes to the system to be made with out the requirement to fundamentally change existing developed functionality or structure.

The design process for the generic modules included a detailed design review, listing all of the functions that would be required for the sub-system. The functional requirements were determined by input from users, existing applications and from review of the literature. The design process identified what would be considered core and slow moving code, and areas of fast moving code subject to review in the future. Slow moving components included the file handling system, display system and known and proven functional algorithms. Areas of the code that required specific extendibility as consideration as fast moving code included the camera, robotic stage and microscope focus devices control software.

As a consequence of the differing requirements for both GUI and functional code implementation, there are essentially two separate design processes completed, the design of the graphical user interface, and the independent design of the "backend" functional code and core data storage systems for the framework. The overall system design required functional schematic diagrams mapping high level system functionality, which were then broken down in subsystem diagrams and further down to pseudo code as required.

In consideration of aesthetical design Visual basic can be considered a rapid prototyping design tool which provides efficient layout tools for the design of user interface environments, and was used for the evaluation of possible user interface designs. Basic aesthetic design considerations were identified at the start of the project such as; no user function will be more than one click away from the main GUI and all buttons would have a graphical illustration the underlying function rather than plan text. The applications developed are image centric, and image positioning and consideration appearance was of primary importance, where graphical control and functions were be fitted around that of the central image, an example of this can be seen in **Figure 4.2** of the alignment user interface. The operation and alignment method used is described in more detail in Chapter 5.
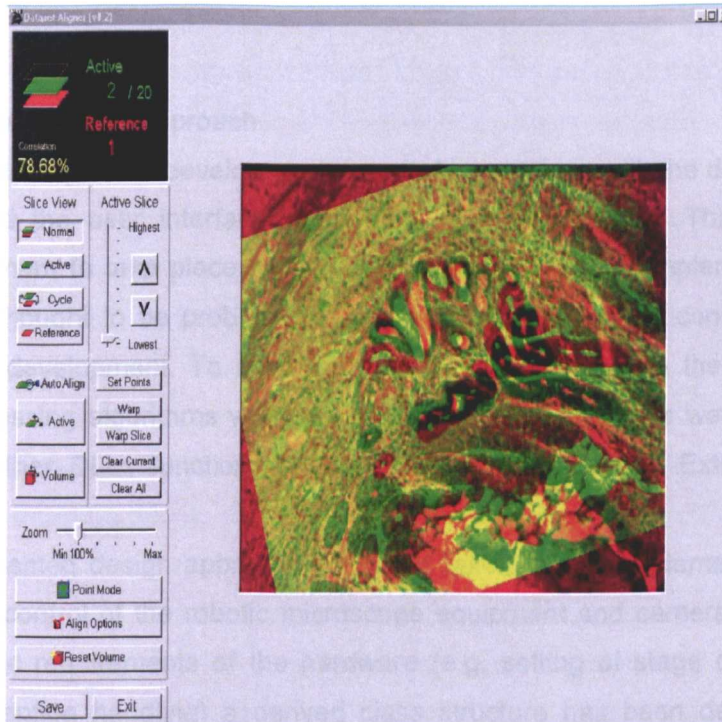
Figure 4.2 Alignment user interface

The lower image shown is placed in the red channel of the displayed image and the top image in the green channel.

At the start of the projects, with the rough specifications agreed as design constraints, and like many other atheistically design driven systems several non-functional basic system prototypes were reviewed, discussed with potential users. The proposed design was then agreed with the management of the company and a more advanced prototype written. This design prototype then formed the stylistic framework for which other applications were developed.

The graphical user interface deviates from the document centric Windows design standard in an attempt to make the application as easy to use as possible as shown in the example in **Figure 4.2** and in the manuals which show many other examples.

Note: As testimony to design of the system and user appeal, an OEM application Laservox (a slightly modified GUI version of FiRender) was commissioned by a major microscope manufacture and 225 units were sold. The ability to provide the software to a third party was only possible due to the ability to change the GUI, without having to change the core functionality and illustrates advantages of having a separated GUI.

4.5   Software Development Approach

As discussed a top down development approach was taken, with the development of back end code and the user interface running in separate streams. This allowed for concurrent development to take place on the core algorithms whose implementation was either not clear or thought to be problematic due to memory or speed constraints at the same time as GUI development. To allow for communication between the GUI and the functional and processing algorithms written in Microsoft VC++ methods were exposed to the GUI through either DLLs function exports or using OLE Control Extension (OCX) components.

An object oriented design approach has been taken for the implementation of the subsystems for the control of the robotic microscope equipment and camera subsystems. Using known generic requirements of the hardware (e.g. setting of stage control speed, movement and exception handling) a derived class structure has been devised. Each separate hardware control system inherits its core structure from a generic class and implements hardware specific functions at a local level. This solution allows further hardware support to be implemented within the system without the need to change the main application code.

A decision was taken not to rely on external software components for the development of core functions. It was considered that the use of external components would limit the flexibility required by the generic framework and may restrict future enhancements that could be required. Most functional and visualisation algorithms have either been written from scratch or implement functionality available in exiting code streams. However Leadtools [132] has been used for the display of the animations where the functionality provided by this tool kit allowed for animations created by the software to be displayed in the application. The automated DNA Image Ploidy system also implements some of the Intel performance library functions for generic image manipulation functions (such as basic kernel operators).

Functional, display and image processing algorithms have been coded with the design constraint that no hardware or structural application dependencies are present, allowing for the code to be used in other applications or platforms and to be replaced in the future with more efficient or effective functions also to be tolerant of microscopy hardware evolutions.

The implementation of each subsystem has been completed in a modular object oriented way. Unit testing each component before fitting it into the main framework, or as it was fitted in dependent on requirements. This methodology was required as the software components made up a suite of commercially available products, so it was not possible to complete all functions and systems before the systems were demonstrated to potential users. As each module was completed rough notes were made, and following the completion of development these notes were then used to construct the full user manuals.

4.6 Core Functionality

The generic functionality that has been developed as part of the framework includes microscope control, image capture, data Input and output (I/O), image display and non specific functional algorithm developments as required by all microscopy applications.

Microscope hardware control. a core class structure and specific device control functionality have been completed. Device drivers have been completed for Proscan stage controller (Prior, UK); Pifoc focusing device (PI, Germany), Ludl stage controllers (Ludl, Germany). Functions are provided for the movement of the stage and associated speed and accuracy settings, monitoring of current position and the handling of exceptions caused by problems.

Image capture, a range of digital cameras are supported including the Hamamatsu C4742 and, C7790, Sony DFW, Basler A101 and Standard analogue RGB cameras, this range provided a choice of camera so selection can be made dependent on that most appropriate for the specific application. The developed generic and specific class structure combination allows for images to be captured from a variety of cameras and provides a generic framework that allows for the support of further cameras in the future without changes to the core application code.

File IO, core functions have been developed that allow for data input and export in standard formats. Microsoft Windows Bitmap (BMP) and TIFF (TIFF) files can be loaded and saved for export to other applications. Export code has been implemented to allow for the saving of Windows video files (AVI). The data storage and I/O functions have been separated from the data processing functions allowing for future system expansions. For collaborative work with other groups a shared memory system has been implemented that allows access to the data volumes for external processes, such as the development of specific segmentation algorithms.

Display, generic display code has been written that provides fast visual display and scaling functionality. These functions are implemented using the Windows DrawDib functions, which at the time of implementation offered the fastest display mechanism on the

Microsoft Windows platform although now there are DirectX functions that could be used to increase display performance if required.

The next chapter describes the algorithms used within the serial section functions alignment introducing a new semi-automatic alignment method using cross correlation as goodness of fit measure. The functionality of the visualisation system is described in full in Section 5.13 but in brief the functions developed include: - Orthogonal slice viewer, non orthogonal slice viewer, various rendering modes, animation and object definition and masking.

Chapter 5 The 3D Reconstruction And Visualisation System

As described in the literature review, 3D reconstruction has found many applications for exploration of specimens within the field of medicine. 3D reconstruction for diagnostic and exploration use within histology and for soft tissue structures remains limited. It can be seen that 3D reconstruction systems for human visualisation are subjective systems where it may be, dependent on the application to provide quantitative data. 3D reconstruction was chosen for study as it encompassed many of the imaging concerns for standard 2D applications in microscopy but also presents extended significant challenges where further research is required.

MRI and CT imaging has been used for the in-situ data capture and visualisation of larger bodies and structures within the human body and CT micro-tomography has been used to successfully study smaller biological structures both in living organisms and in isolated tissue samples. Micro-tomography provides a solution allowing for in-situ visualisation of histological tissue structures without destruction of the specimen, however does not allow the use of routinely used biological markers (bio-markers). The electron microscope has been used to capture data using block faced sectioning techniques and from microtomed serial sections. The techniques have proven application but also do not allow for the study of specimens using biological markers. Confocal microscopy and bright field microscope optical sectioning techniques, while allowing the use of bio-markers are only suitable for the capture of datasets of microscopic objects where the thickness of the specimen is limited. Histological sectioning allows for standard biomarkers to be used and does not have the depth limitation of optical sectioning, specimens can be sectioned finely (down to 2μm) stained with IHC techniques and when reconstructed can provide detail ranging from the sub cellular level to the larger macro tissue structure. As serial sectioning is time consuming, if the method is to find practical clinical application is important that systems are provided that provide the user the ability to complete the required tasks in a timely and robust manner. This chapter describes algorithms that have been used and developed for use in the semi-automatic serial section alignment and the 3D reconstruction systems developed. The work described in this Chapter addresses the aim of development of medical image algorithms for 3D reconstruction and Visualisation as described in Section 1.3.2.

5.1   Software Example - 3D Reconstruction System

Of the three systems designed as part of this study for acquisition alignment and reconstruction, the reconstruction system is detailed below in this section. Further details relating to the user operation of the acquisition and alignment systems can be found in the

user manuals on the attached CD. The algorithms used for the application are provided at the end of this chapter.

5.1.1 Background

In the context of this study, one area in which tools are lacking for allowing Pathologists or other medical professionals to obtain required information is in 3D reconstruction of micro-tomed histology specimens. As such many organs and the structural changes caused by disease is poorly understood. This section explains work that has been completed to allow Pathologists and research biologists to increase understanding allowing current diagnostic practices to be better validated, and also enable for the realisation of the growth pattern of certain diseases.

A system has been designed running on the Windows platform which meets the core need for histological reconstruction of serial sections for biological research and prognostic and diagnostic review of histological samples.

The collaborating establishment (Fairfield Imaging) provided legacy code to the author from a UNIX based visualisation system called Microvision. Microvision had been designed to operate on a Silicon Graphics operating system and employed the use of the Motif window system, this system was not easy to use and many users found problems with its operation and the platform on which it operated. It was first considered that a Linux version running on an Intel based PC may provide a suitable platform, and work was completed by the author to port Microvision to the Linux platform. The Linux port did not meet the needs of the user as it suffered the same acceptance problem as the Silicon Graphics based system. It did prove however that Intel based systems had comparable computing power for Voxel rendering as that of the Silicon graphics machines at a fraction of the cost.

The knowledge that the Intel based PC had sufficient processing speed to develop a viable Voxel rendering system at a greatly reduced cost in comparison to the available Unix based system provided the motivation for the development of a more accessible and user friendly system. The development tools and operating system's display sub-system differ between Unix based and Windows (Microsoft Corporation, USA). Employing the existing Microvision algorithms for Back to Front (BTF), Minimum (M-) and Maximum point rendering (M+); 3D morphological filters and simple 2D orthogonal viewer. A new system was developed and the rendering algorithms extended.

Application developments include development of a new display system using Direct Draw SDK (Microsoft Corporation); Non-orthogonal 2D slice viewer; Extension to supported file formats to include Joint Photographic Experts Group (JPEG) and the Bio-Rad file format

48

(Bio-Rad Laboratories, USA); new colour pallet assignment system; replacement of object generation and presentation system; extension of the haze removal filter (nearest neighbour method) to allow interactive selection of parameters by the user; development of a animation system allowing for the animation of opacities, region of interests and assigned colour pallets as well as including the existing animation capabilities of rotation, azimuth and roll available within Microvision, the output from the animation system was developed to support the Windows AVI format.

The extension of rendering algorithms included in this new application required development to allow: User selection of intensity bounds for M- and M+ rendering; True colour modes for M-, M+ and BTF rendering; Colour encoding of the Voxel Z position in the dataset (true dataset location, rather that visual Z depth from the viewers perspective). The algorithms are given in Section 5.2.4.

5.1.2 Block Diagram
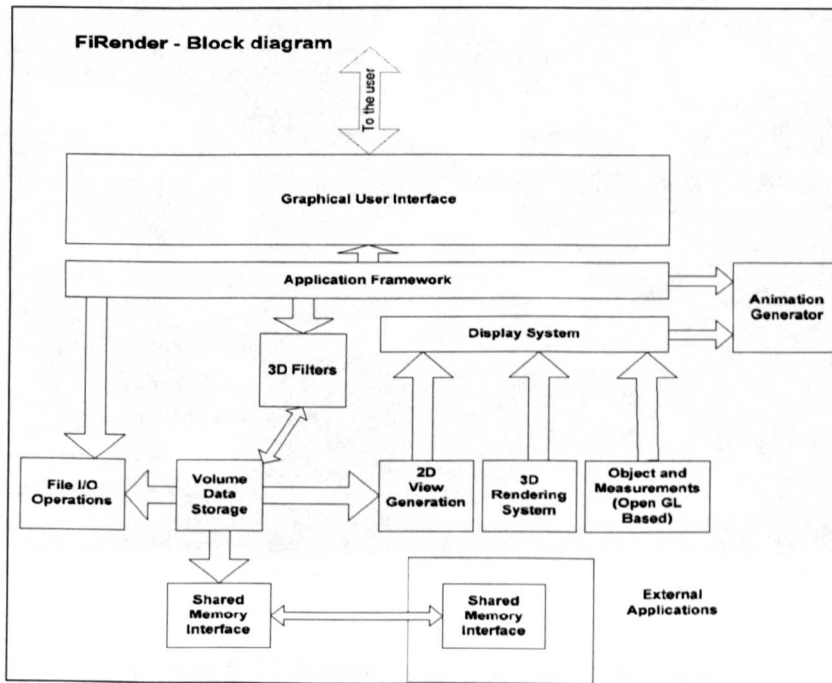
Figure 5.1 FiRender block diagram

The block diagram of the rendering system is shown in **Figure 5.1**. The diagram shows the main components of the system and the flow of data between them. In brief the Graphical User Interface (GUI) provides for communication between the user and the main framework and provides feedback as to the current setting of values represented by various controls. The framework is the central element of the system to which other systems are connected. Independent subsystems include file I/O operations, 3D filters, 2D and 3D view

generation, object display and measurements an animation generator and a shared memory system for data sharing with other external applications. Further explanation as to the functionality of the system is provided in 5.1.3. All functions with the exception of the GUI which has been written in Visual Basic (VB) have been written in Visual C++ (VC). As can be seen from the block diagram the animation creation system is attached to the framework, this allows for the animation of all functions that the user has control over and is not limiting to traditional rotational animations which is the normal case, the use of this is discussed later in this chapter in Section 5.2.5.

5.1.3   FiRender User Interface And Functionality

Figure 5.2 FiRender main application interface

Figure 5.3 FiRender main toolbar

The user interface for the rendering application is shown in **Figure 5.2**. The main tool bar is shown (A) with an expanded view as shown **Figure 5.3** This tool bar is used to

control the display of the control and display windows. **Figure 5.2** (A) shows a tool bar control that specifies the operation to be completed on a selected window, all possible functions are shown all the time, but only enabled when the relevant window is selected. The options include selections such as full dataset position or wire frame position of the 3D view as shown in (C). The 3D visualisation window is shown in (C), this window is the 3D rendered view and is used for the interactive rotation of the dataset; functionality is also included to allow for the rendering to be zoomed by the means of linear interpolation. The visualisation window as with all display windows have a context menu which can be invoked by pressing the right mouse button, this context menu presents options to export the image in various different file formats and to change the contrast, brightness and gamma of the image. The orthogonal slice view is shown in (D), the combination of 3 windows display x-y, x-z and y-z orthogonal views of the dataset, by clicking on any of the three windows the other two windows will update, as with the rendered image window linear interpolation and a context sensitive window is also provided. The histogram of the image is shown in (E), this dialog has dual functionality in that it provides the user with information related to the histogram of the loaded datasets, and provides functionality to allow for thresholds to be set for maximum and minimum point projections or the opacity to be changed, dependent on the rendering mode selected. Functionality is provided to zoom in on ranges of the displayed histogram and to select histograms for any selected sub volume of interest defined. The colour palette editor as shown in (F) provides the functionality to specify, load and save palettes, an interactive method is provided for the selection of colours to be included in the palette, the interpolation between selected colours and a selection of pre-defined palette is provided. The 3D control dialog shown in (G) provides the selection of rendering modes; the azimuth, rotation and roll can be specified accurately using this dialog, as can the application of simple Voxel lighting methods.

Some of the functionality within the system cannot be easily displayed graphically and requires further explanation. The application can load serial Tagged Image File Format (TIFF) and Joint Photographic Experts Group (JPEG) files, selecting the load option shown in **Figure 5.2** (A) displays a load dialog (not shown) allowing for sequentially numbered datasets in either TIFF or JPEG format to be loaded into the system. The software offers functionality to allow for the aspect ratio of the dataset to be changed by the insertion of interpolated or blank serial sections or for the user to resample the size of the original images, as required to insure the aspect ratio of the dataset is preserved.

Animations can be generated for most of the user adjustable settings, Region of Interest (ROI), palette assignments, opacity settings and viewing angles. The animations

are created in standard Windows video (AVI) format, with the user having the selection of the codec to be used.

A linked simple 2D orthogonal slice view is provided allowing the user to explore the original data in the data set, by clicking one of the three views x-y, x-z, or y-z. navigation can be easily achieved through the dataset. This simple viewer also has a feature that allows for the navigation based on the Z buffer of the rendered image on Maximum Point (M+) and Minimum Point (M-) and derived rendering algorithms. The user can select a point on the 3D rendered image and the position in the orthogonal view will be displayed.

The application supports a range of rendering modes, Back To Front (BTF) opacity blending, M+ with threshold, M- with threshold, M+,M- with depth, detailed later in Section 5.2.4. The BTF, M+ and M- rendering modes are a standard implementation of algorithms as detailed later in this chapter. The depth encoding and true colour rendering variants are functions that have been developed as part of this research are area also explained later.

Object modelling and object masks, as discussed in Section 2.3.3 are a form of manual segmentation. An object specification tool has been developed that allows the user to manually select areas to specify objects. Simple drawing and object generation, for functions are provided. These tools allow for flexible user selection of the areas of the dataset to include, exclude or change in the rendering process. The object generation functions allows for the user to generate seed filled objects, which can be rendered in isolation or can be used to act as masks to arithmetically or logically alter the rendering process for the area of the dataset defined. Functions such as increasing opacity or changing colour. Open GL has been used to implement the drawing functions of the objects and allows for future potential of including geometry based rendering systems. The user interface for the object generation system is shown in **Figure 5.4**. The system allows for objects to be inserted as shown **Figure 5.5** each generated object can have a Voxel colour assigned for clear visual review. **Figure 5.5** shows the visualisation where the area defined by mask is removed from rendering view. The windowed interface shown here allows the user to directly interact with the wire frame around the object by manipulating the elevation, azimuth and roll by dragging the wire frame.

A non-orthogonal slice view has been developed as shown in **Figure 5.6**, the simple user interface used to allow the user to select the position of the non-orthogonal slide within the dataset. This functionality allows for an intersecting plane to be inserted in the dataset at a user definable location and with a defined thickness, offering more flexibility to explore the dataset than the orthogonal view alone, but is more difficult to use for the novice user.
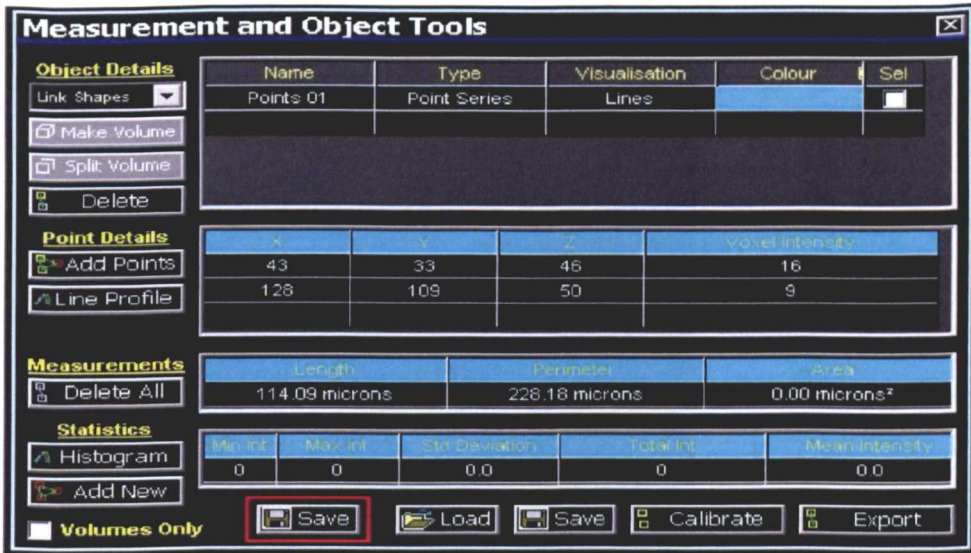
Figure 5.4 Graphical User Interface for object specification

The user controls for the measurement and object specification tool shown in the left of **Figure 5.4**, allow for the user to covert point lists into areas, areas into volumes and to add to and delete defined objects. A histogram of the area of the dataset defined by the object mask can be generated. The panels from top to bottom show object group names and type; coordinates of individual pixels defined by the object; spatial measurements of the defined object and basic statistical measures of the Voxels defined by the mask. The buttons at the bottom of the dialog control file and calibration operations.
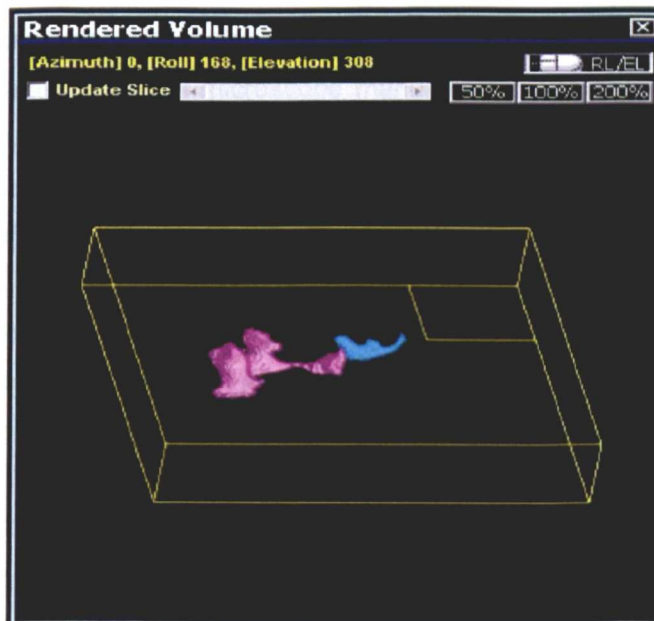
Figure 5.5 Display of generated objects
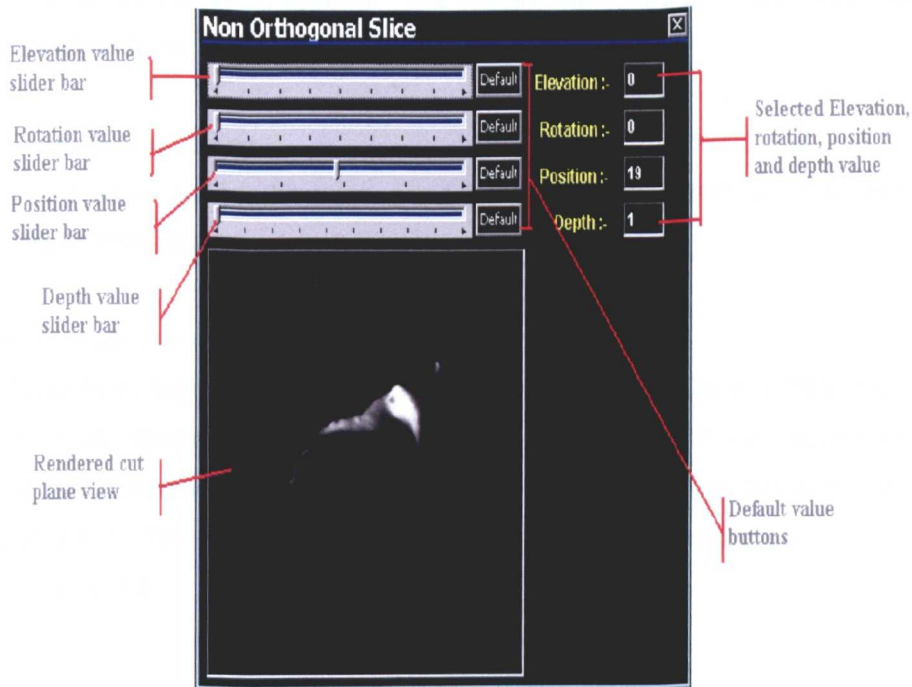
Figure 5.6 Non Orthogonal slice viewer

5.1.4 Commercialisation

The three elements of this system for acquisition, alignment and reconstruction have been commercialised and have found application in a range of academic and commercial projects.

The 3D application, FiRender has been sold directly to academics for biological research into 3D histological structures. An OEM version of this reconstruction software was also licensed to a major confocal microscope manufacturer who chose the product due to its ease of use an uncomplicated graphical user interface. The reconstruction system has also been used in the successful completion of an EU funded project Vascan (funded by EC FP5 (QLG1-CT-1999- 00084)) for the study of 3-Dimensional Analysis of Vascular Structure, Function and Receptor Distribution Using Confocal Laser Scanning Microscopy (CLSM) this work resulted in two co-authored publications [4;133]. A commissioned project for the reconstruction and annotation and reconstruction of female human subject has also been completed for the National Radiation Body (NRB) using the developed software.

5.2 Algorithms For Medical Image Processing

This section presents the algorithms used and developed for the applications as detailed in Chapter 4 and 5. This chapter is separated into four sections, image manipulation, image enhancement, algorithms used in the alignment system and algorithms

used in the 3D visualisation system. The results from medical image application obtained from these algorithms can be found in Chapter 7.

5.2.1 Image Manipulation

The following algorithms are used for data manipulation as used within the serial section registration system.

a) Transformation And Rotation Matrix

Solid body transformation and rotation has proved to be a reliable method however without manual interaction this method is time consuming and not intuitive for the user to use. The transformation matrix can be rapidly used to complete this and rotation is shown in **Equation 5.1**. The effect of the application of this transformation can be seen in **Figure 5.7 and Figure 5.8.**

$$\begin{bmatrix} x' \\ y' \\ 1 \end{bmatrix} = \begin{bmatrix} s.\cos\alpha & s.\sin\alpha & t_x \\ -s.\sin\alpha & s.\cos\alpha & t_y \\ 0 & 0 & 1 \end{bmatrix} . \begin{bmatrix} x \\ y \\ 1 \end{bmatrix}$$

..(5.1)

Where x' an y' are the pixel coordinates after application of the transformation matrix. s scale factor applied the images, α rotation, t_x and t_y, x and y translation. x and y are the original pixel coordinates.

The system designed allows for interactive solid body transformation and rotation, fiducial point alignment in real time. For fiducial point operation, the user is prompted to select fiducial points on one image and then on the second, the average rotation and translation is then calculated and the image processed using the equation shown.
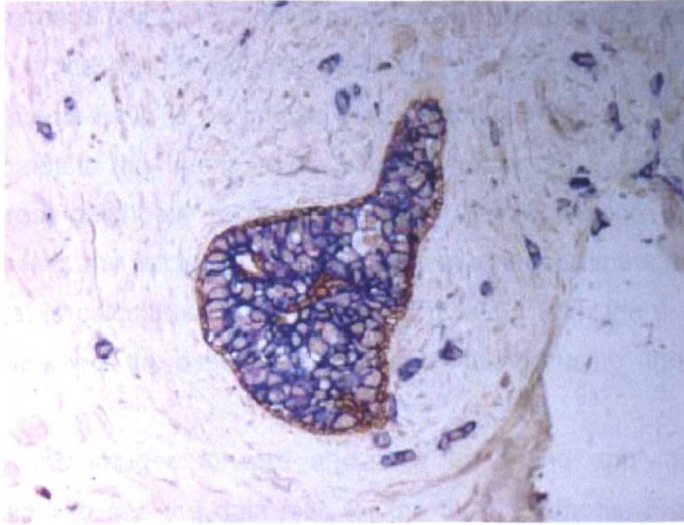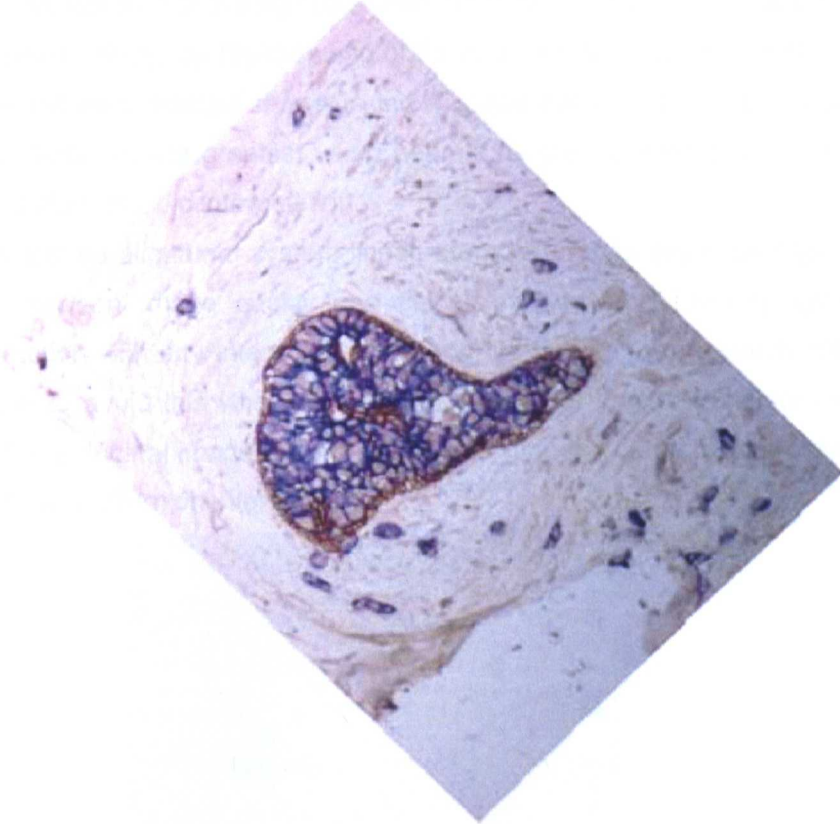
Figure 5.7 Original image before transformation

**Figure 5.8** Image after transformation

Rotating an image using the algorithm shown in **Equation 5.1** results in data loss as each pixel location in the destination image will not exactly exist in the source image and intermediate data points have to be interpolated. The three standard methods exist which can be used to complete this interpolation, which in order of quality and processing time required are: nearest neighbour replication, where the destination pixel is taken to be nearest pixel, removing any fractional element of the image coordinate; bilinear interpolation the destination pixel is calculated using linear interpolation from the 4 nearest pixels and; bicubic interpolation where the destination pixel is calculated using the 16 nearest source pixels.

By rotating the images forward and then back and applying the interpolation methods it is possible to see the data loss for the three methods. **Figure 5.9** shows the original image taken from subsection of a microscopy image. **Figure 5.10** shows the effect of nearest neighbour interpolation, **Figure 5.11** shows bilinear interpolation. **Figure 5.12** shows bicubic interpolation. For the figures shown the areas of dark pixel values around the edge of the images is caused by the cropping of the rotated image to the size of the original image. From the resultant images shown in the **Figures 5.9 – 5.12** it is possible see the individual pixel differences are greatest using nearest neighbour interpolation, followed by linear interpolation then bicubic interpolation.

In the developed alignment system linear interpolation has been used as it offers a good comprise between image quality and calculation speed. Iteratively applying the rotation transformation with any interpolation method will result in progressive degradation of the final image, to avoid this when an image is rotated or indeed translated within the alignment system the original image is always used, as such the output image only contains errors from interpolation from one iteration.

206	197	199	172	168	199	210	224	202	228
179	183	177	162	138	174	210	220	218	227
182	183	167	180	160	184	215	197	208	214
185	176	160	201	206	212	218	188	161	208
165	158	156	200	225	216	208	191	179	194
167	175	191	203	226	209	211	181	205	181
178	199	225	202	210	194	212	164	166	184
220	198	211	185	212	197	205	148	152	172
210	185	199	177	200	185	195	167	163	174
193	164	181	167	185	175	186	222	192	190

Figure 5.9 Orginal Image
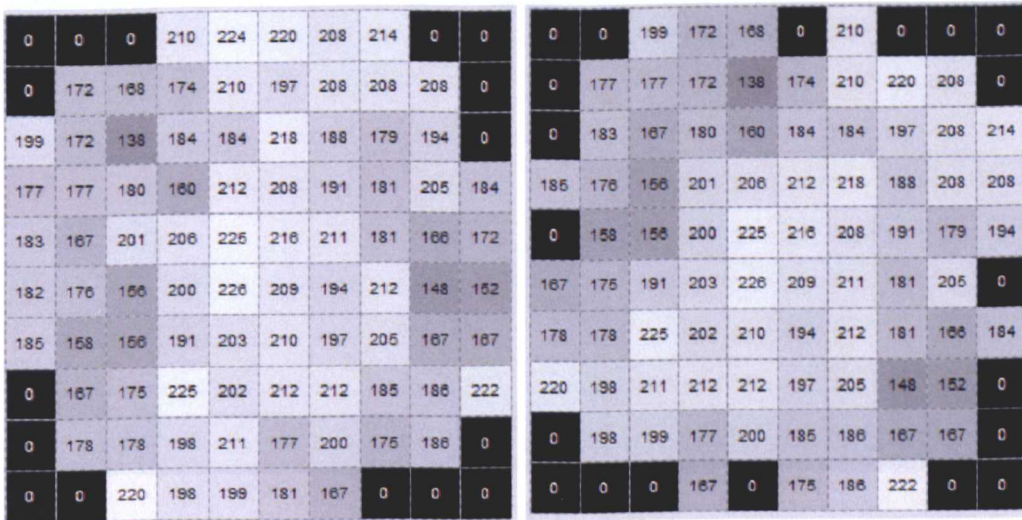
(A)

(B)
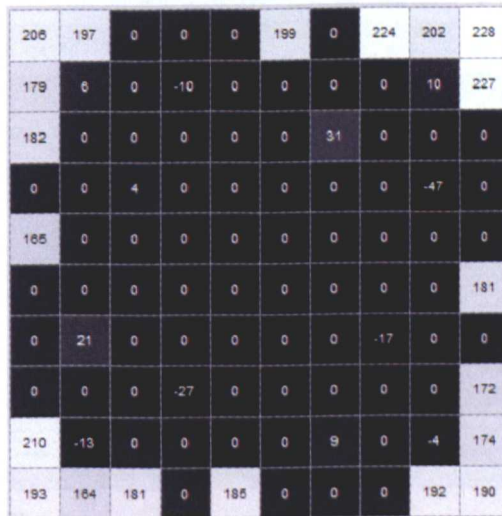
(C)

Figure 5.10 Nearest neighbour interpolation.

(A) orginal image rotated 33 degrees; (B) rotated image rotated back 33 degrees; (C) difference between orginal image shown in **Figure 5.9** and (B).

0	0	71	188	216	219	214	203	24	0
21	112	172	185	211	203	191	187	133	0
187	169	145	168	200	210	186	175	189	67
184	172	173	181	210	213	198	189	195	166
183	168	184	206	219	213	210	178	166	169
182	171	163	199	221	212	205	194	151	156
163	163	168	195	207	208	197	202	175	174
60	167	181	215	203	201	201	188	191	208
0	114	190	204	205	180	193	180	119	23
0	22	206	197	194	181	157	67	0	0

(A)

0	21	178	136	150	150	179	79	0	0
0	121	178	165	153	180	208	216	142	24
66	180	169	175	173	187	206	200	202	194
153	172	171	192	199	210	211	192	185	154
134	165	169	199	217	215	207	192	179	168
147	177	191	204	216	211	209	186	193	149
148	195	211	205	208	203	198	174	170	152
195	200	205	197	201	198	197	158	159	61
23	129	191	181	195	189	188	176	109	0
0	0	67	149	144	157	151	195	21	0

(B)

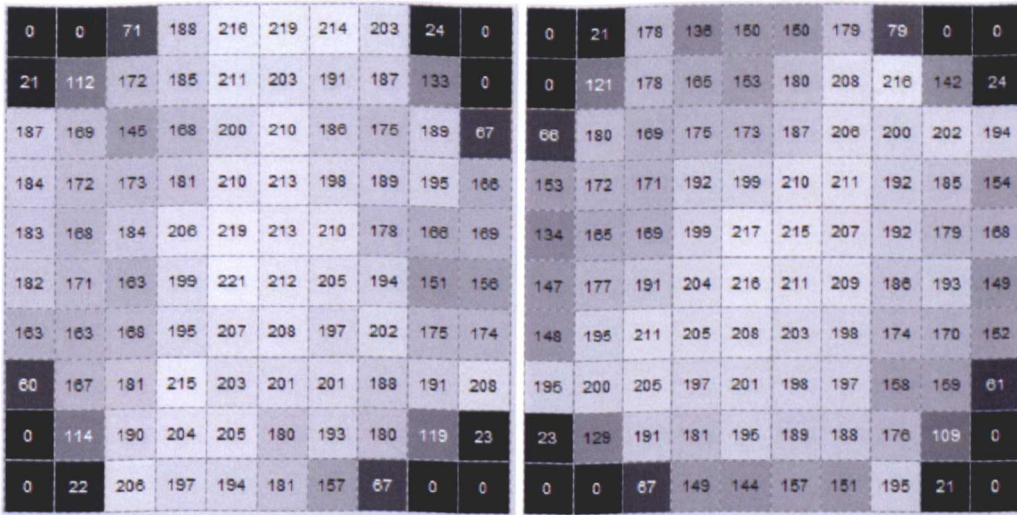| 206 | 176 | 21 | 36 | 18 | 49 | 31 | 145 | 202 | 228 |
179	62	-1	-3	-15	-6	2	4	76	203
116	3	-2	5	-13	-3	9	-3	6	20
32	4	-11	9	7	2	7	-4	-24	54
31	-7	-13	1	8	1	1	-1	0	26
20	-2	0	-1	10	-2	2	-5	12	32
30	4	14	-3	2	-9	14	-10	-4	32
25	-2	6	-12	11	-1	8	-10	-7	111
187	56	8	-4	5	-4	7	-9	54	174
193	164	114	18	41	18	35	27	171	190

(C)

Figure 5.11 Bilinear interpolation.

(A) orginal image rotated 33 degrees; (B) rotated image rotated back 33 degrees; (C) difference between orginal image shown in **Figure 5.9** and (B).

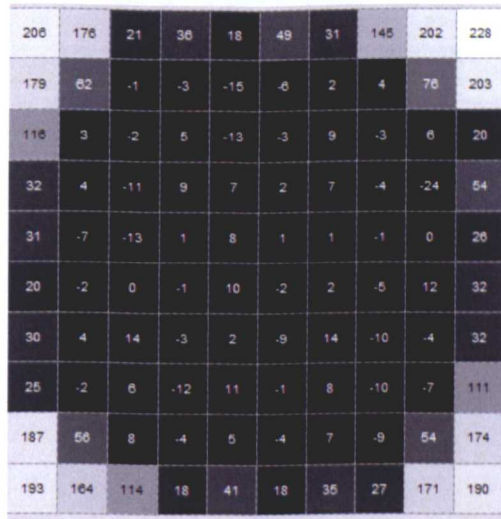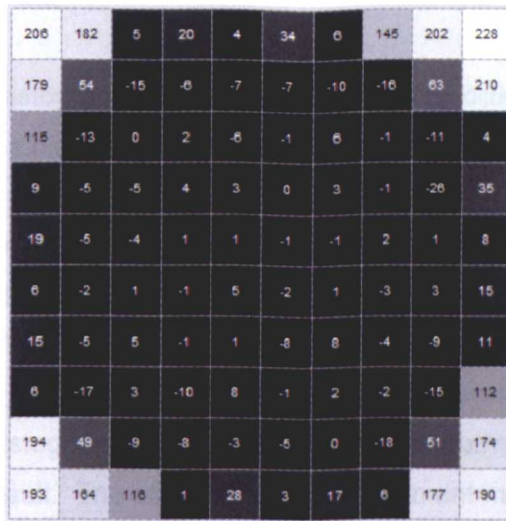(A)   (B)

(C)

Figure 5.12 Bicubic interpolation.

(A) orginal image rotated 33 degrees; (B) rotated image rotated back 33 degrees; (C) difference between orginal image shown in **Figure 5.9** and (B).

5.2.2 Enhancement

As discussed in Chapter 2, images obtained using the bright field microscopes are particularly prone to changes in the colour temperature and intensity of the illuminating light source. This issue must be addressed in order to allow for the reconstruction of sequential images for both human review and quantification.

a) Histogram Equalisation

Histogram equalisation shown in **Equation 5.2** and is commonly used to correct intensity changes of images [134].

$$P_{new}(k) = \sum_{j=0}^{k} \frac{n(p_{org}(j))}{n_{total}}.P_{(max)}$$

..(5.2)

Where P_{new} is the new histogram value, k the value of the pixel (0-255), n total the total number of pixels, $P_{(max)}$ the highest probability of any pixel.

The histogram for the image is remapped to provide an image which has equal representation across the whole intensity range, however the difference in colour temperature limits the effectiveness of this method for quantitative systems, and can be seen to modify colour so it has limited use for visualisation systems. Sample images are shown in **Figure 5.13**. Histogram equalisation has been performed and the images shown **Figure 5.14** shows the result. The other histogram adjustment method that was considered was histogram specification.

As the sectioning procedure will result in a sections obtained both before and after the main area of interest of specimen histogram adjustment can be problematic, using either 2D or 3D correction. The biasing of the histogram by the inclusion of dominate features such as that of areas outside the main area of interest causes issues when the pixel probability is calculated on the whole image space. There are adaptive techniques where constrained 1D, 2D or 3D areas are mapped using rolling grey scale transformation. While these regional methods can improve visibility, the resultant grey scale map is no longer unique in terms of the original data values as such can cause issues for intensity based segmentation methods and requires that the resultant image is segmented using gradient based methods.

Standardisation of the captured images is important for the measurement and visualisation of microscopy images, standardisation of the microscopes illumination conditions can be provided by shade correction as described in Section 5.2.2.2. Efforts

have to be taken to ensure consistency of laboratory preparation of specimens prior to imaging, rather than reliance on post imaging histogram normalisation procedures.
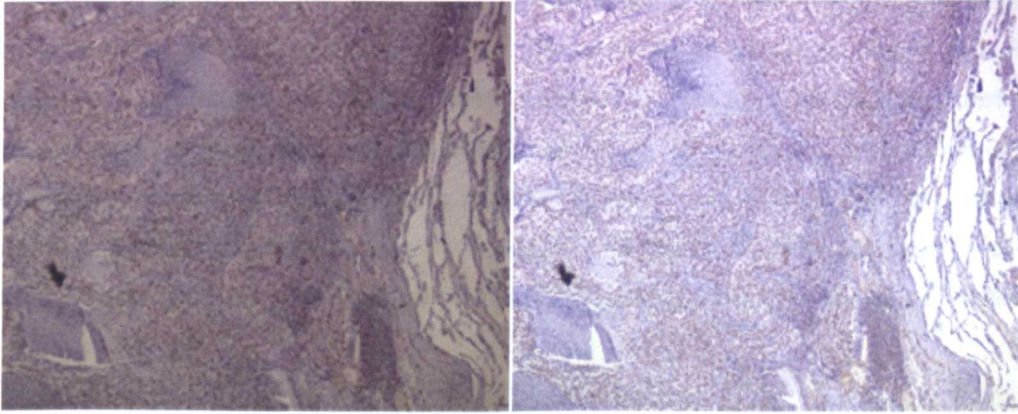

Figure 5.13 Images at different colour temperatures
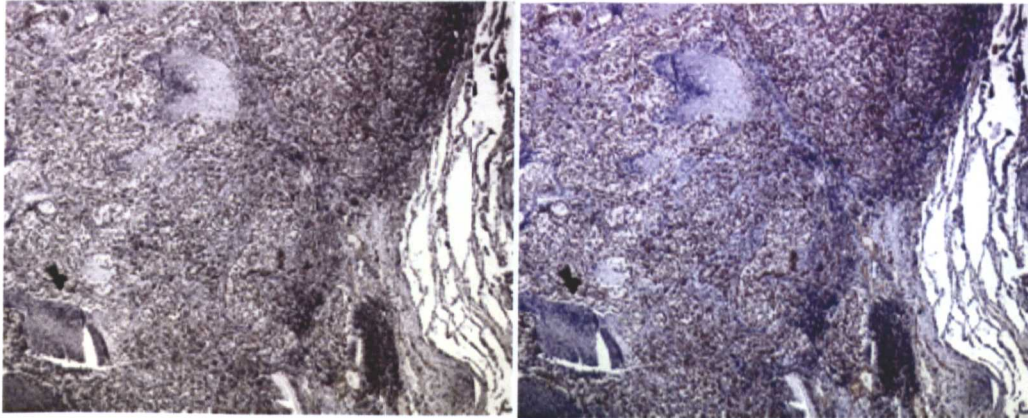

Figure 5.14 Histogram equalisation

b) Shade Correction

Shade correction using a reference image can be used to address the requirement of intensity correction, as illustrated in **Equation 5.3**.

$$P_{out} = \frac{P_{image}}{P_{background}}.S$$

..(5.3)

Where P_{out} is the output pixel value, P_{image} the original pixel value, $P_{background}$ pixel value. S the scaling value, 255 to achieve saturation in blank areas for 8 bit images. The function can be applied to RGB images where each pixel is considered for its individual Red, Green and Blue components.

The shade correcting function requires that a blank image is captured. Using a bright field microscope this can be easily achieved by moving the stage either manually or automatically to an area of the slide where no specimen is present. **Figure 5.15** shows the respective reference background images for the two images shown in **Figure 5.9**. Results from the procedure is shown in **Figure 5.16**. While it can be seen that it is not perfect, the extreme examples given illustrate the effectiveness of the method. This method is also advantageous over the histogram correction method as it corrects for illumination unevenness in the background image and any dust particles either on the camera or within the optical tract. This effective method has been implemented in the developed system.

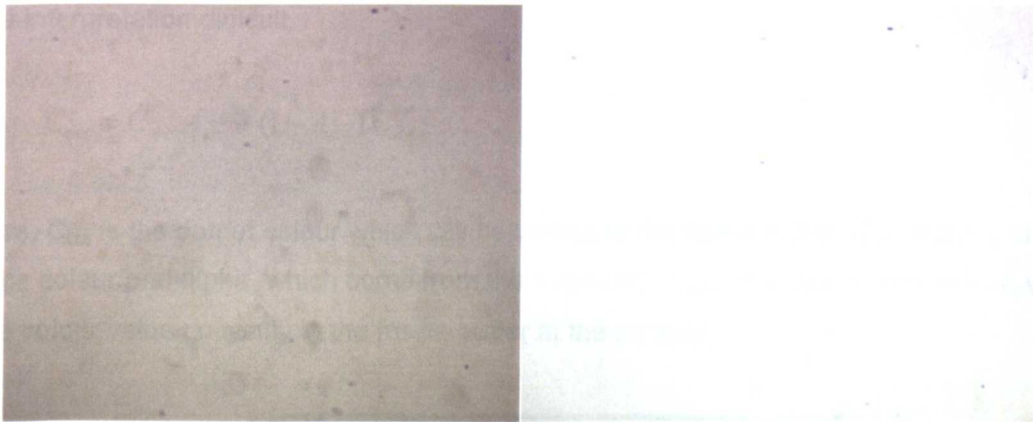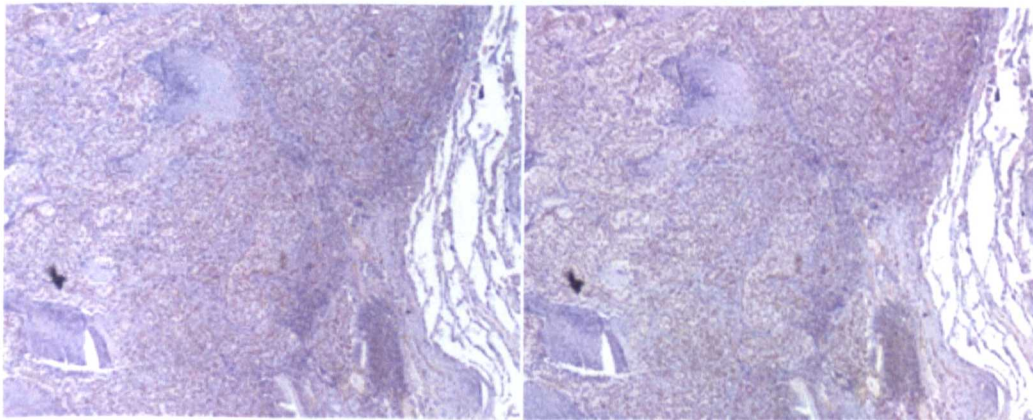**Figure 5.15** Reference background images

Figure 5.16 Shade corrected images

5.2.3   Alignment And Visualisation

The following algorithms are of use in the alignment of serial section images and for the visualisation of 2D medical image data.

a) Opacity Blending Of Two Images

In order to allow for manual registration to be completed an image has to be presented to the user so that the two sequential images can be viewed simultaneously. Methods available to complete this include the use of simple opacity blending of the two images so that a second image can be seen through the first as shown in **Figure 5.13**. The calculation for opacity blending is given in **Equation 5.4**. Although this method can be used and preserves original colour in images, in practice the calculations required to perform this in combination of the application of the transformation and rotation matrix as shown **Equation 5.1** could not be used to provide a real time interactive system. A further disadvantage as can be seen in **Figure 5.17** the similarities between the two images can make interpretation difficult.

$$C_{out} = C_{src}.A_{src} + (1 - A_{src}).C_{dst}$$

..(5.4)

Where, C_{out} is the output colour which will be written to the frame buffer. C_{src} and A_{src} are the source colour and alpha, which come from the fragment. C_{dst} is the destination colour, which is the colour value currently in the frame buffer at the location.
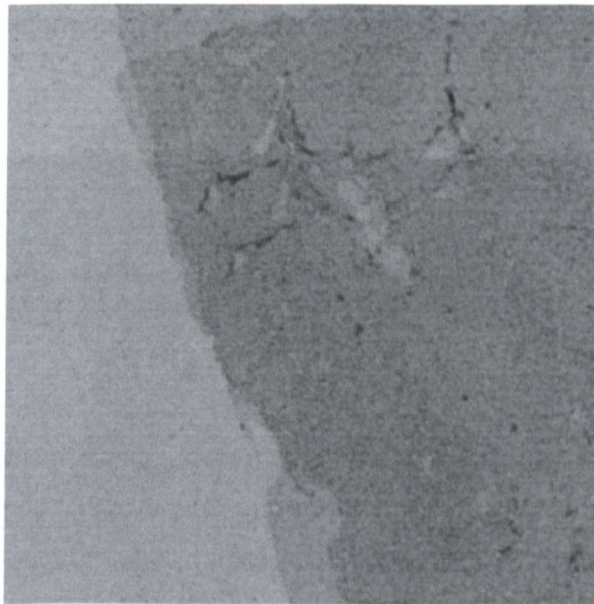

Figure 5.17 Opacity blending of serial section images

b) Red Green Colour Merge

A red-green merging algorithm as shown in **Equation 5.5** can be very efficiently implemented as it just requires the sequential placing of the two grey scale image directly into an RGB image buffer.

$$Pout_{RGB} = Pslice_{green} + Pslice_{red}$$

..(5.5)

Where $Pout_{RGB}$ is the output pixel, $Pslice_{green}$ the green element of the slice pixel and $Pslide_{red}$ the red.

The system implemented uses the method of placing the two serial section images data into a three channel Red, Green and Blue (RGB) image buffer and then displaying the image. The resultant image appears yellow in areas of high intensity and correlation and black in areas of low intensity and high correlation, as shown in **Figure 5.18**. This method provides the user with a simple but effective method to visually view the alignment of the two images, and requires minimal processing to complete. The image is rotated around its central point, allowing the user to finely control the amount of rotation that is applied accurately. The values obtained from this user interaction are applied to the transformation matrix as shown **Equation 5.1**. Due to the efficiencies of this algorithm and the fast implementation of the transformation it is possible to manipulate the images in real time.
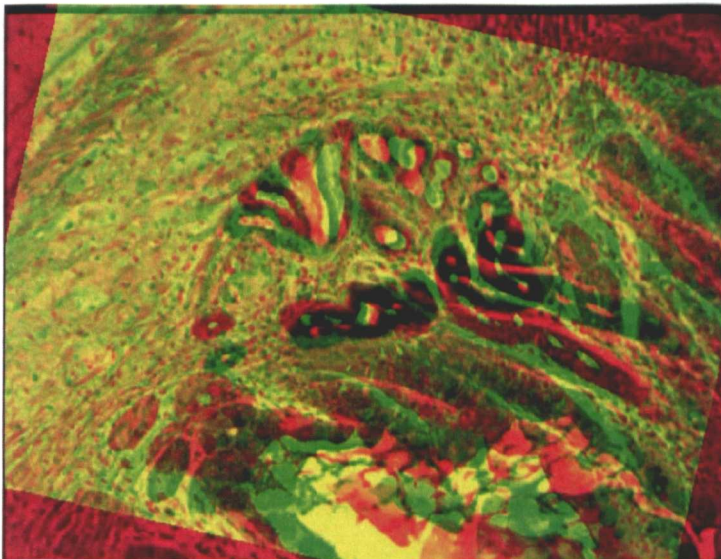

Figure 5.18 Red/Green channel merging of images
The red plane shows the bottom image and the green plane the top Image.

c) Intensity Calculation

$$I = 0.6.green + 0.3.red + 0.1.blue$$

..(5.6)

The commonly used intensity calculation as shown in **Equation 5.6** allows for intensity information to be extracted from a colour image. This equation finds application in many areas, not only in extraction of grey scale image but in the extraction of intensity data from colour images as required by quantification. As the method implemented in Section 5.2.3.2 operates on the intensity of image, when aligning colour images to create red/green composite images the images have first to be transformed into grey scale prior to application of the function, **Figures 5.19** and **5.20** show the images before and after this operation.
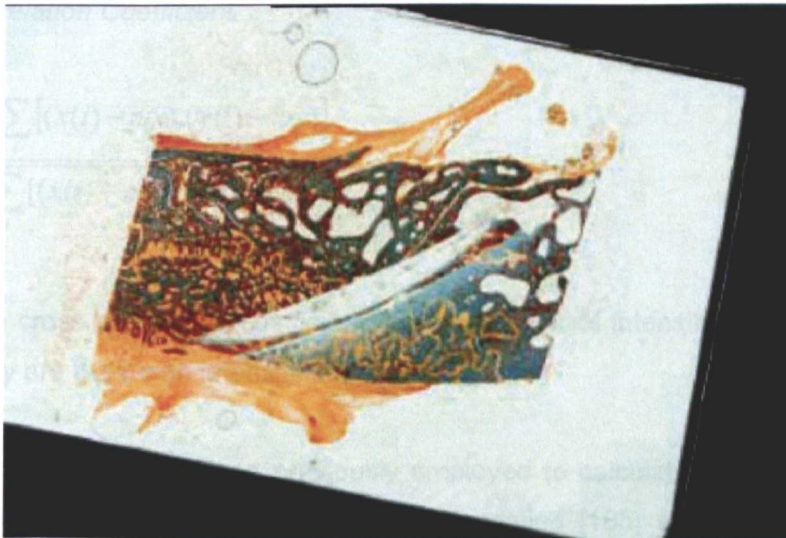

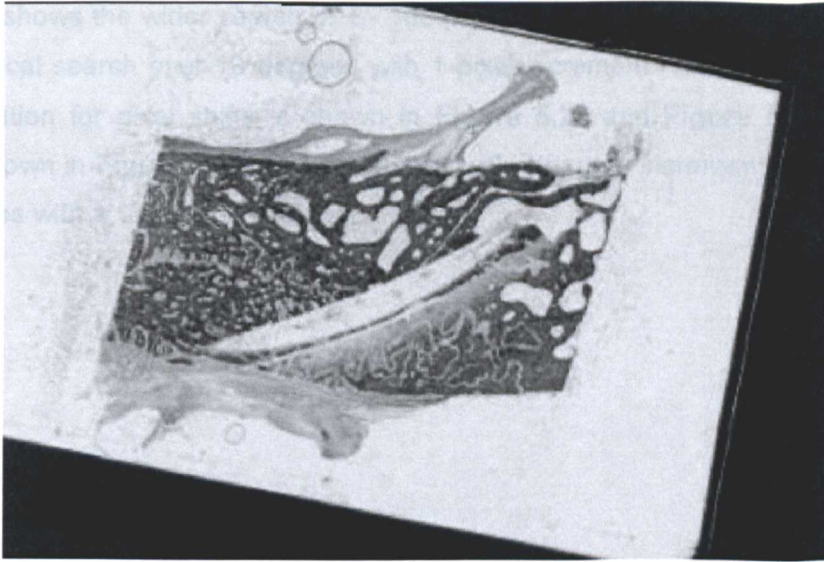**Figure 5.19** Original image for greyscale conversation

Figure 5.20 Grey scale image

d) *Cross Correlation Coefficient*

$$r = \frac{\sum_i [(x(i) - mx).(y(i) - my)]}{\sqrt{\sum_i [(x(i) - mx)^2.(y(i) - my)^2]}}$$

..(5.7)

Where *r* is the cross correlation coefficient, *x(i)*, *y(i)* are pixel intensities for the two slices, and *mx* and *my* are the mean intensities for the images.

Other methods have been previously employed to calculate the best alignment of the two sequential images, such as simulated annealing [135] which prevents incorrect alignment due to local areas of high cross correlation and while the method is effective at ensuring true correct alignment this method can be slow [136]. The use of cross correlation as a comparison method as shown in **Equation 5.7** has been chosen due the speed of calculation and its global operation on the image does not require identification of the structural components of the dataset.

While areas of cross correlation match can be seen when aligning adjacent serial histological sections as shown in the following figures, these tend to be soft peaks of low magnitude in comparison to the optimum alignment position **Figure 5.21** - **Figure 5.24** shows the results of an exhaustive search using cross correlation, due to the time taken to calculate the results and in the interest of clarity a wide search has been combined with a finer local search of the within proximity to the location with maximum cross correlation.

Figure 5.21 shows the wider search of +/- 100 pixels with a 5 pixel increment, Figure 5.22 shows the local search over 10 degrees with 1 pixel increment. The location of maximum cross correlation for pixel shifts is shown in Figure 5.21 and Figure 5.22 the effect of rotation is shown in Figure 5.23 +/- 180 degrees with 5 degree increments and Figure 5.24 +/- 10 degrees with a 1 degree increment.
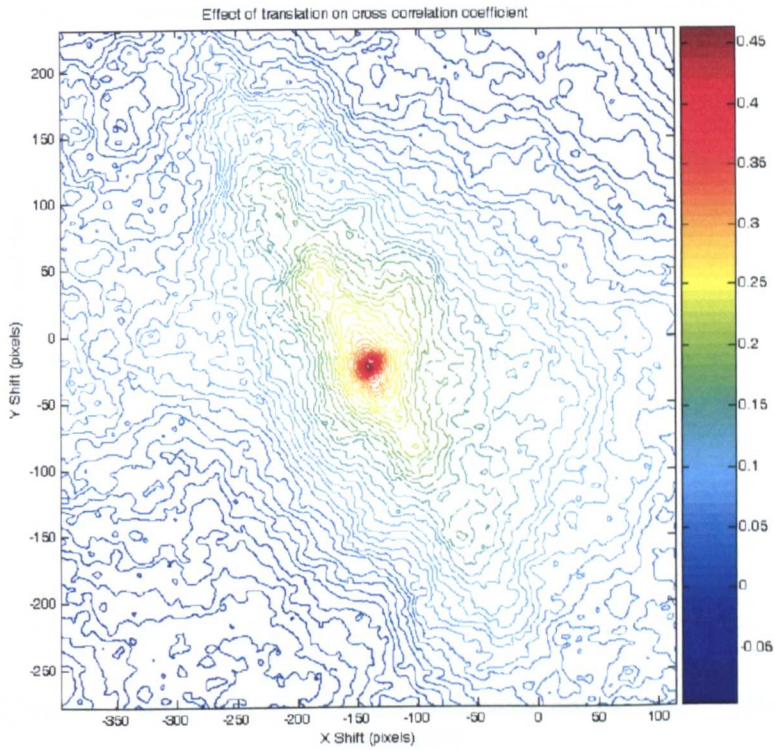
Figure 5.21 Effect of pixel shift on cross correlation coefficient (+/-100 pixels in 5 pixel increments).
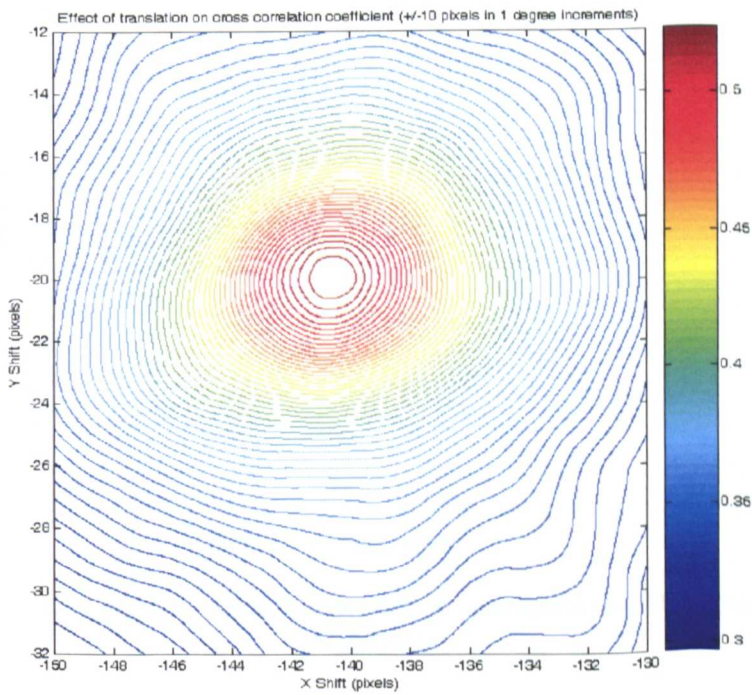
Figure 5.22 Effect of pixel shift on cross correlation coefficient (+/-10 pixels in 1 pixel increments).
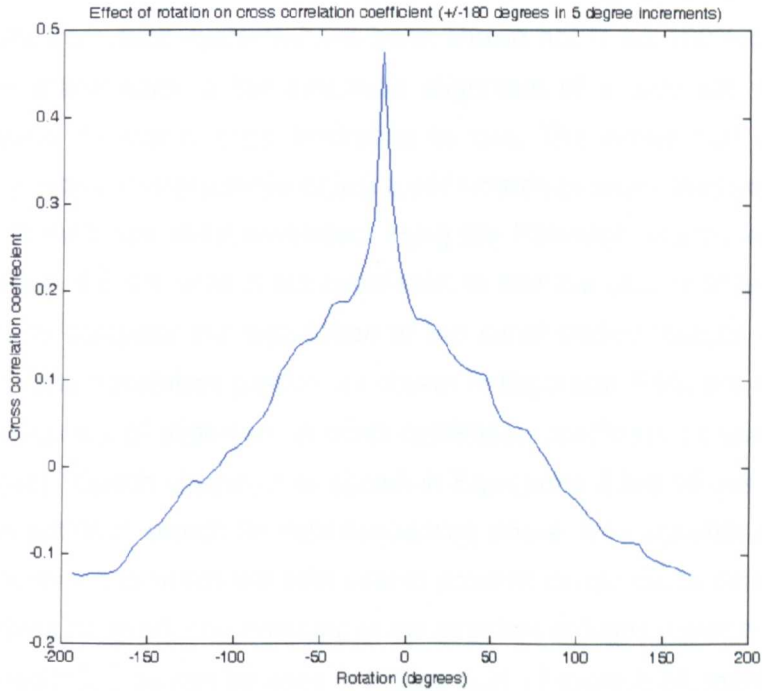
Figure 5.23 Effect of rotation on cross correlation coefficient (+/-180 degrees in 5 degree increments).
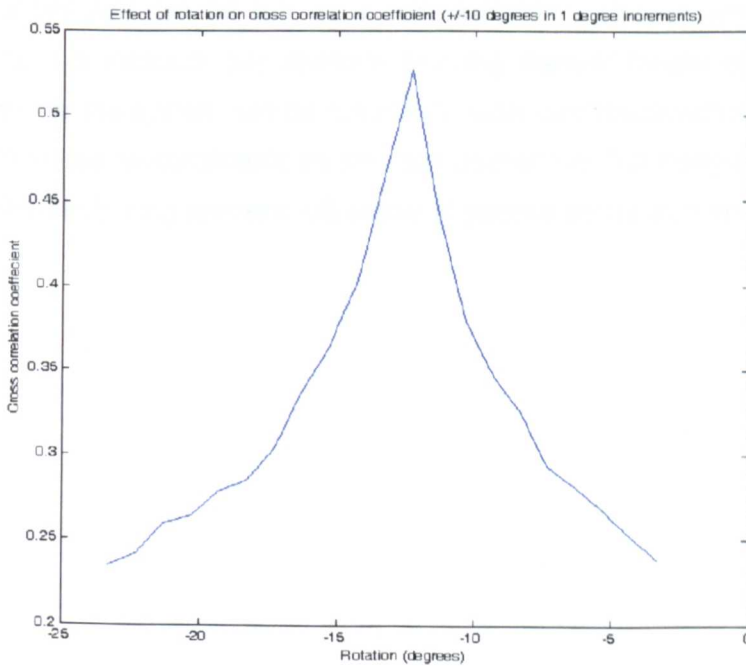
Figure 5.24 Effect of rotation on cross-correlation coefficient (+/-10 degrees in 1 degree increments).

e) *Automatic Alignment, Fibonacci Search Method*

Automatic alignment systems currently implemented using cross correlation require that the whole data set is automatically tested in all ranges of X,Y and rotation the image,

this iterative method takes an extended length of time excluding its use in a semi-automatic systems. Results from such systems have been shown not to be 100% reliable as errors that have been made early in the automatic alignment of a data set would propagate through the whole dataset proving frustrating to use. The errors can be the result of specimen preparations, missing slices or just a poor match between the two images.

A new method has been developed using the Fibonacci search algorithm, and as shown in **Equation 5.8-5.9** uses cross correlation to find the best fit of two images in the search process, to complete the registration of two serial section images by searching for the best rotation and translation position as shown in **Equation 5.10**, the measure used to determine the accuracy of alignment is cross correlation coefficient as shown in **Equation 5.7**. The Fibonacci search algorithm as shown in **Equations 5.8-5.10** has previously been shown to be the optimum search for data sequences where local maxima are not an issue, requiring less iterations to reach the best search position compared to other methods such as binary searching or iteratively searching in the direction of highest match until a minimum change is reached [137], as can be seen in **Figure 5.21 - Figure 5.24**, there is a very sharp peak around to optimum alignment location which allows the use of this search algorithm. The use of new method of serial section alignment dramatically increases the search speed and means the process can be run as a semi automatic process with each automatic alignment taking 1-2 seconds per sections allowing manual review of each section. If required by the user the system can be run in fully automatic mode without user interaction but suffers from the same constraints as previous methods in that badly deformed sections as a result of the sectioning process will cause alignment errors to propagate through the whole dataset.

The Fibonacci numbers are defined as:

$$F_0 = F_1 = 1$$

and

$$F_n = F_{n-1} + F_{n-2}, \text{ for } n=2, 3, 4, ...$$

yielding the sequence 1, 1, 2, 3, 5, 8, 13, 21, 34, 55, 89, ...

The search function is

$$L = (F_{n-2} / F_n) (b-a)$$

Where L is the size of the initial step

The first two points are $X1$ and $X2$, found by

$$X1 = a + (F_{n-2} / F_n) (b-a)$$

$$X2 = b - (F_{n-2} / F_n) (b-a)$$

The cross correlation function f is evaluated at these points: $f(X1)$ and $f(X2)$, comparing these function values to see if $f(X1) > f(X2)$ or $f(X1) \leq f(X2)$.

If $f(X1) > f(X2)$

Discard the interval $[X2, b]$. The new interval of interest is $[a, X2]$.

Let a= current interval end-point

Let $b = X2$

Let $X2 = X1$

Find the new X1 point by:

$$X1 = a + [F_{n-k-2} / F_{n-k}] (b-a)$$

..(5.8)

Evaluate $f(X1)$ and $f(X2)$ and compare.

If f(X2) > f(X1)

Let *b*= current right hand end-point

Let *a* = *X1*

Let *X1*=*X2*

Find the new X2 by :

$$X2 = b - [F_{n-k-2} / F_{n-k}] (b-a)$$

..(5.9)

And the function used to determine the best alignment is given by

$$f_r = f_x(f_y(f_c))$$

..(5.10)

Where f_r is the function used in **Equation 5.7-5.8**, and f_x, f_y represent Fibonacci searches in both the x and y direction of the images and f_r the Fibonacci search of rotation.

5.2.4   3D Visualisation

The developed application contains standard rendering functions Back To Front (BTF), minimum and maximum point projections, the algorithms used have been detailed for completeness. The volume data is traversed as shown in **Figure 5.25**, applying the specified transfer function [138]. Developed extensions for this study have been to modify maximum and minimum point rendering functions so that the rendered data can be limited by intensity. Both minimum and maximum point projection functions have been extended to include depth encoding of the Z positions of the Voxel in dataset in the displayed visualisation.   24 bit rendering systems have been developed based on Maximum and minimum point projections and BTF rendering functions, allowing multiple pallet assignments. In the following section both the standard algorithms for the rendering modes are given and the extensions and explanation for the developed 24 bit versions. In the development of the new system decisions were taken not to develop surface rendering methods as previous work as discussed in Chapter 2 had shown that Voxel rendering techniques had greater acceptance than Geometric (or surface) rending for complex datasets, such as required for histology studies due to the methods ability to more accuracy represent original data. Minimum and maximum projection are found to work well when rendering datasets containing fine structures, however there is no user control of the intensity range to be included in the final visualisation, so methods were developed which

allow for these algorithms to be applied to a given intensity range. Under some circumstances it is difficult for the user to orient the visualisation, this can particularly be the case with complex datasets with fine structures. The M+ and M- projections are good methods for visualising this type of data as the fine changes sometime lost with other methods such as BTF rendering remain visible. The M+ and M- methods have been extended to allow for the encoding of the position of each visualised Voxel with it Z location in the dataset.

BTF rendering offers the most flexibility for rendering histological data, for new users it can be hard to learn how to optimally set the opacity curve for best results, consequently when designing the new animation system, the animation of the opacity curve was included. As well as producing informative visualisations itself, opacity animation allows for a range of visualisations to be completed using a wide range of settings and the visualisations from the animation can be subsequently extracted.
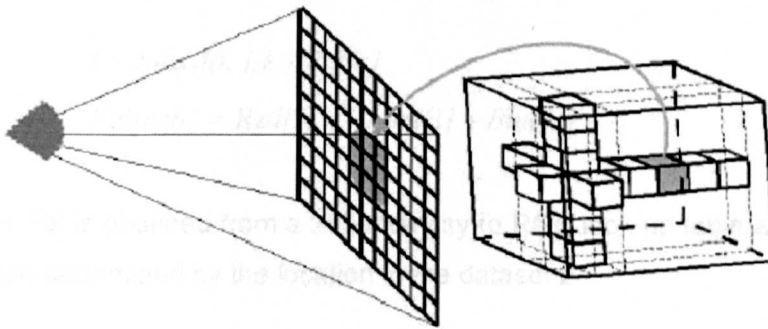
Figure 5.25 Back to front rendering

a) *Maximum (M+) And Minimum (M-) Point Modes*

$$I = Max(f(i,j,k)).Bright$$

$$P_{RGB} = Pal[I]$$

..(5.11)

Where Intensity *I* is calculated as the maximum pixel encountered by the ray projecting through the volume *f* in all volume locations determined by *I*, *j*, and *k*, following *3D* transformation. An RGB look up table *Pal* is applied to pseudo colour the calculated intensity *I* to determine the final image P_{RGB}.

Maximum point and minimum point rendering modes project the intensity for the brightest/darkest Voxel normal to the viewing plane. An example rendering is shown in **Figure 5.26**. Parallel rays are cast through the volume at right angles to the viewing plane, one ray for each pixel in the final image. The value associated with each ray is that of the highest Voxel value encountered during its traverse of the volume. For M- each ray returns the lowest Voxel value which encountered. The choice of which option to use is dictated by the location of significant detail in the Voxel histogram of the volume of interest. **Figure 5.26** shows the colour pallet applied is shown below the main rendering in window. The rendering modes require few decisions to be made by the user other than the initial choice of using either M+ and M- (for example, there is no opacity curve to be drawn). Extensions have been made to the rendering engine system that allow for a upper and lower threshold to be set when performing M+ and M- rendering, this allows for removal of background noise and rendering to be performed solely in defined intensity ranges.

b) Maximum (M+) And Minimum (M-) Depth Rendering Modes

$$I = Max(f(i, j, k)).Pal[z]$$
$$Pal[rgb] = Red[I] + Green[I] + Blue[I]$$

$$..(5.12)$$

Where the pallet *Pal* is obtained from a 255 intensity to RGB look up table and the location in the lookup table determined by the location in the dataset *z*.

Visualisations of histological datasets can be hard to interpret and it can be difficult to see the location of structures within the 3D projection. In normal maximum point projection the intensity of the Voxel of highest intensity normal to the viewing plane is the one that enters the viewing window. Including Z position in the M- and M+ rendering methods replaces the intensity value of the brightest pixel with a value that corresponds to the distance from the top of the dataset. This value is then remapped to its corresponding pallet entry. **Figure 5.26** shows normal Maximum point projection of a neuron captured using a confocal microscope. **Figure 5.27** shows the same dataset with depth encoded maximum point projection. As can be seen in **Figure 5.27** the same level of detail can be seen in the final image with the added information as to the path of the dendrites through the specimen. In the figures shown dendrites are the branching filament like structures that can be seen to be emanating from the cell nucleus which is the central object in **Figure 5.26** and **5.27**. As can be seen in **Figure 5.27** the maximum point rendering with the dataset depth encoded the location and path of the dendrites can be determined visually. The

location of the dendrite in the dataset can be observed by viewing the changing colours in the applied palette with the highest location being maroon, green the centre of the dataset and red the lowest point.
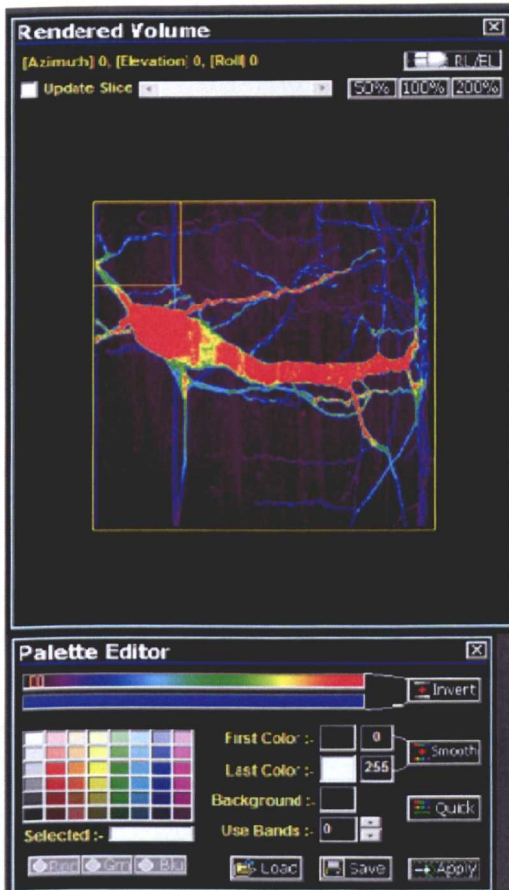
Figure 5.26 M+ projection of a neuron
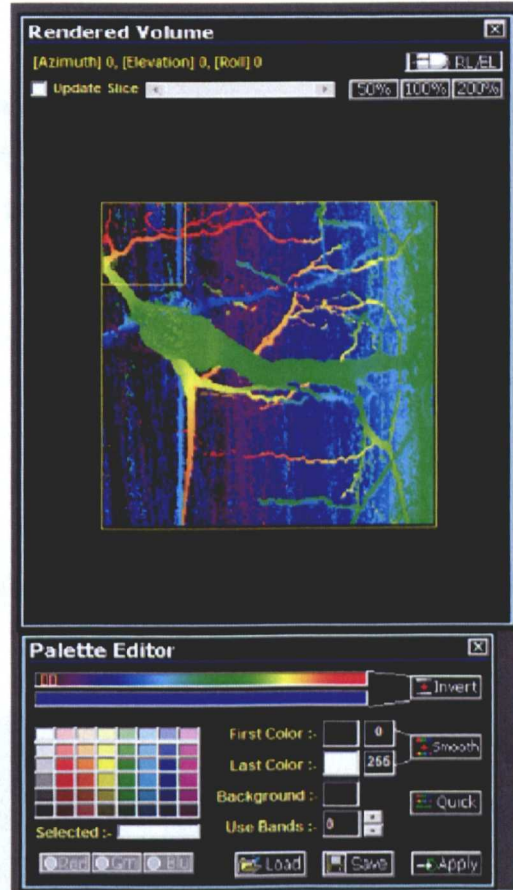
Figure 5.27 M+ depth encoded projection

c)   Rendering Multi Channel Data

So far rendering modes considered in this section have worked on single 8 bit datasets where the final colour for each Voxel has been determined by an applied colour palette, and the rendering operation applied. In many situations there is a requirements to visualise true colour datasets. True colour rendering algorithms have been developed as part of this study, the equations as shown in **Equation 5.13** are similar to the standard 8 bit version of the functions.

With true colour data-sets the way the rendering operations work is principally the same as the gray level rendering systems. The green component of the Voxel is used to determine the Voxel to be rendered and the highest colour component in the selected Voxel

is the actual colour that is displayed in the final rendered output, an example rendering output can be seen in **Figure 5.28** here the dataset consists of both a green and blue channel, the equation for true colour rendering is shown in **Equation 5.13.**

$$I = Max(f(i, j, k)).G$$
$$P_{rgb} = I_r + I_g + I_b$$

..(5.13)

Where the Voxel to be displayed I is determined by the green component of the data volume and the displayed image P_{rgb} is the original RGB values of the selected Voxel I_r, I_g and I_b for the Red, Green and Blue components respectively.

For example:-

Given

	R	G	B
1	234	50	70
2	200	190	89
3	34	17	120

If the rendering mode was M+ then Voxel number 2 would be chosen, and the output colour seen would be R with an intensity of 200.
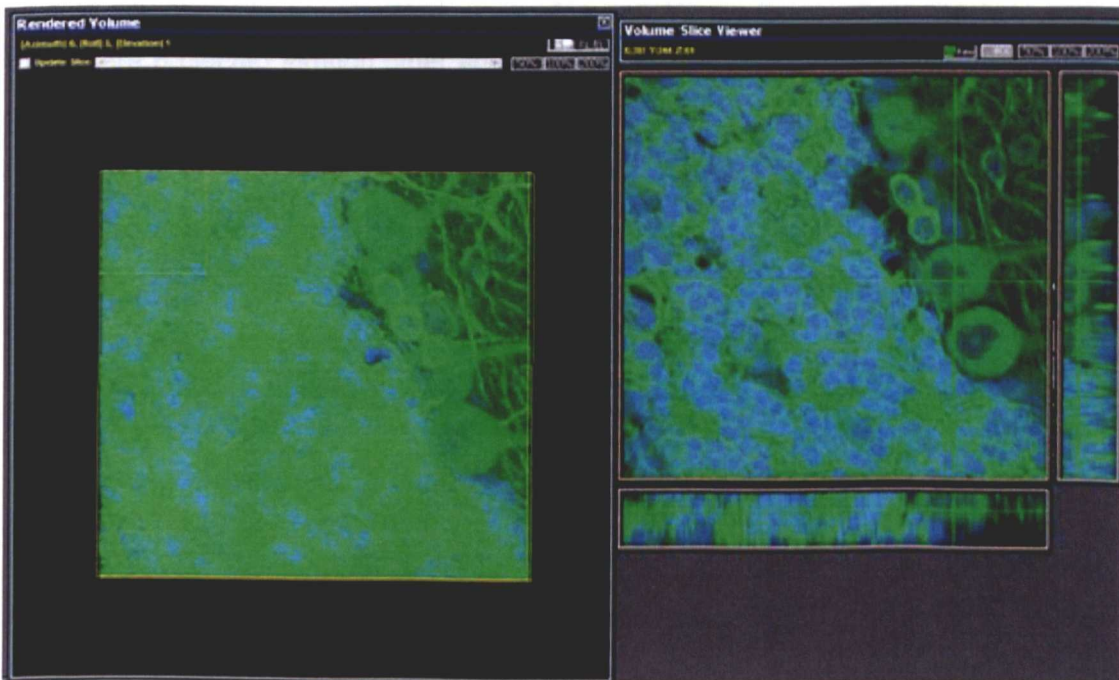

Figure 5.28 Three channel confocal dataset of a brain cross-section

d) 3D Rendering With Opacity Blending

Back to front opacity blending has also been included to allow for precise control of individual Voxel values as given in **Equation 5.14**.

$$I_{out} = F_{ijk}.A_{src} + (1 - A_{src}).I_{dst}$$

$$P_{rgb} = Pal[I]$$

..(5.14)

Where, I_{out} is the output colour which will be written to the frame buffer. F_{ikj} is the Voxel determined by the position being rendered the dataset and A_{src} are the source alpha, which come from the fragment. I_{dst} is the destination visualisation buffer.

With opacity blending each of the 256 possible Voxel values must be assigned an opacity, or alpha factor. Because there are many ways to draw the opacity curve, there are many visual effects which can be created using the method. Each will emphasise a different property of the distribution of Voxel values in data space. This method allows for advanced histogram segmentation to be completed. The use of the opacity tool allows not only binary segmentation to be completed but for control of specific opacity to be controlled for each Voxel intensity. As shown in **Figure 5.29**, increased control of the rendered object can be obtained, and the results are more pleasing for visual review as the opacity of the dataset objects are correctly accumulated, unlike M+ and M- rendering where the light and dark Voxels are projected through other areas of the dataset based on intensity and irrespective of position.
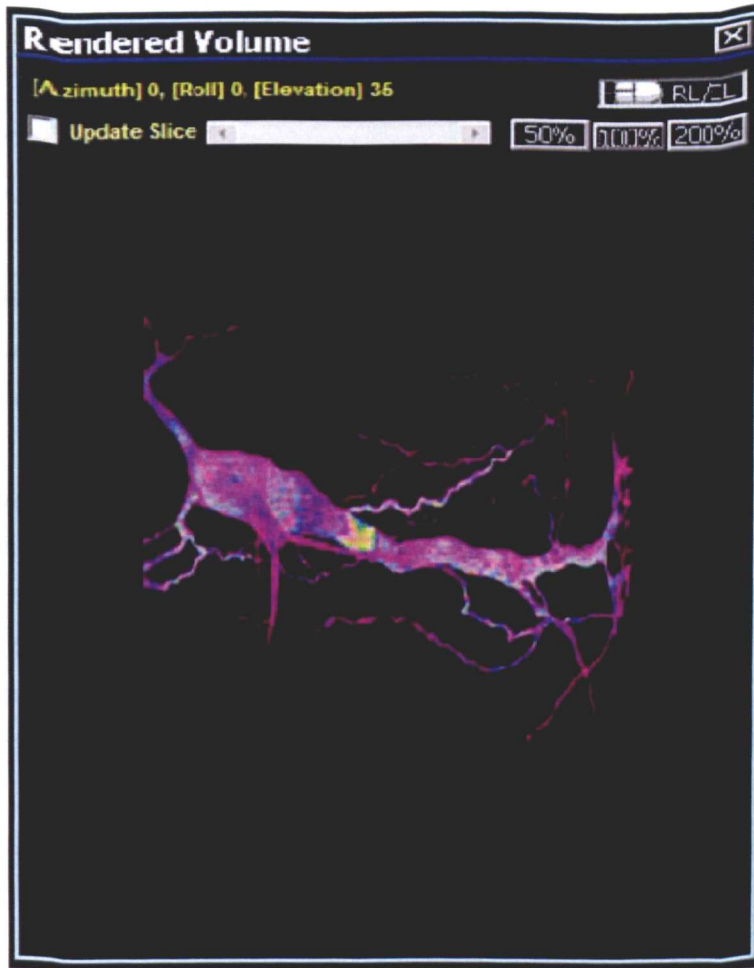
Figure 5.29 Neuron rendered with opacity rendering

5.2.5   Opacity Animation

Animations are a valuable tool in the understanding of 3D visualisations, which are missing real depth information to the human eye, stereo anaglyphs can also be produced to improve this perception but without movement 3D images are hard for the human brain to interpret effectively. Opacity animation allows for the user to define the changing opacity of a selected intensity Voxel. In the same way that animations of the 3D visualisation can help the human observer to visualise the dataset in its 3D form the animation of the opacity of the data set allows the user to visualise the data and to understand its structure.

$$\Delta i = \frac{(O_{start} - O_{end})}{N_{frames}}$$

$$Opacity_i = O_i + \Delta_i . n_{frame}$$

..(5.15)

Where Δi is the change in opacity per animation frame, O_{start} is the starting opacity for the specified Voxel value, O_{end} the ending opacity the result is an opacity for each N_{frame} in the animation is calculated.

The illustration show in **Figure 5.22** is a static representation of an animation produced by the developed system. Frame (A) the varying opacity of the object can be seen with the main body of the dataset becoming transparent. As can be seen the opacity of the rendered animation changes over time, allowing the context of the red area of interest to be considered within the rest of the object. Frame (B) shows the main body of the image almost completely transparent and frame (C) the main body of the visualisation becomes opaque again (NB: The original form of this data is a Windows .Avi file). It is difficult to illustrate the effect of an animation using static images, but in the moving animation the structure of the selected area can be seen in context to the rest of the data.
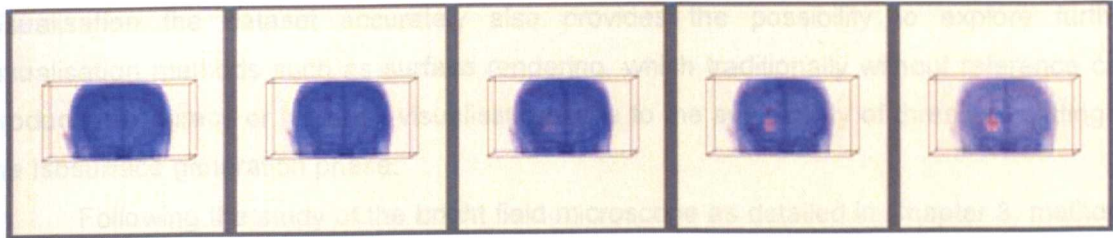
(A)
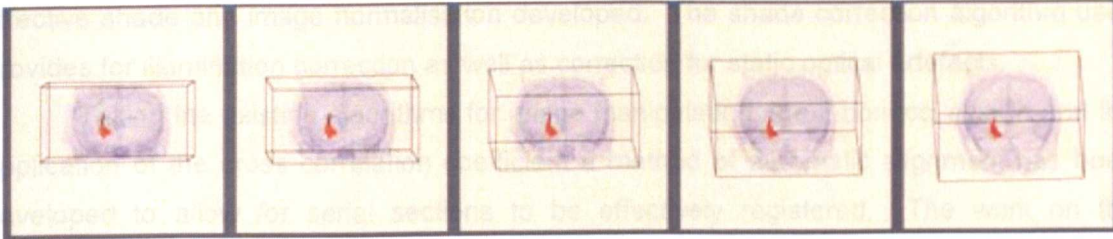
(B)
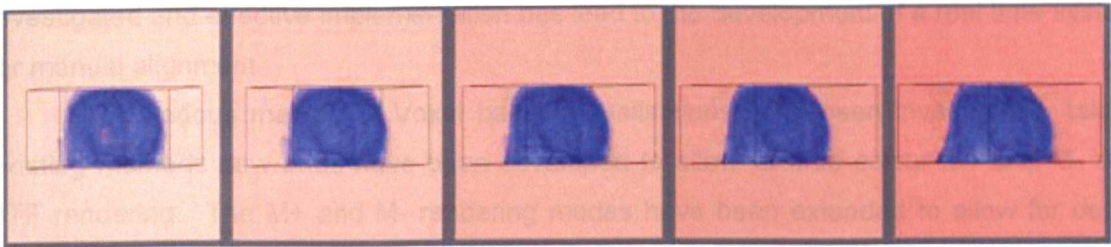
(C)

Figure 5.30 Opacity animation of MRI data showing surrogate cell injection.
The frames from an animation A, B and C in order show the effect of animating the opacity of the dataset, where the area of interest (red) is first fully obscured by the high opacity setting of the surrounding data (blue), becomes visible in as the surrounding opacity setting is reduced and then becomes obscured again as it is increased.

5.2.6 The Major Contribution Of The Aims

The framework that has been developed for clinical image processes provided core microscope automation functionality and an image capture framework. Image processing techniques have been used to counter optical deficiencies are observed from the bright field microscope. The framework provides a functional code base for the development of specific software components. Built upon this are specific applications one for serial section alignment and the other for 3D visualisation, both have been implemented to address specific aims in medical imaging. A system has been designed and implemented for serial section capture system that overcomes the optical limitations of imaging from low NA objectives. Allowing source images to be captured of histological datasets free from

illumination artefacts using objectives that offer a higher resolving power than would be achievable using other non microscope based imaging systems. The ability to view visualisation the dataset accurately also provides the possibility to explore further visualisation methods such as surface rendering, which traditionally without reference can produce inaccuracy or incorrect visualisations due to the subjectivity of threshold setting in the Isosurface generation phase.

Following the study of the bright field microscope as detailed in Chapter 3, methods of correction of local image deformations have been completed and an algorithm for effective shade and image normalisation developed. The shade correction algorithm used provides for illumination correction as well as correction for static optical artefacts.

Taking the existing algorithms for image manipulation, the Fibonacci search and the application of the cross correlation coefficient a method of automatic alignment has been developed to allow for serial sections to be effectively registered. The work on the alignment system required that the various techniques for the merging of two images be investigated and effective implementation has lead to the development of a real time system for manual alignment.

The various method of Voxel based visualisations have been investigated, taking existing methods new ones have been developed to allow for true colour M+ and M- and BTF rendering. The M+ and M- rendering modes have been extended to allow for depth information to be combined with these methods allow the user to interoperate depth information without the loss of existing data. A method of including a time base in the rendering system has been developed. Opacity animation allows for animation to be completed which keep the visual keys within the data set while allows for complex and difficult segment structures to be viewed.

The methods that are used for the reconstruction of datasets are dependant on the data understudy, the way that the methods have been employed are explained in Chapter 7, where the visualisations from three example datasets are presented. The work that has been presented in this chapter for the development of medical image algorithms for 3D reconstruction and visualisation is contribution towards aim 1.3.2.

The systems that have been developed allow for the study of histological serial sectioned datasets to be completed efficiently with uncomplicated tools, these allow for further independent study of soft tissue structures stained with regular biomarkers and for serial section registration and reconstructions to be completed on readily available and cost effective personal computing platforms. Authored and co-authored papers show the practical application of the developed systems [129-131].

The work that has been described in this chapter provides a foundation in terms of the hardware data capture requirements and development of basic image processing algorithms such as the shade correction algorithm as well as a software base required for further application development on the Windows based systems.

The following chapter describes the automated DNA Image Ploidy system developed. Presenting the algorithms used and developed, allowing automated image capture, segmentation and classification. The clinical studies that have been completed using the system are introduced in Chapter 7.

Chapter 6 Automated DNA Image Ploidy System

The three main compartments of a cell are the nucleus, the cytoplasm and the membrane. The nucleus is the control centre of the cell and located in the centre. The nucleus determines how the cell will function. The cytoplasm is a gel like fluid and provides a platform in which many organic operations takes place such as cell growth and replication. The cell membrane is the boundary structure between the structures outside the cell; it maintains the integrity of the cell as well as being the interface for control signals. DNA Ploidy acts on the cell nucleus and laboratory preparation removes most of the other compartments however parts of the cytoplasm remain present in the final prepared slide.

DNA Image Ploidy is a quantitative test, as discussed in the literature review in Chapter 2. Ploidy is a cytogenetic term for the number of single sets of chromosomes in a cell or an organism. As a recap of the descriptions given in Chapter 2, diploid cells contain one pair of chromosomes, as found in normal cells. If the DNA duplicates without a following cell division, the cell will contain two pairs of chromosomes and will be called tetraploid. Aneuploid cells contain a number of chromosomes that is not an exact multiple of the normal, diploid number. In humans, aneuploid cells are considered abnormal and are a strong indication of malignancy. The amount of DNA in the nuclei can be expressed as the amount of light absorbed by the Feulgen stain over the nuclei. Optical density (OD) is, for a given wavelength, an expression of the transmittance of an optical element. DNA Ploidy is set by calculations of integrated optical density (IOD), the sum of all OD values for all the optical elements in a cell nucleus. Image cytometry has the advantages of morphological verifiable nuclei and results in limited or no debris being included in the analysis. Increased automation allows for the number of cell nuclei it is practical to capture to increase, in turn increasing to ability to review the statistical significance of what could be sub populations with limited number of events. Accurate grouping of cell types will again further reduce manual burden, and increased automation decreases subjective variations introduced by the user.

It can be seen that the challenges for the development of an automated DNA Image Ploidy system can be broken down into three elements 1) Location, focusing and capture of cell nuclei; 2) Segmentation and calculation of image characteristics as required for DNA Ploidy classification; 3) Classification of both intact nuclei from artefacts and classification of cell populations. The higher the accuracy of the automatic focusing methods and parametric calculations the clearer the aneuploid nuclei populations will be in respect to normal either diploid or tetraploid populations.

.

New methods are described which provide efficient focusing, employing the use of linear regression to predict the general focus plane of the specimen and object based methods for refined image focus. The methods allows for time efficient and independent optimum focus position to be selected for each object. A method is also presented that allows for a hybrid textual segmentation to allow segmentation in presence of residual cytoplasm following specimen preparation.

There are some minor hardware changes to the system that have been made to account for the specific imaging requirements as detailed in Chapter 4. The implementation of the classification system is described. At the end of the chapter the algorithms used and introduced are presented. A full user manual for the system can be found on the accompanying CD.

The method used to prepare the specimen prior to imaging is illustrated in **Figure 6.1** A block of paraffin embedded tissue (1) is cut in sections and mounted on to a slide, To visualize the tissue, the slides are stained with haematoxylin and eosin and the tumour areas are defined by a pathologist (2). The tumour area is micro-dissected from the paraffin block (3) and cut in thick sections (4). A suspension of nuclei is created from the sections (5) and put on to a slide in form of a monolayer (6). The monolayer is stained with Feulgen's reagent ready for imaging. (7) and Ploidy classification (8).
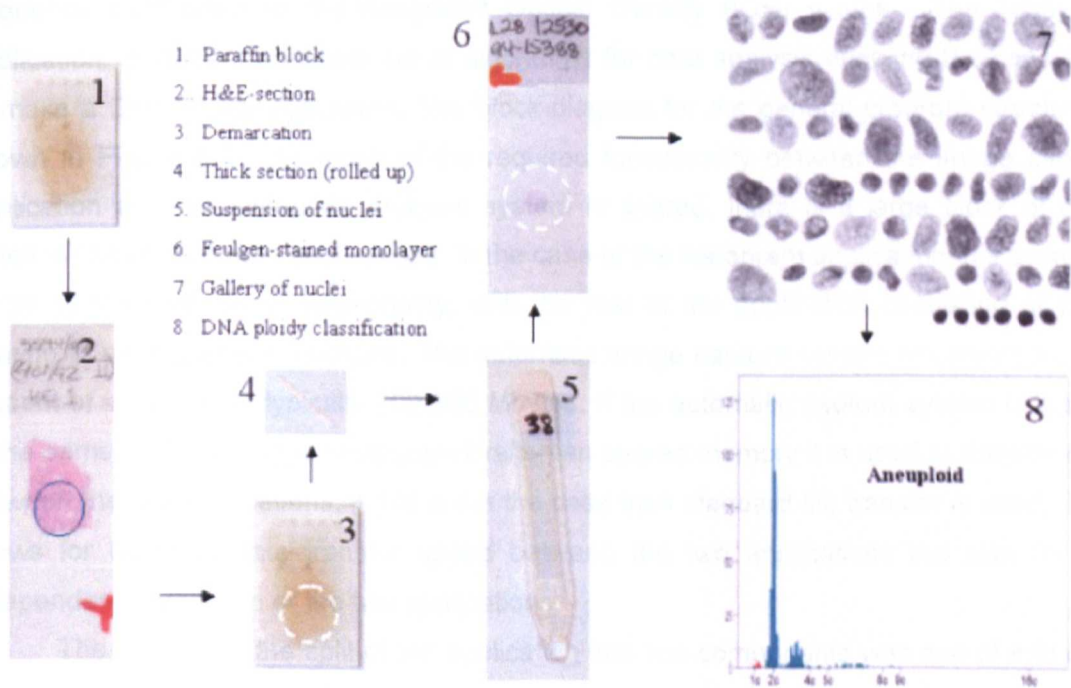

1. Paraffin block
2. H&E-section
3. Demarcation
4. Thick section (rolled up)
5. Suspension of nuclei
6. Feulgen-stained monolayer
7. Gallery of nuclei
8. DNA ploidy classification

Figure 6.1 Preparation of Feulgen stain mono layer

6.1 Hardware Requirements

Specific imaging requirements for this system is that a 546 nm interference filter is used as the Feulgen stain used is only quantitative in a narrow spectral window, 546 nm is the centre wavelength of it quantitative absorption range. The preparation that is used for DNA Image Ploidy is a cytospun mono layer, cell nuclei are spun onto a glass slide using a centrifuge. It can be understood that due to different cell structures and densities some cells are flattened more than others, as a result cell nuclei within a single field of view can have different optimum focal positions (a problem well known in cytology). A Piezo focusing unit with it short settle time of approximately 30ms and high accuracy ±20nm provides a good solution as it allows rapid and accurate movements ensuring maximum slide throughput, where multiple focus positions are required to achieve optimum results.

6.2 Software Design And The User Interface

The automated DNA Ploidy system is made up of two separate applications, one for data acquisition and for histogram analysis. The data acquisition program is called the 'DNA Ploidy Cell Capture Program' and the data analysis program is called the 'Histogram Draftsman'. The DNA Ploidy Cell Capture Program automatically captures cell nuclei, classifies and places them into galleries. The Histogram Draftsman program uses the data captured from the DNA Ploidy Cell Capture Program to calculate a histogram showing the frequency distribution of the Integrated Optical Density (IOD) values. The histogram application includes a complete set of algorithms for data analysis enabling the consultant to make a DNA Ploidy evaluation. The block diagram for the general program structure is shown in **Figure 6.2**. As much of the required functionality between the image capture application and the histogram analysis system is shared, there is a large block of code which is common to both applications. In the case of the histogram application this accounts for all of the lower level functionality, with the rest of the application consisting of code relating to user interface functions. The automatic image capture system generates a large amount of image data, typically 200-300 Mbytes. If the automatic capture system is loaded in the same machine as the Histogram Draftsman shared memory it is used to transfer data between the two applications, if this is not the case then standard file transfer is used. This allows for optimum data transfer speed between the two applications but also for the independent installation of the two applications.

The reason for the split of the application into two components was one of end user practicality, efficient use of time and system resources. The capture system in practice will be running on the analysis machine situated either in a lab, where the results viewing and histogram viewing and classification will be completed by the pathologists in office locations.

This two component approach allows for a dedicated analysis application be designed for use on the capture system and a dedicated analysis system for the pathologist.
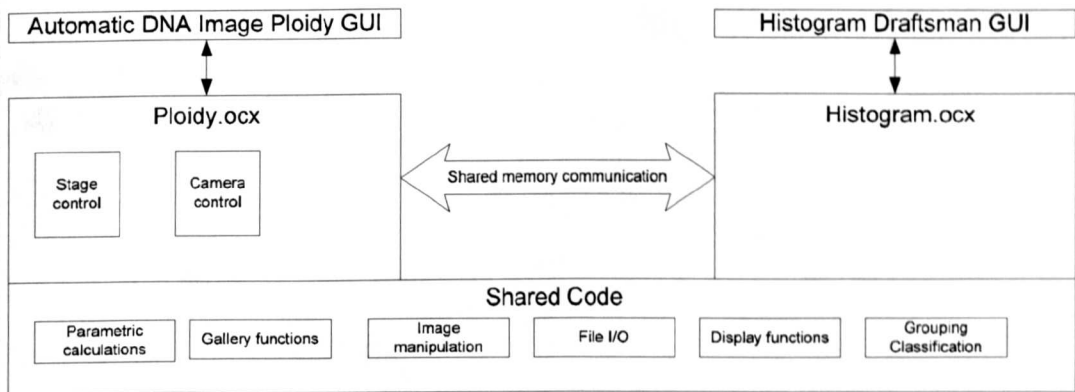

Figure 6.2 Automatic DNA Image Ploidy program structure

6.2.1 DNA Ploidy Capture Program

The main interface for the DNA image Ploidy capture system is shown in **Figure 6.3**. The centre image shows the raw image captured from the microscope with the user interface shown in the right hand side. The application has features that allow the user to calibrate the automated stage system, select the segmentation parameters, and specify the number of nuclei to be collected. In practice user interaction is limited, required to select and place the slide on the microscope verify the illumination intensity and press the 'GO' button. After the system has collected the defined number of nuclei images and classified them into appropriate groups the user must then verify this classification and specify a Ploidy result based on the histogram. To allow for future algorithmic development the data file saved included the original and relevant area of the image used for shade correction.
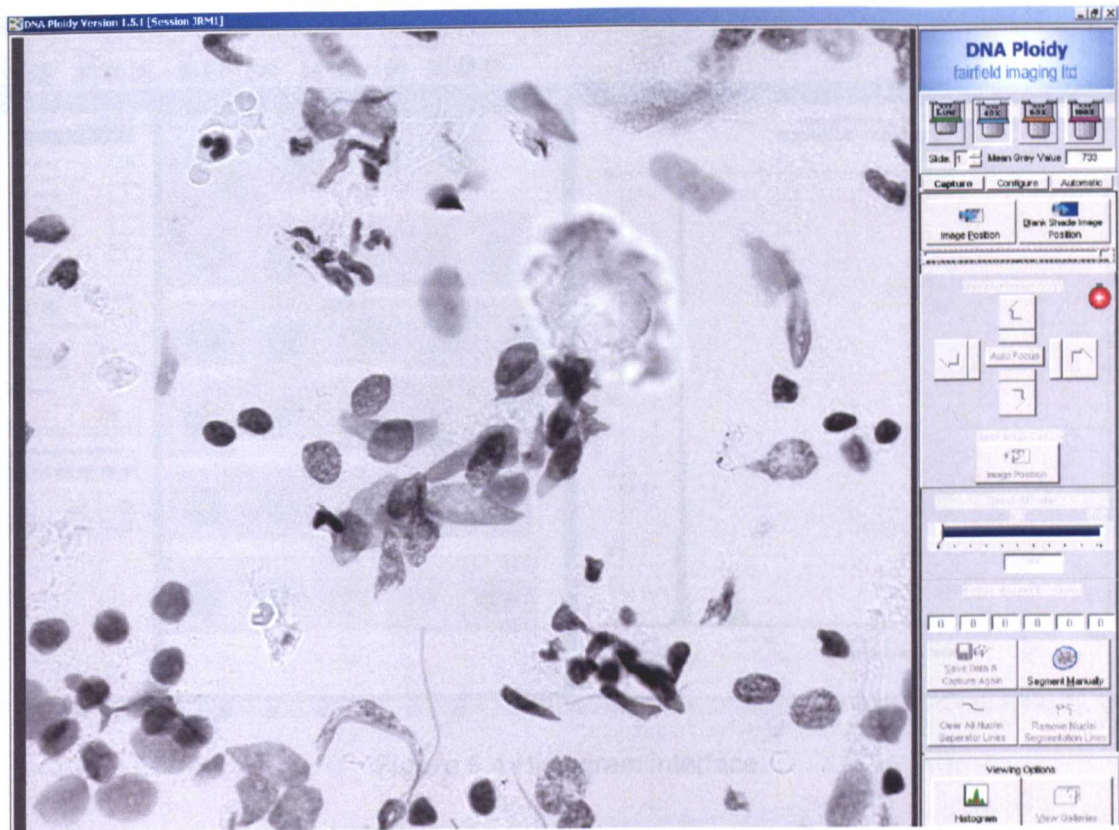
Figure 6.3 DNA Image Ploidy main interface

From top to bottom the interface shows: Lens selection icons; mode classification (manual capture, automatic controls, calibration); Stage movement control; Threshold selection slider; I/O functions and Gallery view selection.

6.2.2 Histogram Draftsman

As with the automated capture application the full application and its features are described in the user manual. In brief the application allows the user to manually move captured nuclei from one gallery to another, perform statistical analysis and annotation the results data with selected statistical measures. The user interface for the histogram draftsman is shown in **Figure 6.4**. It is the histogram application that is also used to specify the parameters used for automatic cell grouping classification.
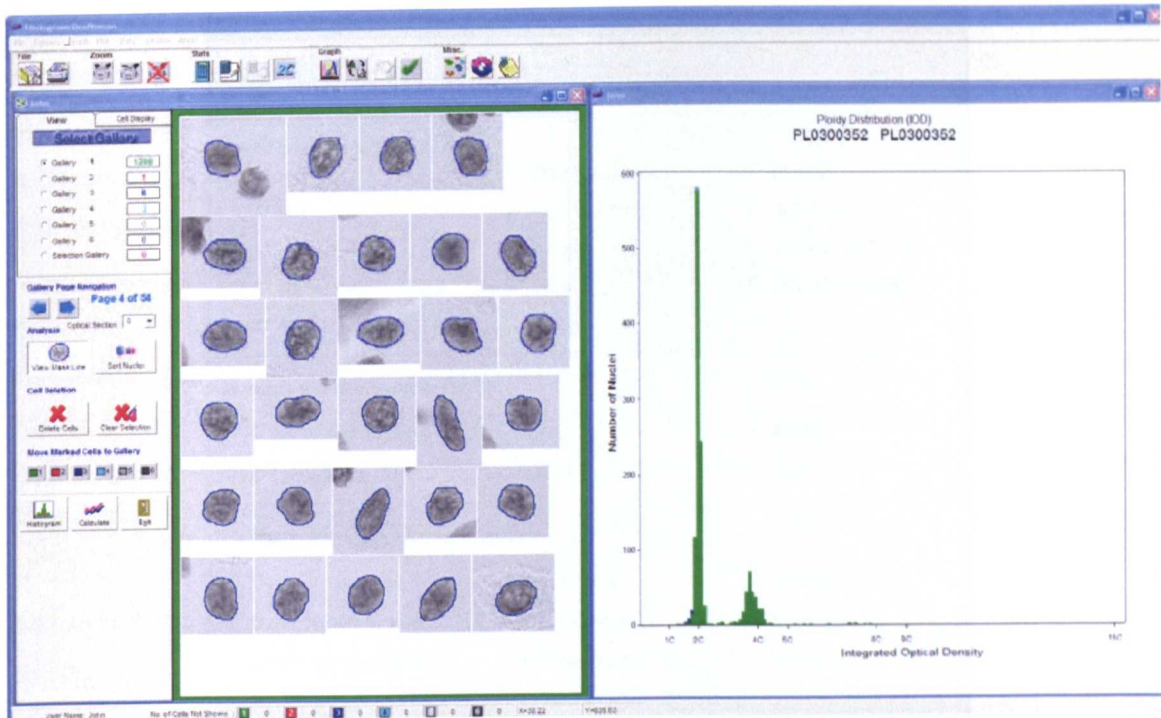
Figure 6.4 Histogram interface.

The user interface shown in **Figure 6.4** has three main elements graphical display, cell selection window and control bars. Top tool bar: File control, print, zoom control, statistical output options, graph type selection (histogram/scatter), Annotation options. Left tool bar: Cell selection options user selectable gallery, sorting options and nuclei deletion and movement functionality. Left Window: display of captured nuclei, the user can select individual images to gain individual parametric information; nuclei can be selected and moved between galleries. Right window: Graphical histogram display window, the scale can be changed and the user has selection of the parameters that are plotted in either scattergram or histogram format. Brushing allows the cell nuclei denoted by graph points in the graphical display window to be selected is included both for histogram displays and for scattergrams. The brushing functions allows the user to view nuclei that fall within specific limits, grouped together, have specific diagnostic concern or may be outliers. The application can be run on systems that support dual monitors, where it is possible to display the nuclei gallery on the left hand screen and the graphical display on the right.

The statistical algorithms are presented at the end of this chapter. Dependent on the statistical measure, these can be selected for all of the data or for user selected ranges of the graph, the available measures are shown in **Figure 6.5**.
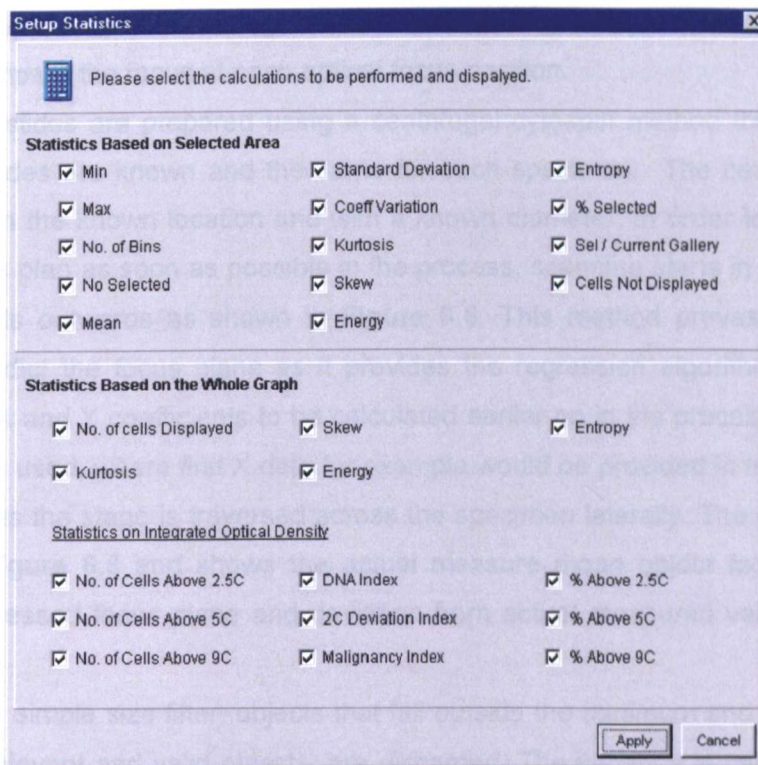
Figure 6.5 Statistics calculation options

6.3   Auto-focus And Image Capture Method

Traditional methods of auto-focus work on the whole field of view, where a search algorithm is used to determine the optimal focus position for the whole field of view based on a defined accuracy of focus measure. Using the whole field of view to determine the best focus position has disadvantages in that it makes the basic assumption that all objects within the field are on a singular focus plane. While this can be seen to largely be the case for histological sections, as routinely used in pathology review it is not the case for cytological preparations such as in DNA Image Ploidy.

Image capture and auto-focus methods used to capture cell nuclei must overcome two main difficulties. First, not all of the cell nuclei appear in the same optical plane. Second, each field of view will contain artefacts as a result of preparation procedure that must be ignored by the auto-focus algorithm. An Image example from a preparation is shown in **Figure 6.3** as can be seen in the figure the cell nuclei are of differing size and shape as well as there being large number of artefacts.

For each field of view, images are taken in ten different optical focus planes. A cell nuclei showing pixel variances at 10 sequential focus positions spaced at 1µm is shown in **Figure 6.7**. These image frames are shade corrected. Object segmentation is completed using a fixed binary threshold locating the bounding box for each object and identifying each

object in a separate mask. This segmentation technique is adequate for object location as required to compare the focus at each optical focus position.

As the slides are prepared using a centrifugal cytospin method the location of the cells on the slides are known and the same for each specimen. The centrifuge leaves a disk of nuclei in the known location and with a known diameter. In order to create the best predicted focus plan as soon as possible in the process, scanning starts in the centre of the disk and spirals outwards as shown in **Figure 6.6**. This method proves to be far more efficient to predict the focus plane as it provides the regression algorithm with data that allows for the X and Y coefficients to be calculated earlier on in the process than if a raster type scan were used, where first X data for example would be provided in isolation and then Y data points as the stage is traversed across the specimen laterally. The regression plane is shown in **Figure 6.8** and shows the actual measure mean object focus position, the calculated regressed focus plane and deviation from actual measured values of the fitted plane.

Using a simple size filter, objects that fall outside the minimum and maximum range expected for relevant and valid objects, are discarded. The variance is calculated for each object in each optical plane. Only the image with the highest variance for each object is selected for further processing, all other images are discarded. If less than 80% of the selected objects have an optimum focus (greatest variance) in one of the eight centre optical sections, this signifies that the objects as a whole within the field of view are not optimally focused and a new focus position should be selected. Once an acceptable linear focus plane has been calculated the number of optical sections needing to be captured and examined is reduced as an estimation of the linear focus gradient of the specimen will have been described. The decision as to if the focus plane is acceptable for use is again calculated by linear regression and determined by examination of the R^2 value, which an expression of the accuracy of the calculated fitted linear plane with respect to the current data As explained in Section 3.7.2, a low R^2 value signifies that multiple regression does not find a representative linear representation of the focus plane to represent the current data, caused either by lack of data or the measured plane not being linear.

In short the steps taken by the implemented auto focus algorithm are:-

1. Capture image, locate objects using the seeded flood fill algorithm.
2. Collect optical sections (10 sequential focus positions), select objects from field.
3. Test that 80% of objects have an optimum focus plane with the current centre stack positions, if not move in determined Z direction as provided from calculation of the mean highest variance.
4. Select optimum plane for each object from focus stack and complete parametric calculations.
5. Insert current X,Y and Z mean best position into 2D regression matrix.
6. Move to next position in a spiral movement as shown in Calculate Z position using 2D regression (as explained in Section 3.7.2.). If R^2 value is greater than 80% reduce number of collected optical sections to 5, collect optical stack. Loops to 3 until specified number of nuclei or fields of view have been reached.
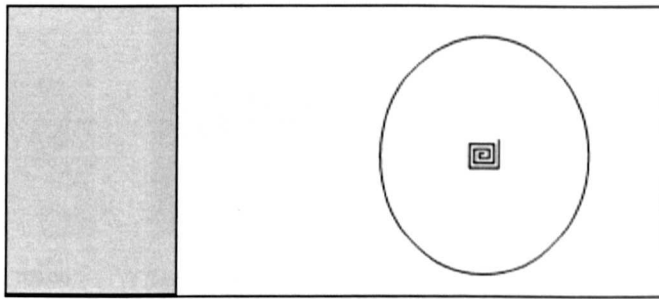

Figure 6.6 Spiral scanning motion of the DNA Ploidy system
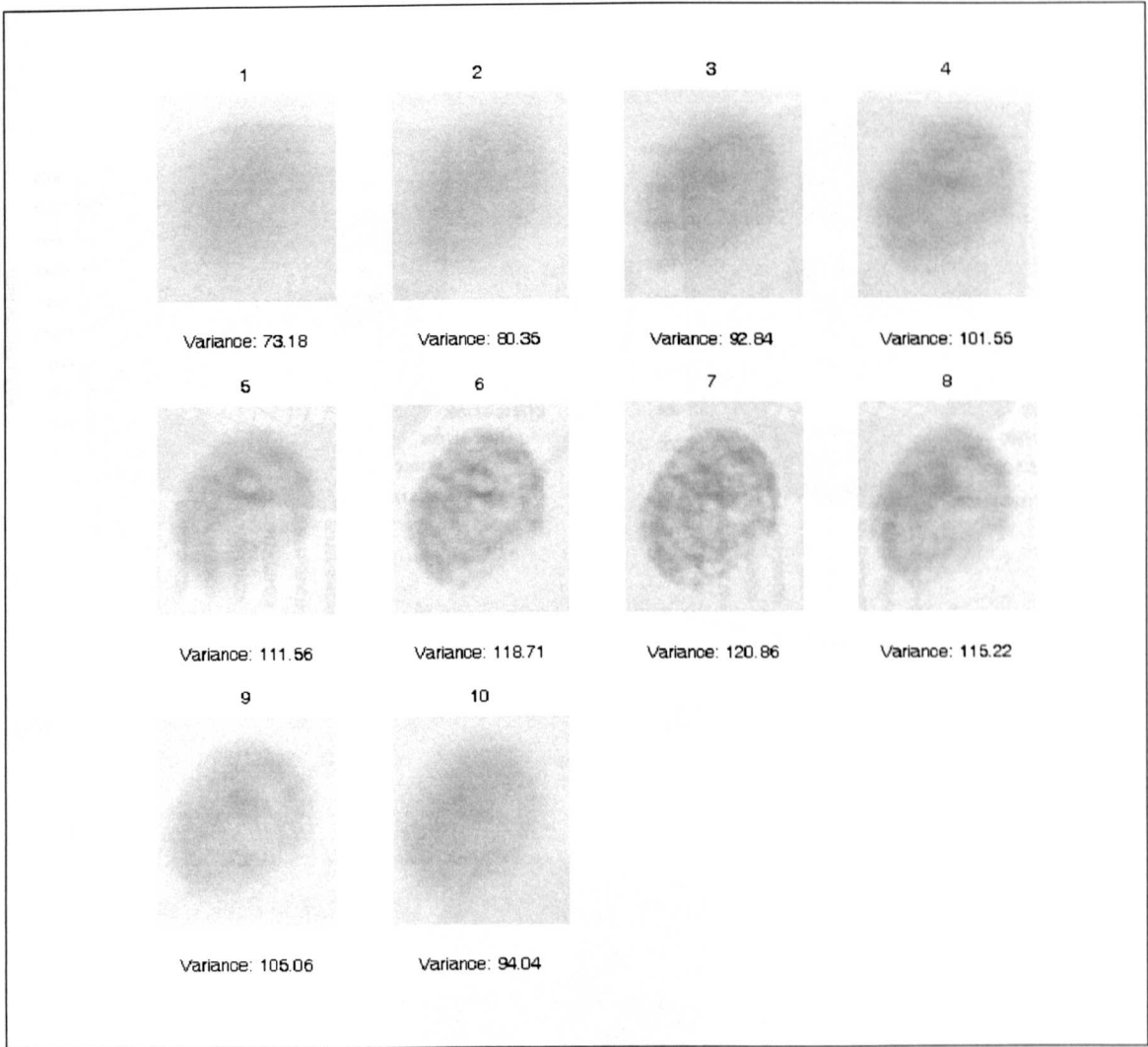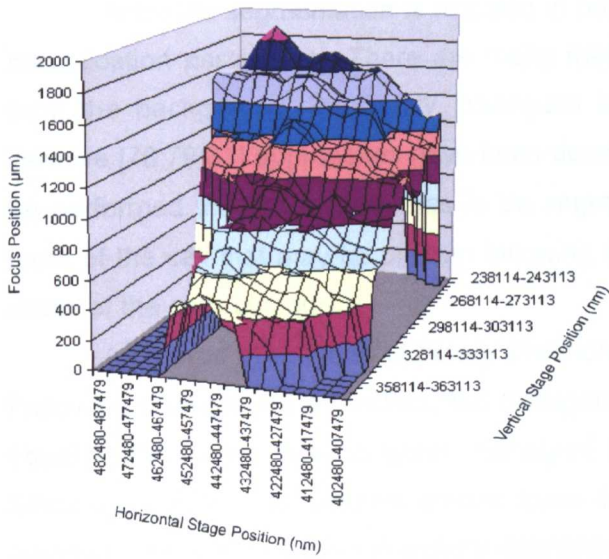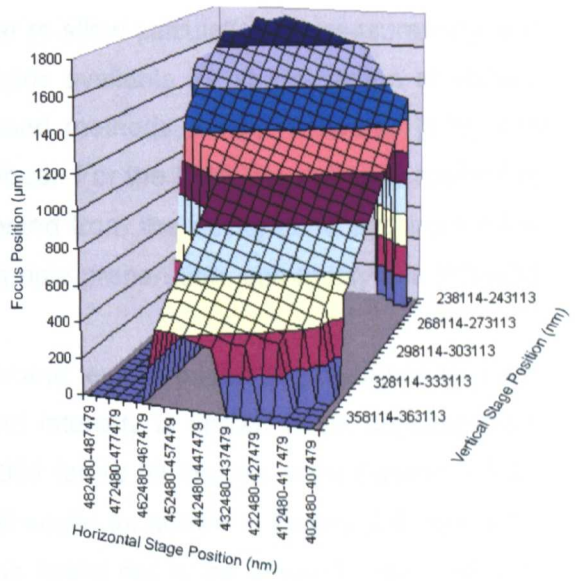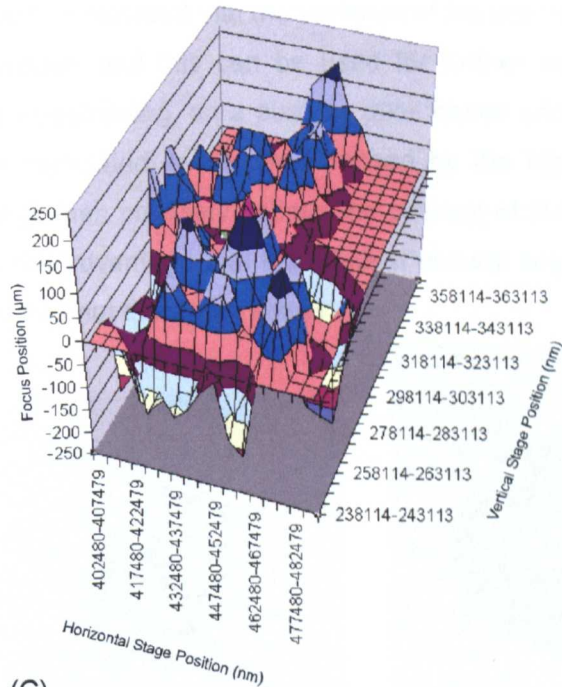
Figure 6.7 Sequential optical section with variances

(A)

(B)

(C)

Figure 6.8 Focus planes

A. Original measured focus plane, B. Fitted plane using 2D linear regression. C. Difference between predicted and actual focus plane.

6.4 Segmentation

Accurate segmentation is required in order to allow calculation of measurement and classification parameters. There are many methods available for segmentation of objects from the background. Previously, histogram based methods, neural networks [139] and iterative [78;79;81] approaches have been described. For the DNA image Ploidy method to be performed the cell nucleus has to be segmented from the background and from other parts of the cell that may be present following sample preparation, commonly this included areas of the cells cytoplasm.

A method of a hybrid of binary thresholds and texture based segmentation is used. Following background correction, the background intensity is known to be approximately equal to the scaling factor S (pixel intensity of 1024 for 10 bit images, from **Equation 5.3**). Since cytoplasm is still present around some cell nuclei as shown in **Figure 6.9**, simplistic automatic histogram based threshold detection is found not to be efficient. Low and high static segmentation thresholds are set leaving only a small area of uncertainly where the boundary between foreground and background is known to lie but its exact location is not defined, as shown in **Figure 6.8**, where the annotated black line marks the boundary. It is known and can be easily understood that the variance of the cell nuclei is higher than that of the surrounding cytoplasm, and this can be used for further textual segmentation step. Following fixed binary thresholding, on a pixel by pixel bases and using a 3 x 3 kernel the grey-level variance is calculated in the area defined by the high and low thresholds. A threshold of the variance then precisely defines the position of the segmentation boundary. This method provides the advantage that the efficient textural segmentation is only used in the area of uncertainty and not the whole image.

(A)   (B)
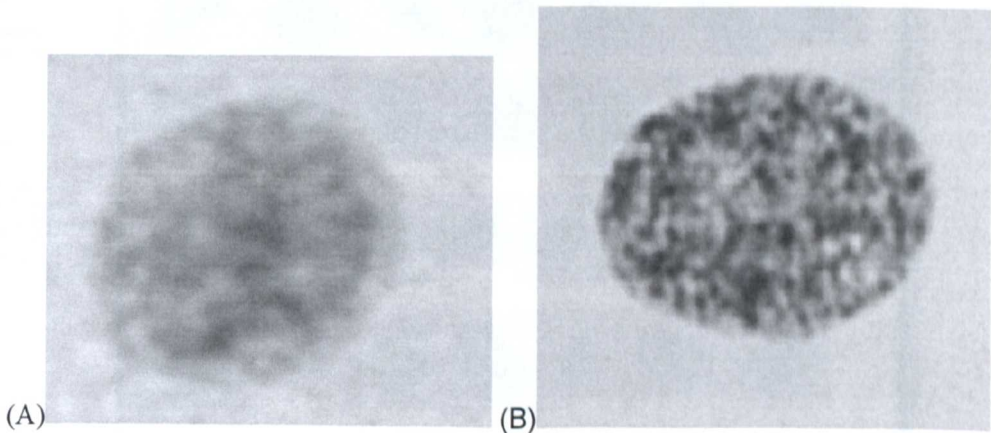
Figure 6.9 Original nuclei images
(A) Cytoplasm around cell; (B) No Cytoplasm visible

Figure 6.10 Area for texture based segmentation.

Example of the segmentation results are shown in **Figure 6.11**, as can be seen the segmentation remains reliable even with a large amount of cytoplasm still present. After segmentation has been completed it is the local background which is used for the calculation of IOD as described later.

Figure 6.11 Segmentation results. Blue lines show segmentation borders.

This system has been tested with many different samples to test its robustness, as detailed in Chapter 7.

6.4.1 Shade Correction On Greyscale Images

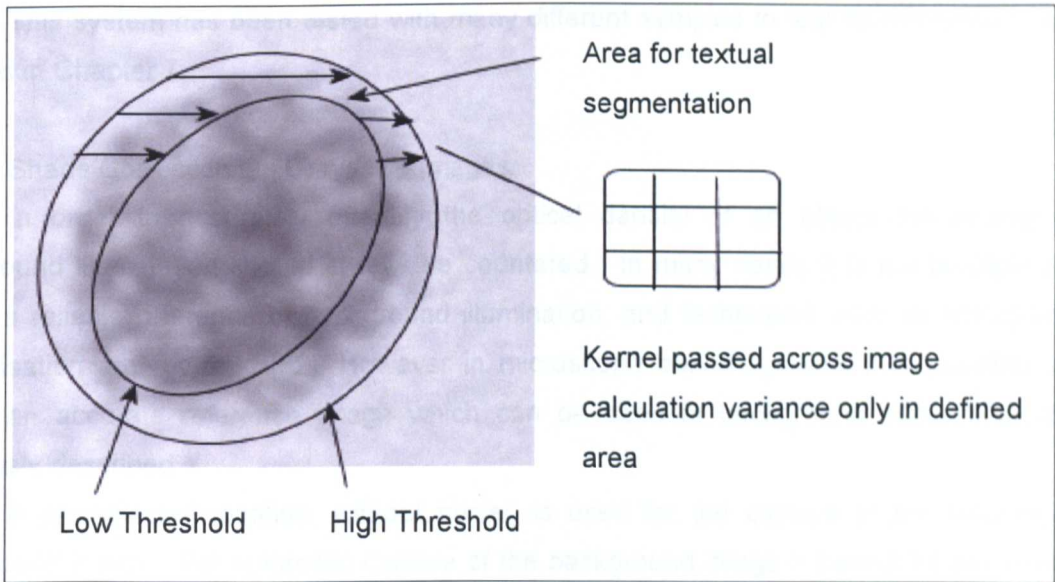In order to accurately quantify the optical density of an object the changing background illumination should always be countered. In many cases it is not possible to obtain a reliable reference of background illumination, and techniques such as histogram normalisation are required [62]. However in microscope based systems it is possible to obtain an accurate reference image which can be used in background subtraction as previously described.

A pre-selected location, without nuclei, is used for the capture of the reference background image. For automatic capture of the background image it cannot be assumed that the pre-selected position is free of artefacts. In the implemented system two images are captured. In order to ensure that the images are free from local artefacts, these images are compared to each other. If there is more than 3% difference in intensity between the two images, the shade image is rejected and the system automatically captures two further images in an adjacent location. The figure of 3% was chosen after practical experimentation to provide a good difference level between two genuinely blank images that are subject to unavoidable small amounts of image noise and other physical debris on the slide.

Once the image to be used for shade correction is selected, a shade correction algorithm as shown in **Equation 5.3** (Page 60) is applied, and the resultant image is used for all further image processing. **Figure 6.12** shows captured cell nuclei before and after shade correction.

(A)

(B)

Figure 6.12 Captured cell nuclei with and without shade correction

(A) Without shade correction. (B) Shade corrected nuclei.

6.5   Parameter Calculation

For each of the captured objects parameters are calculated that parametrically express nuclei captured objects as shown in **Table 6.1**. The new measures that have been developed allow for the classification system to determine if the objects under test are either intact nuclei of interest, a cut or folded nucleus, a double (two nuclei connected together) or an artefact. The newly developed algorithms marked with an * are presented at the end of this chapter, along with any of the less obvious implementations of existing algorithms.

Parameter
1. Area
2. Perimeter
3. Optical Density
4. Integrated Optical Density
5. Maximum Diameter
6. Minimum Diameter
7. Sum Of Intensities
8. Sum Of Square Intensities
9. Number Of Grey Levels
10. Form Factor
11. Shape Factor
12. Symmetry*
13. Jaggedness*
14. Biggest Flat Spot*
15. Concave*
16. Radial Variance*
17. Calibrated Area
18. Calibrated Maximum Diameter
19. Calibrated Minimum Diameter
20. Angular Change*
21. Grey Level Variance
22. Grey Level Variance * Area
23. Kurtosis

Table 6.1 Calculated parameters

To determine the importance and redundancy of the calculated parameters for classification, a test set comprising of objects and cell nuclei from 5 clinical cases were captured using the system. Following automatic classification the objects were manually edited giving a total number of 19,117 objects, classified as: Gallery 1 Epithelia cells (cells from the tumour); Gallery 2 Lymphocytes (white blood cells); Gallery 3 Plasma cells (a mature Lymphocyte); Gallery 4 Fibroblasts (cells contributing to the connective tissue of the

body) and; Gallery 5 Artefacts or nuclei that had been damaged during the slide preparation procedure. Linear discriminate analysis was completed to determine the importance of individual parameters in the classification of nuclei from artefacts as shown in **Table 6.2** and the importance of individual parameters for the classification of cell nuclei types as shown in **Table 6.3**. For all the analysis the Integrated Optical Density (IOD) parameter was removed as this is the parameter using within the DNA Image Ploidy test to determine the quantity of DNA within the cell nuclei so it is not appropriate to consider IOD as a classification parameter.

Feature	Classification correctness from discriminate analysis of a single variable
Symmetry	72.90%
Concave	72.40%
Angular Change	66.60%
Shape Factor	64.90%
Kurtosis	57.30%
Grey Level Variance * Area	55.70%
Biggest Flat Spot	55.40%
Form Factor	55.00%
Grey Level Variance	54.60%
Colours Used	52.50%
OD	51.70%
Jaggedness	51.20%
Perimeter	49.70%
Calibrated Maximum Diameter	48.20%
Maximum Diameter	48.20%
Radial Variance	46.70%
Sum Of Square Intensities	45.50%
Sum Of Intensities	45.00%
Area	44.60%
Calibrated Area	44.60%
Minimum Diameter	37.60%
Calibrated Minimum Diameter	37.60%

Table 6.2 Classification potential between cell nuclei and artefacts resulting from linear discriminate of single variables.

Feature	Classification correctness from discriminate analysis of a single variable
Minimum Diameter	77.80%
Calibrated Minimum Diameter	77.80%
OD	73.40%
Grey Level Variance * Area	72.60%
Maximum Diameter	69.20%
Calibrated Maximum Diameter	69.20%
Sum Of Intensities	66.50%
Area	66.00%
Calibrated Area	66.00%
Sum Of Square Intensities	65.50%
Perimeter	62.60%
Symmetry	62.50%
Concave	54.60%
Kurtosis	53.90%
Biggest Flat Spot	53.70%
Jaggedness	52.90%
Shape Factor	40.40%
Form Factor	32.40%
Radial Variance	26.40%
Colours Used	23.90%
Angular Change	22.70%
Grey Level Variance	22.10%

Table 6.3 Classification potential between cell nuclei types resulting from linear discriminate of single variables

In order to determine the redundancy of the parameters stepwise linear discriminate analysis was performed, again between cell nuclei and artefacts and on the cell nuclei only. The results of this are shown in **Table 6.4** and **Table 6.6** respectively. The Wilks' Lambda statistic shown is a statistical measure used to measure the difference between the group populations at each step of the stepwise linear discriminate analysis process.

Step	Variable Entered	Wilks' Lambda Statistic
1	Symmetry	0.75542
2	Angular Change	0.69729
3	Minimum Diameter	0.65600
4	Jaggedness	0.63905
5	Concave	0.63549
6	Calibrated Area	0.63135
7	Kurtosis	0.63006
8	Optical Density	0.62849
9	Grey level Variance	0.62615
10	Sum Of Square Of Intensities	0.62261
11	Colours Used	0.62087
12	Perimeter	0.61826
13	Maximum Diameter	0.61678
14	Grey Level Variance * Area	0.61532
15	Biggest Flat Spot	0.61504
16	Shape Factor	0.61487

At each step, the variable that minimizes the overall Wilks' Lambda is entered.
Maximum significance of F to enter is .05.
Minimum significance of F to remove is .10.

Table 6.4 Stepwise discriminate analysis of parameters to determine parameter redundancy when classifying between artefacts and cells.

Parameter Name

Area
Sum of Intensities
Form Factor
Radial Variance
Calibrated Minimum
Diameter
Calibrated Maximum
Diameter

Table 6.5 Parameters excluded from stepwise discriminate analysis between artefacts and cells

Step	Variable Entered	Wilks' Lambda Statistic
1	Optical Density	0.25276
2	Form Factor	0.17805
3	Shape Factor	0.13878
4	Colours Used	0.11436
5	Grey Level Variance * Area	0.10423
6	Concave	0.09971
7	Sum Of Square Of Intensities	0.09680
8	Perimeter	0.07662
9	Calibrated Maximum Diameter	0.07523
10	Symmetry	0.07395
11	Angular Change	0.07308
12	Minimum Diameter	0.07234
13	Sum Of Intensities	0.07190
14	Grey Level Variance	0.07143
15	Jaggedness	0.07111
16	Kurtosis	0.07082
17	Radial Variance	0.07058
18	Biggest Flat Spot	0.07043

At each step, the variable that minimizes the overall Wilks' Lambda is entered.
Maximum significance of F to enter is .05.
Minimum significance of F to remove is .10.

Table 6.6 Stepwise discriminate analysis of parameters to determine parameter redundancy when classifying between nuclei types.

Parameter Name

Area
Maximum Diameter
Calibrated Area
Calibrated Minimum
Diameter

. **Table 6.7** Parameters excluded from stepwise discriminate analysis between cell types.

As can be seen from **Table 6.2** and **Table 6.3** Minimum Diameter and Calibrated Minimum Diameter; Maximum Diameter and Calibrated Maximum Diameter; Area and Calibrated Area have the same importance when considering individual classification importance. These parameters only differ in that the calibrated values have been scaled to represent real world measures from the pixel equivalents. One of the pairs was removed by the stepwise discriminate analysis as shown in **Table 6.4 - Table 6.7**. Discriminate analysis also found that Sum of Intensities; Form factor and; Radial variance did not contribute to discriminate classification effectiveness in the case of classifying between artefacts and cell

nuclei as shown in **Table 6.5**. Area was completely excluded when classifying between cell types. The only parameters that are seen to be redundant when considering both classification requirements are the parameters that express size characteristics in calibrated units where a non calibrated equivalent exists or visa versa. The one excluded is dependant on the arbitrary order in which the parameters are listed for stepwise discriminate analysis.

The results from linear regression show that the parameters related to the shape of the object in terms of its symmetry and perimeter characteristics are most important for determination if the object under study should be considered an artefact or an real nuclei. This is because the artefacts are fragments of other cell compartments or nuclei that have been damaged during the preparation process. For determination of the cell type the optical density and shape of the object are found to be of most importance, this is because all of the intact nuclei have a generally smoothed surface and the size, shape and compactness of the DNA contributing to the optical density is what characterises the difference between the cell groups.

6.6 Classification

There are different forms of classification systems that can be used to provide the classification of cell nuclei. Existing classification systems include neural networks [140-143] and genetic algorithms [140-143] and decision tree based methods [144-146]. When selecting the classification system for inclusion in the system, a method had to be chosen which was both understandable by biomedical scientists and provided the ability to discretely control the selection criteria to ensure that selection was not made on criteria that could adversely effect the final DNA Ploidy classification. A further consideration was also that the use of neural networks for the classification on cell types has Intellectual Property (IP) protection in the form of a granted patent and to use this method would have incurred either commercial risks or costs. The use of a decision tree based method was selected, where the selection criteria are defined by a set of rules. The parameters to be used can be discretely selected, each stage in the classification process can be verified independently, and the selection parameters can be iteratively tuned. The decision tree implementation allowed for each rule to define a minimum and maximum value for each parameter and a definition of the process to be followed if the rules was either passed or failed. The processes that are supported are, to apply another rule, delete the cell nucleus or move it to a cell gallery. The decision tree used is shown in **Figure 6.13**.
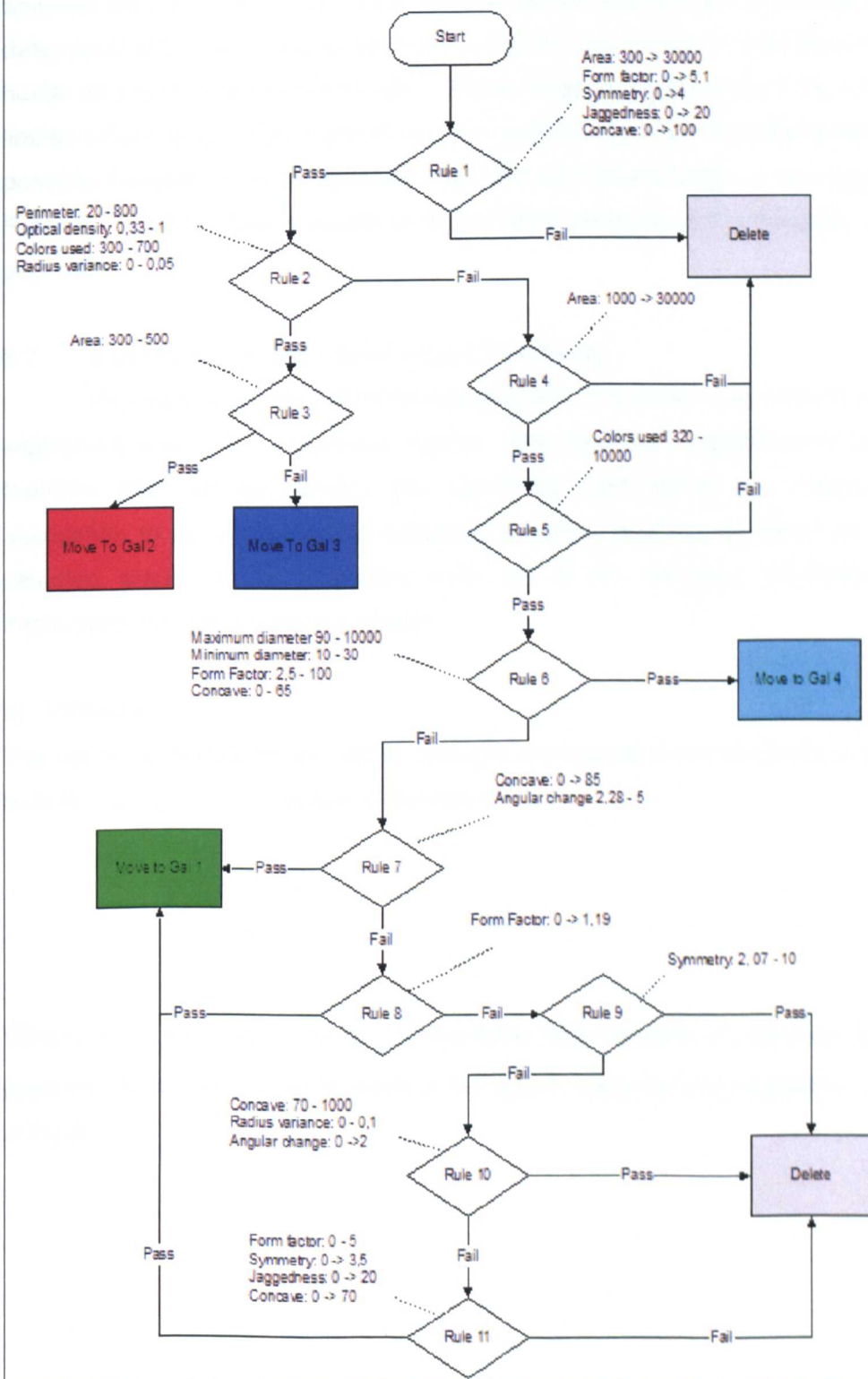
Figure 6.13 Decision tree used for classification.

As shown in **Figure 6.13** four classification galleries are used: 1. assumed epithelial cells; 2. assumed lymphocytes; 3: assumed plasma cells; 4: assumed fibroblasts. Rule 1 rejects very small and large objects; Rule 2 filters nuclei that are below the expected size for epithelia cells and have a OD range as expected for lymphocytes or plasma cells; Rule 3 determines if the nuclei is a lymphocyte or plasma cell, based on size; Rule 4 rejects large nuclei as a further refinement of rule 1; Rules 5 rejects objects likely to be artefacts due to limited colour range; Rule 6 places nuclei in gallery 4 that fulfil the criteria selected for possible Fibroblasts; Rule 7 classifies epithelia cells on the bases of cell regularity and Rules 8-11 reject artefacts based on shape factor measures and irregularity of the boundary perimeter.

6.7 Algorithms For Quantitative Image Processing

This section is split into three sub-sections. The variance and the multiple regression algorithms used in the auto-focus system. The parametric algorithms to calculated object features and the last section the algorithms used within the Histogram Draftsman application to allow the user to complete statistical analysis on either the whole or user selected areas of the histogram data. All of the following parameters have been implemented in the developed systems.

a) Variance

The variance calculation is used to calculate a measure of the accuracy of the focus in the auto-focus algorithm explained in Section 6.3.

$$\sigma^2 = \frac{\sum (\overline{P}_{im} - P_{im})^2}{N}$$

.. (6.1)

Where σ^2 is the pixel variance, $\overline{P}_{im}$ the mean pixel intensity, P_{im} the pixel intensity for each pixel and N is the number of pixels in the object. Variance is increased for objects that are in focus.

b) Multiple Regression

$$Z = a_0 + b_1 x_1 + b_2 y_1$$

The residual is given by

$$R^2 = \sum [y_i - (a_0 + b_1 x_1 + b_2 y_1)]^2$$

.. (6.2)

Where a_0 is the offset Z axis offset, b_1 and b_2 are calculated factors for the stage positions x_1 and y_1. R^2 represents the residual error. For the calculation of the coefficients in the implemented system a standard least squares fitting algorithm has been used.

6.7.1 Parametric Calculation

Following accurate segmentation, parametric calculations are performed on each cell nuclei. These calculations make it possible for the decision tree classification system (explained below) to remove artefacts, to sort the nuclei into different galleries as well as providing information that will be used to create the IOD histogram to be used for DNA Ploidy classification.

a) Perimeter

$$P = 1.41.N_{Diagonal\_Pixels} + N_{Vert\_Hoz\_Pixels}$$

.. (6.3)

Perimeter P is the number of boundary pixels in the segmented object. $N_{DiagonalPixels}$ is the number of pixel on the perimeter of the object diagonally connected to neighbours and $N_{Vert\_Hoz\_Pixels}$ is the number of pixels connected to neighbouring pixels either vertically or horizontally.

b) Mean Intensity

$$\overline{Intensity}_{im} = \frac{\sum_{n=0}^{n=N_{im}} Intensity_n}{N_{im}}$$

.. (6.4)

$\overline{Intensity}_{im}$ is the mean intensity inside a segmented area and N_{im} is the number of pixels within the object, *Intensity$_n$ is the pixel intensity for individual pixels.*

c) Shape Factor

$$ShapeFactor = 2.\left(\frac{Area}{Perimeter.(\frac{Diameter_{max}}{2})} \right)$$

.. (6.5)

Shape factor is a parametric measure used to describe the circularity of an object where shape factor for a circle=1. *Area, Perimeter* and *Diameter* are object dimensions in pixels.

d) Form Factor

$$FormFactor = \frac{Diameter_{max}}{Diameter_{min}}$$

.. (6.6)

Form factor is the measure used to describe the shape in terms of the length of its minimum and maximum diameters, as opposed to shape factor in Section 3.2.3 which references object to a circle using perimeter and area measures. *Diameter$_{min}$* and *Diameter$_{max}$* are the minimum and maximum diameters of the segmented cell.

e) Optical Density

$$OD = -\log(\frac{MeanIntensity_{im}}{MeanIntensity_{bk}})$$

.. (6.7)

Where Optical Density is OD. MeanIntensity$_{im}$ is the mean intensity of the segmented object and *MeanIntensity$_{bk}$* is the mean intensity of the background area.

f) Integrated Optical Density

$$IOD = \sum_{n=0}^{n=N} -\log(\frac{Intensity_n}{MeanIntensity_{bk}})$$

.. (6.8)

Where *IOD* is the integrated optical density of the object, *N* is the number of cells in the segmented cell nuclei image. *Intensity_n* and *MeanIntensity_{bk}* are the object and background intensities. In this case the background intensity is the area inside the bounding box, but excluded by the generated segmentation mask.

g) Centroid

$$Cx = \frac{\sum_N m_i . x_i}{\sum_N x_i} \quad and \quad Cy = \frac{\sum_N m_i . y_i}{\sum_N y_i}$$

..(6.9)

Where *Cx* and *Cy* are the centroid coordinates for both the *x* and *y* axis *m* is the number of points for in the corresponding image positions *x* and *y*.

h) Symmetry
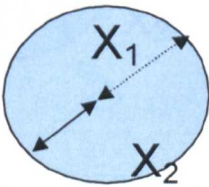
$$Symmetry = \left(\frac{\sum_{n=i}^{N} \sqrt{(X_{n1} - X_{n2})^2}}{N} \right)$$

.. (6.10)

Symmetry is used to detect uneven of cut cells or cells that are touching each other. X_{n1} and X_{n2} are vector pairs, π radians around the perimeter of the object with the centroid at the centre There are *N* equally spaced paired vectors.
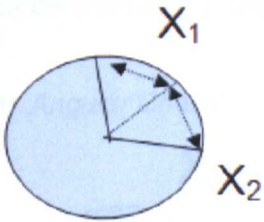
i) Jaggedness
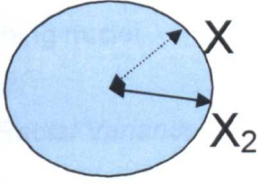
$$Jaggedness = \left(\frac{\sum_{n=0}^{n=N} \sqrt{\left(X_n - \left(\frac{median(X_{(n-n+5)})}{5} \right) \right)^2}}{N} \right)$$

.. (6.11)

Jaggedness is the measure of the roughness of the object. By calculating local differences in radial distance, this measure can be used to detect cut nuclei or to distinguish artefacts from nuclei that are of interest. X_n is the distance from the perimeter to the centroid of the object.

j) Biggest Flat Spot

$$MeanLengthOfPerimeterSections = \left(\frac{\sum_{n=0}^{n-N} X_n}{N} \right)$$

$$BiggestFlatSpot = \frac{Max_x}{MeanLengthOfPerimterSections}$$

..(6.12)

Where the perimeter of the object is first divided into N angularly equal sections. The biggest flat spot is then calculated as a ratio of the longest vertices and the mean length of all of the perimeter sections. This parameter is useful for use within the classification system to determine if the object is a cut nuclei.

k) Concavity

$$Concavity = \frac{ConvexHull_{Area}}{Mask_{Area}}$$

.. (6.13)

Concavity is the area difference between the true area and that of a convex hull of the perimeter. This parametric measure is used to detect touching nuclei. $ConvexHull_{Area}$ is the

area defined by the convex hull of the object and $Mask_{Are}$ is the area of the segmented object. This parametric measure can be used to determine if a object comprises of two touching nuclei.
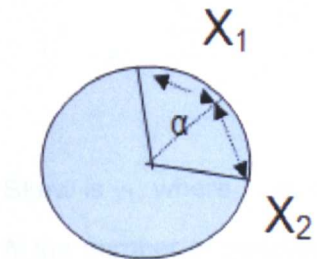
l) Radial Variance
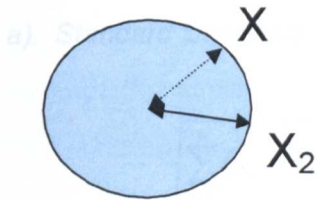
$$RadialVariance = \left(\frac{\sum\limits_{n=1}^{N} \sqrt{(x_i - \bar{x})^2}}{N} \right)$$

.. (6.14)

Radial variance is the parametric measure used to determine how much the radial distance deviates around the perimeter of the measure nuclei. x_i is the distance from the perimeter to the centroid of the object and $\bar{x}$ is the mean radius.

m) Angular Change

$$AngularChange = Max_{\alpha}$$

..(6.15)

Where the perimeter of the object is first divided into N angularly equal sections. The *AngularChange* is then calculated as the largest angle α, between any two adjacent vertices.

6.7.2 Statistical Calculations Used Within The Histogram Draftsman

The following calculations act on the selected histogram display, in most cases this will be the IOD (Integrated optical density) histogram of the captured objects. These algorithms have been defined for inclusion within DNA Image Ploidy applications in the ESACP consensus report of DNA image Ploidy [64].

a) *Standard Deviation*

$$\sigma = \sqrt{\frac{\sum_{i=1}^{N}(x_i - \bar{x})^2}{N}}$$

.. (6.16)

Standard deviation is σ, where $\bar{x}$ is the mean value, x_i the sample value and N the number of samples.

b) *Skew*

$$\gamma_1 = \frac{\sum_{i=1}^{N}(x_i - \bar{x})^3}{N.\sigma^3}$$

.. (6.17)

Skew is γ_1, where $\bar{x}$ is the mean value, x_i the sample value and N the number of samples, N the number of samples, σ the standard deviation. The measure shows the distribution of the histogram.

c) *Kurtosis*

$$\gamma_2 = \frac{\sum_{i=1}^{N}(x_i - \bar{x})^4}{N.\sigma^4} - 3$$

.. (6.18)

Skew is γ_2, where $\bar{x}$ is the mean value, x_i the sample value and N the number of samples, N the number of samples, σ the standard deviation. The measure shows the degree of peakedness of the distribution.

d) Coefficient Of Variation

$$CV = \frac{\sigma}{\overline{x}}.100$$

.. (6.19)

CV is Coefficient Of Variation, where σ is Standard Deviation and $\overline{x}$ the mean. This measure is used to measure the spread of each of the histogram peaks, it can also be used as a quality of data measure or when reviewing a single cell line.

e) Entropy

$$H(x) = \sum_{x=1}^{N} p_i Log_2(p_i)$$

.. (6.20)

Entropy is *H(x)*, where p_i is the probability of each histogram bin *(x/X)* and represents the level of order of a histogram.

f) Exceeding Rate

$$5cER = \frac{N(>5C)}{N}$$

.. (6.21)

The *5cER* is the percentage of cells with a DNA content of *5C* or above, for this parameter to be calculated the 2C point must first be defined. Exceeding rates are also calculated for 2.5C, 5C and 9C.

g) 2C Deviation Index

$$2cDI = \frac{\sum_{i-1}^{N}(x_i - \overline{x})^2}{N}$$

..6.22)

2cDI is the variance of the 2C histogram peak as defined by the user. Where $\overline{x}$ is the Mean and N the number of samples in the selected area.

h) DNA Index

$$DI = \frac{Mode(peak)}{Mode(2c)}$$

.. (6.23)

The *DNA Index DI* is the calculated of a selected histogram peak based on the *2c* reference point.

i) Malignancy Index

$$MI = 2cDI.5cER$$

.. (6.24)

Malignancy Index (MI), where *2cDI* is the 2C deviation index and *5cER* is the 5C exceeding rate.

6.8 Contribution To The Aims

A novel automatic DNA Image Ploidy system has been presented, showing the practical application of the developed methods meeting the aim to develop an automated DNA Image Ploidy system as described in Section 1.3.3. A new method for obtaining optimum focus of a specimen prepared onto a cytospun monolayer which uses multiple linear regression to allow optimum focus to be achieved on a per object basis something that normally would not be attempted due to the processing time taken to focus each field with traditional methods. The automatic segmentation method presented accounts for the residual cytoplasmic overlap on some cell nuclei and uses a combination of textural and binary segmentation techniques. Parametric feature calculations performed on each nucleus have been presented and using these measures a binary decision tree method allows for the classification of each object into galleries that contain specific cell groups. The classification method serves to reject artefacts and incomplete nuclei which have been captured from the specimen.

System validation and clinical tests are provided in Section 7.2. The system has been used by customers and collaborators in different areas these include, Oral Leukoplakia, Hydatidiform moles and Ovarian cancer information of this clinical work has been in the clinical papers published by collaborators and are listed in the initial sections of

this Thesis, this work has been introduced in Section 7.3. A technical paper describing the method described in this chapter has been produced [147].

The next chapter presents experiential results obtained using the developed system in clinical and biological studies. This work has been completed in collaboration with various academic sites and is testimony to the ease of use of the developed systems. For the reconstruction and visualisation system three different datasets are presented, the preparation techniques, the methods used and any new findings are described. The results of the experimental studying for the automatic DNA Image Ploidy system are presented showing comparisons between manual and automatic measurements as well as clinical studies using the automatic system.

Chapter 7 Experimental Test Results

This Chapter has three sections. The first section presents results obtained using the 3D reconstruction and visualisation system as described in Chapter 5. The second section presents results from the automatic DNA Image Ploidy system described in Chapter 6. The third section clinical studies which have been completed using the automated DNA Ploidy system are introduced. The results shown in this section are a result of individual work and collaboration with academic groups. . The work detailed in this chapter represents to work required to meet the aim of evaluation of completed work using clinical tests as described in Section 1.3.4.

7.1 3D Reconstruction And Visualisation

The work presented here is novel in respect to the visualisation of datasets from serial sectioned histological samples using the developed systems. It has been proven by these results that the developed systems can be used by biomedical scientists to provide valuable insight.

In considering the following datasets, it is possible to see visually if a dataset has been successfully re-registered, through the detail of structure that can be observed in the x-z and y-z planes. This chapter also does not include all datasets that have been aligned and reconstructed using the systems, as these have been successfully commercialised there have been many instances of reconstruction of datasets both with and without input from the author. For the work shown here the author configured hardware systems used for both the data capture and subsequent software manipulation, aided in the data capture, serial section alignment and use of the developed systems in order to gain he visualisations shown. Three datasets are presented in this chapter showing results obtained using the systems. The three experiential results shown all have associated co-authored publications, these are Three-Dimensional Reconstruction of Human Breast Carcinoma [129], 3D Reconstruction of Human Axillary Lymph Nodes [130;148] and; Imaging of Afferent Neurons from Semi-thin Sections of Drosophila Ganglia [131], which is the nervous system within the fruit fly.

7.1.1 Three-Dimensional Reconstruction Of Human Breast Carcinoma

The aim of this study was to determine if the developed systems could be used to explore the 3D biological structures involved in invasive ductal carcinoma which is a type of breast cancer, using normal laboratory equipment.

a) *Dataset Preparation*

1cm^3 sample of breast tissue obtained from a case of invasive ductal carcinoma. 128 sequential serial sections 20µm apart and a thickness of 4µm were cut and mounted on glass slides. An antibody is a protein used within the immunohistochemical technique to identify an area of interest in the tissue. For this study a primary antibody a mouse monoclonal anti-human cytokeratin (clone AE1/AE3) used in an optimal dilution anti-c-erbB-2 antibody, the secondary antibody (biotinylated goat anti-Mouse/Rabbit immunoglobulin; Duet K 0492, DakoCytomation, Denmark). 3-3'Diaminobenzidine tetrahydrochloride (Dako liquid DAB plus, K3468, Denmark) was used as a chromogen which is used within the immunohistochemical process to enable visualisation of the antibody [129].

b) *Methods*

Images were captured on a DMRXA microscope (Leica, Germany), equipped with a Proscan stage and controller (Prior scientific, UK) and a Pifoc focus device (PI, Germamy). Images captured using a C4742 camera (Hamamatsu Photonics, Japan).

Data were captured using the automated system with the selection of the 5x objective lens, a larger area than required was scanned to avoid later problems due to misalignment and mismatched image sizes.

As can be seen in **Figure 7.1** there were large translational differences between the serial sections as seen on the orthogonal views by the jagged dark areas. The dataset has been converted to grey scale intensity in preparation for 3D reconstruction after image capture, and as can be seen in **Figure 7.2** the actual sample has very poor contrast with that of the background of the slide. The poor contrast shown in this dataset made alignment and reconstruction difficult.

The dataset was aligned using the semiautomatic method described in Chapter 5 and shown in **Figure 7.1**. Before reconstruction the dataset was median filtered to remove noise and to limit minor mismatches from the alignment process. Reconstruction has been completed using a variety of rendering techniques to review the most applicable method as shown in, reasonable representation of the dataset has been achieved. BTF rendering was chosen selecting a colour pallet which showed normal tissue in yellow and Ductal Carinoma In Situ (DCIS) in blue as shown in **Figure 7.2**. Opacities were chosen so that the DCIS areas were more opaque than the normal tissue which was used as a reference for the location of the DCIS areas.
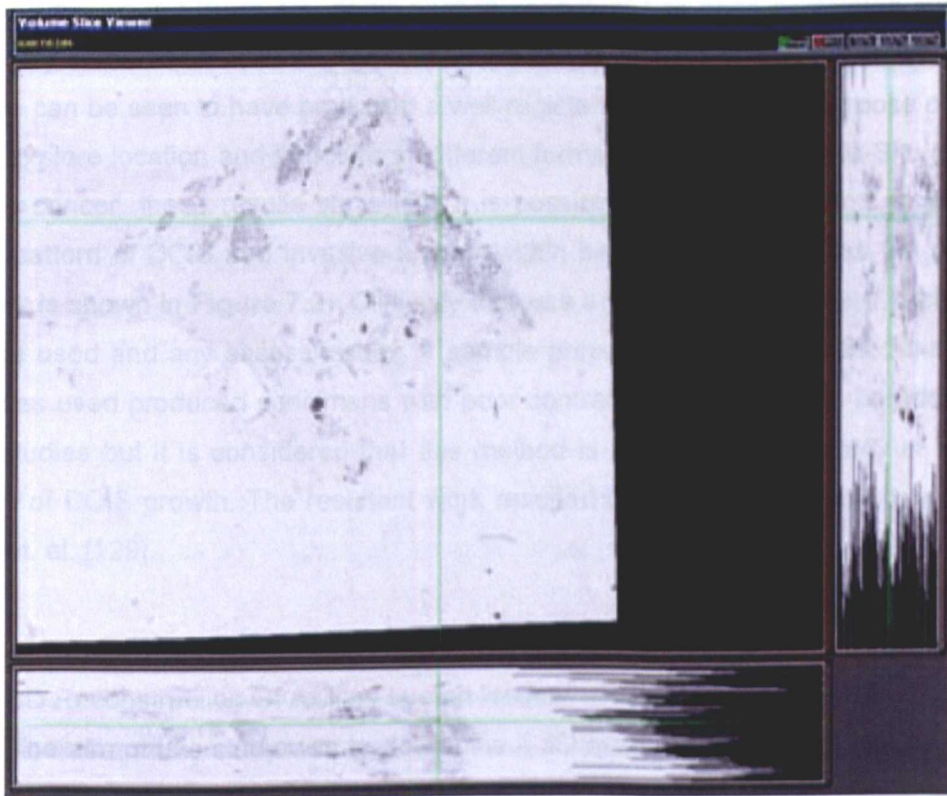
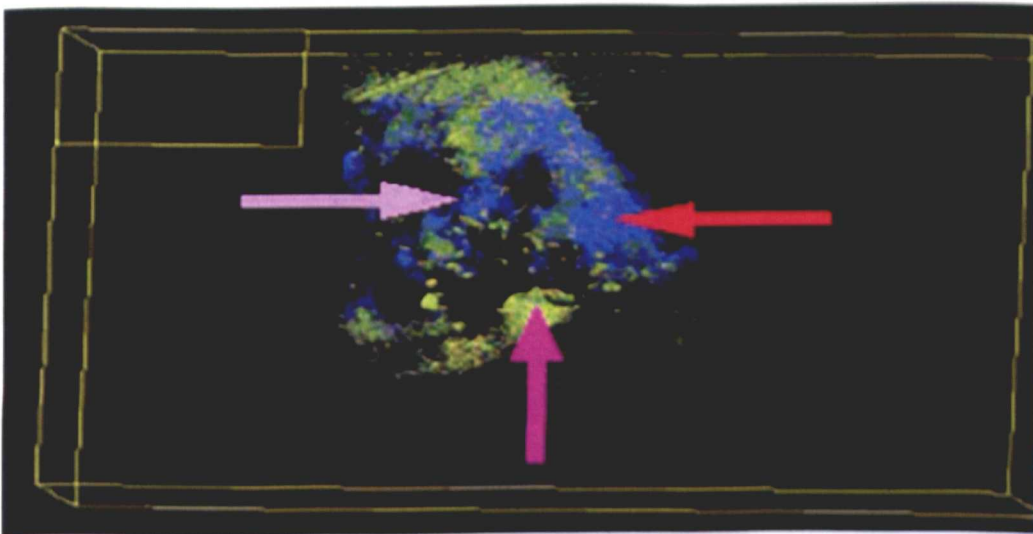**Figure 7.1** Aligned breast tissue dataset

Figure 7.2 Maximum point rendering of DCIS

c) New Findings

As shown in **Figure 7.1**, serial section alignment has been completed successfully. The quality of the serial section alignment can be seen in the X-Z and Y-Z views, where the software can be seen to have produced a well registered dataset. The purpose of the study was to explore location and structure of different forms Ducal Carcinoma In-Situ (DCIS) and invasive cancer, these results show that it is possible to use the systems to explore the growth pattern of DCIS and Invasive tumour within breast cancer samples. An example of this work is shown in **Figure 7.2**. Clinically this was a pilot study to review if such a system could be used and any assess issues in sample preparation. As mentioned the choice of antibodies used produced specimens with poor contrast, this will need to be addressed for future studies but it is considered that this method is viable for larger study of the growth patterns of DCIS growth. The resultant work resulted in a paper co-authored with Thomas Kurien et. al. [129].

7.1.2   3D Reconstruction Of Axiliary Lymph Nodes

The aim of this study was to determine if 3D reconstructions could be completed of Axiliary lymph nodes using the developed system, and standard laboratory equipment. Axiliary lymph nodes are glands which help the body fight infection and can become affected by breast cancer. This study has been completed in collaboration with Claire Paish, Nottingham University, and credit is given for the preparation and the image capture of data using the systems provided. The data in brief and method was presented by the Author July 05 at Medivis (London).

a) Dataset Preparation

Axiliary lymph nodes from breast cancer patients, containing areas of metastatic tumour signifying the spread of cancer from one area to another were selected. In the following images blue areas represent normal nodal tissue, and red areas define the areas of spread of cancer (metastasis). Each lymph node was serially sectioned at 4µm, and sections at 20µm intervals were selected and stained immunohistochemically a process where an antibody is bound to a specific biological instance and then has another compound attached so it can be seen with a bright field microscope. In this case with a broad spectrum cytokeratin antibody (AE1/AE3) in order to localise the metastatic tumour cells. Each node yielded, on average approximately 100 sections for 3D reconstruction.

b) Methods

Images were captured on a DMRXA microscope (Leica, Germany), equipped with a Proscan stage and controller (Prior scientific, UK) and a Pifoc focus device (PI, Germany). Image have been captured used a C4742 camera (Hamamatsu Photonics, Japan). This dataset has been captured using systems designed as part of this report, aligned and rendered using the system developed with advice and help from the author.

The dataset has been aligned using the systems as described in Chapter 5, as shown in **Figure 7.3**, it has been possible to achieve good segmentation between the metastatic and normal areas within the captured dataset.

c) New Findings

The 3 dimensional reconstruction of tumour-containing lymph nodes enables the area of metastasis to be visualised from all angles, rather than just 2 dimensions as routinely the case in normal evaluations performed by pathologists using serial sections. By viewing the tumour in 3 dimensions, it is possible to evaluate if certain growth patterns are associated with particular tumour types and grades. Evaluation of the significance of the location of the metastatic deposit within the node is also possible. The results of this work resulted in two papers co-authored papers [130;148].
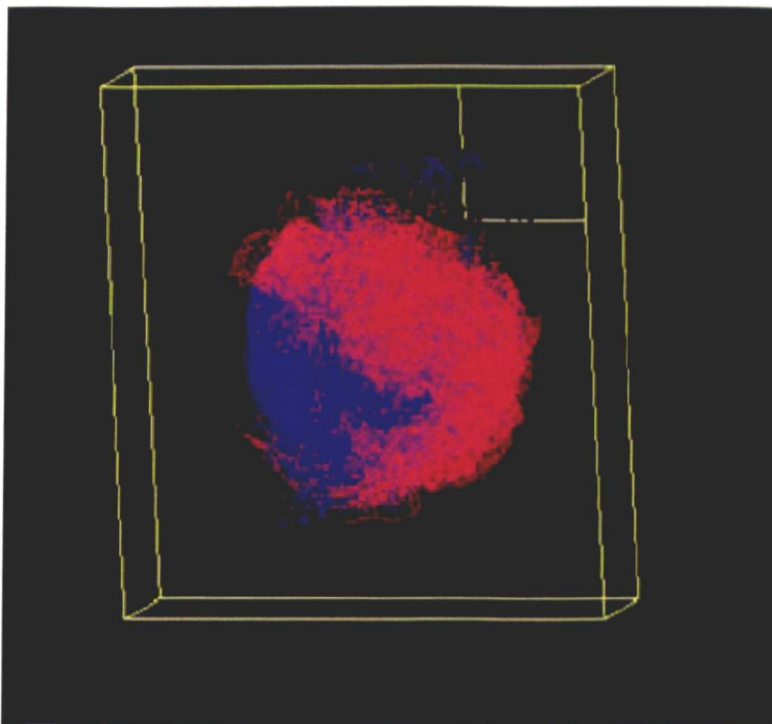
Figure 7.3 Flood filled and Object rendered Lymph node

Using this data as a reference, initial study was completed to review if it would be possible to correctly set isosurface thresholds as required by surface rendering. Reviewing if the results obtained were comparable to that obtained using the developed Voxel rendering system. The comparison was completed using the results shown in **Figure 7.4** which was produced using Matlab (Mathworks, USA) and then Bryce (Corel Inc, USA). Results using contoured isosurfacing were also produced and are shown in **Figure 7.5.** using VTK (Kitware Inc) to TCL script for this is shown in Appendix C.
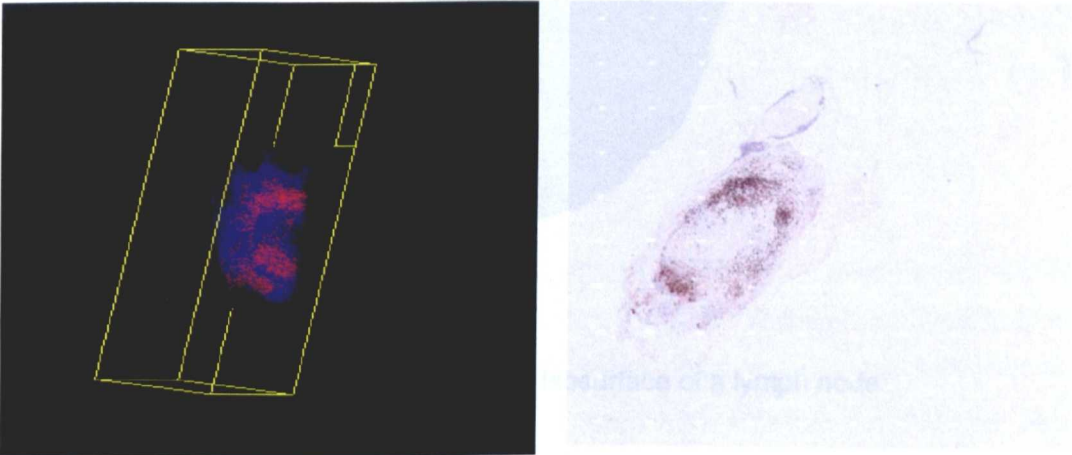
Figure 7.4 Reconstructed Lymph node (left). Original image (right).

Figure 7.4 Isosurfaced and ray traced lymph node
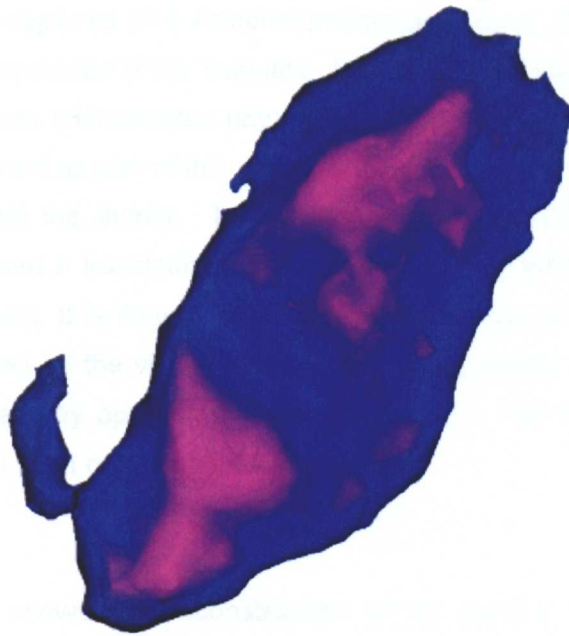
Figure 7.5 Contoured Isosurface of a lymph node

7.1.3 Imaging Of Afferent Neurons From Semi-Thin Sections Of Drosophila Ganglia.

The aim this study was to develop protocols for computer imaging of the thoraco-abdominal ganglion (nervous structure) of Drosophila (a family, within in a genus of fruit fly) from serial semi-thin sections, in which specific neurons were stained and related by immunohistochemistry, Nomarski optics (differential interference contrast) were used to show motor neuron targets in the neuropil (complex mesh of nerves). While not a clinical application of 3D reconstruction and visualisation the method has clinical application the same techniques can be applied to clinical specimens.

a) Dataset Preparation

The Thoraco-abdominal ganglion complex from adult fruit flies were dissected from the GAL4 enhance trap line c42. After fixation the Green Fluorescent Protein (GFP) was made visible to white light. The ganglia was soaked over night at 4°C in anti-GFP antibody (Boehringer-Mannheim) at a concentration of 1:200. The ganglia were embedded and sections cut (approx 200) following the celloidin wax sandwich method [149]. 2μm sections were cut, and dried at 60°C. After dewaxing and rehydrating the sections were mounted in glycerine jelly and imaged.

b) Methods

Images were captured on a Aziophot microscope (Zeiss, Germany), equipped with a Proscan stage and controller (Prior scientific, UK). 8 bit grey scale images were captured using a C4742 camera (Hamamatsu photonics, Japan). This dataset has been captured using systems designed as part of this report, and aligned using the system developed with advice and help from the author. In the alignment of the objects a manual bias was discovered that caused a translational and rotational skew, while this effect could not be seen on other datasets. It is thought that due to the structure of the dataset the user was prone to be influences by the visible neuropil (nervous system). The dataset rotation was removed by systematically applying a correction factor to individual slices of the dataset based on the rotation seen on the dataset as a whole.

c) New Findings

Figure 7.6. shows the reconstruction of fly ganglia from serial sections, to understand how a given neuron interacts with others required that the identity of which it makes contact is known, such information is known about very limited number of neurons. This study has been to evaluate both imaging and microscopy methods using the drosophila as very complex example with high levels of image detail. The same strategy has particular utility for the analysis of regions of the mammalian brain, that like Drosophila ganglion are not organized in a regular spatially ordered pattern. This study resulted in a co-authored paper with M. Tyler, et al. [131].
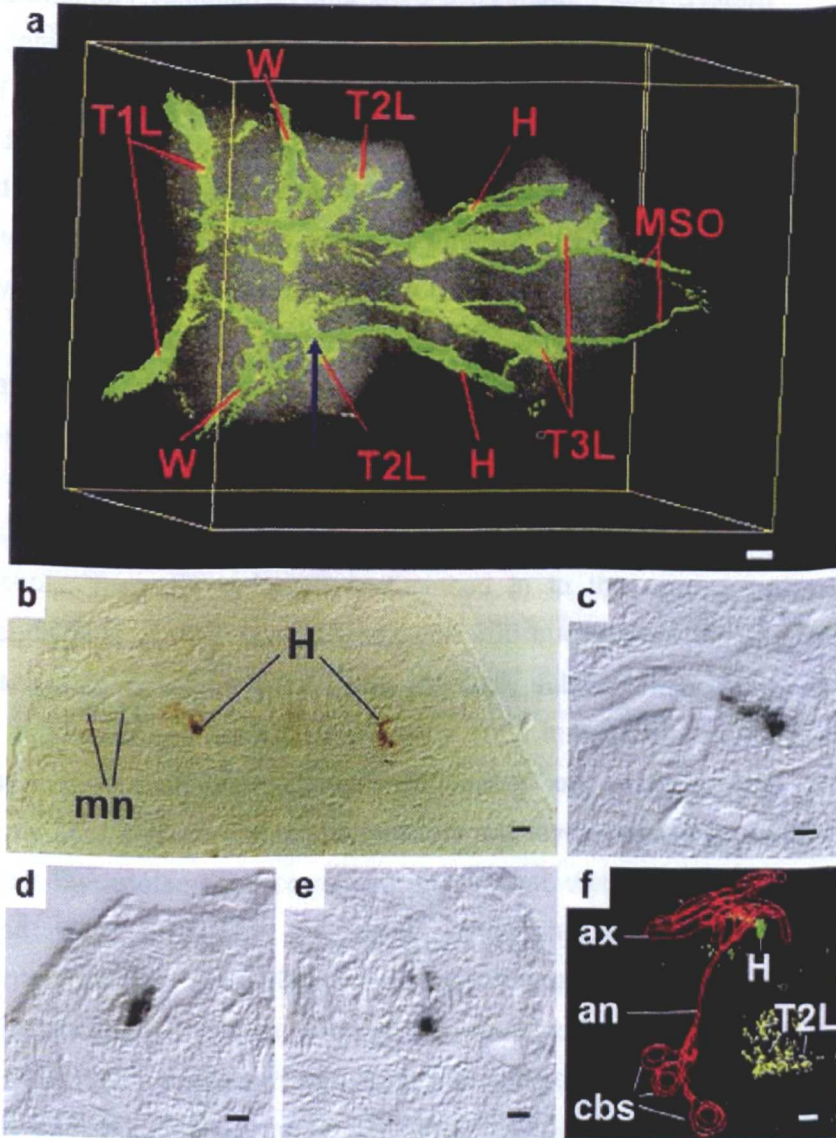
Figure 7.6 Reconstructed fly ganglia

(a) Dorsal view of 212 2 µm sections transgenically labelled, anterior is to the left. Section b is taken from location of the blue arrow. (b) Dorsal region of section 62 from the image assembly, showing projections of chordontonal afferents from the halteres immmunostained with peroxidase and neuropil features revealed with Nomarski optics. (c-e) Examples of contacts made by branches of haltere chordontaonal afferents (f) Assembly of images from sections 53-62 with contiguous profiles.

7.2   Experimental Evaluation – Automated DNA Image Ploidy System

To determine if there is a reduction in manual burden any effects on the final outcome of the Ploidy classification, 141 cases of prostate cancer from a retrospective clinical study were selected (cases from 1987-1995). Both manual and automated cell capture and classification has been performed on these cases.

The cases measured were prepared as follows. The tissue area of current interest, identified by a pathologist, was selected (microdissected) from paraffin embedded material. The tissue was enzymatically digested to yield a suspension of nuclei, centrifuged and placed on a slide to form a monolayer. The monolayer was stained with Feulgen's stain to verify the nuclei. The monolayer was then put under a microscope attached to a camera and robotic stage-focusing unit as described in Chapter 6. For manual collection, each field of view was focused and the nuclei were thresholded manually by interactive selection of a binary threshold, manually selected and placed in to the correct gallery. For manual collection, each field of view was focused and 300 nuclei were thresholded manually by interactive selection of a binary threshold, manually selected and placed in to the correct gallery. For automatic collection approximately 1500 images were automatically captured and put in different folders/galleries, depending on nucleus type. For automatic measurements after capture, trained technicians visually assessed the nuclei, excluding the ones affected by artefacts or correcting those that were misclassified. The resulting classifications were QA'd by the same cyto-technicians that made the manual measurements. The final DNA Ploidy classification was made from an Integrated Optical Density (IOD) histogram, based on information calculated from the different galleries.

The DNA Ploidy histogram was classified using the following criteria. A sample was considered to be diploid if only one 2C peak (first major peak in the histogram) was present and 4C peak did not exceed 15% of the total epithelial cells. If the 4C peak was larger than 15%, or there was a peak present in the 8C position, the sample was considered tetraploid. The 15 % limit was set on the basis of DNA Ploidy analysis of normal prostate tissue from autopsies. The sample was considered aneuploid when a peak appeared outside 2C, 4C or 8C ranges.

System speed, quality of captured data, accuracy of classification and final Ploidy histogram classification has been compared for data collected by automated and manual methods.   System speed was assessed to review the potential of time saving that this new system provides. The quality of data was reviewed by comparing Coefficient of Variation (CV) where (CV = StdDev/mean*100) of 2C peak of the collected data samples to review accuracy of the automatic system with that of existing manual methods, in terms of segmentation and cell nuclei focusing. The correctness of cell classification was reviewed,

as this is the most significant task requiring human interaction. Finally a comparison was made on the final DNA Ploidy classification between manual and automatic methods, as any differences in these classifications could affect patient treatment in a clinical setting.

Basic summary statistical descriptors have been used to compare the two sets of results for system speed, correctness of automatic cell grouping classification and final DNA Ploidy classification. A paired T-Test was used to compare the difference in the quality of data captured.

7.2.1 System Speed

Approximate time of cell capture of automated and manual data collection was recorded for 24 cases measured manually and 14 measured automatically. 350 nuclei on an average were captured for the manual timings and 1200 on an average for automatic capture. Mean collection time was 85 minutes for manual measurement and 68 minutes for automatic measurement. The data collected automatically required approximately 20 minutes per case to edit and review the collected galleries. This is not required for manually collected data as the user selects the nuclei prior to inclusion in to specified galleries. Summary results are shown in **Table 7.1.**

	Mean number of nuclei captured	Mean capture time (minutes)	Mean editing time (minutes)	Manual interaction required (minutes)	Interaction time per nuclei (seconds)
Manual	350	85	-	85	15
Automatic	1200	68	20	20	1

Table 7.1 Nuclei capture times

In terms of elapsed time, automatic collection of data was found to be faster than manual collection on a per nuclei basis. However more significantly was the reduction in manual intervention where the operator was only required for placement of the slide on the system. The collection time of approximately 85 minutes for manual measurement required continual manual intervention, where as for automatic cell capture this is reduced to approximately 20 minutes to verify the classification of the capture nuclei. Automated operation has allowed the number of cell nuclei that are collected to be dramatically increased. The automated system can practically collect 1500 epithelial nuclei in approximately one hour, with a subsequent editing time of 20 minutes. It would take a manual operator up to five hours to collect the same number which is impractical.

7.2.2 Quality Of Data Capture

To determine if the data collected by the automatic system was as accurately collected in terms of segmentation and automatic focusing, the CV for the 2C peak for both the automatic and manual system were compared. Using a paired T-Test, the differences between the CV of the two sets of data were checked for statistical difference. The mean CV's were 3.75 and 3.66 for the manual and automatic system, respectively. The differences between the two groups was not statistically significant ($p = 0.3$). A summary of the results is presented in **Table 7.2**.

	Automatic	Manual
Number of patients	141	141
Mean CV of 2C peak	3.66	3.75

Table 7.2 Summary measurements for manual and automatic data capture

The novel methods introduced using object based auto-focus method and the segmentation system are found to work well. The new hybrid segmentation system was found to be an effective method to automatically segment the nuclei from both the background and the surrounding cytoplasm. As well as producing well segmented nuclei the hybrid method allows for the segmentation to be completed rapidly as required due to the large number of nuclei captured.   The object based multilevel auto-focus system implemented allows for effective and rapid focusing of cell nuclei of multiple planes following monolayer preparation. The accuracy of data collection in terms of the calculated CV of the data collected between manual methods and the automatic system were found to be statistically equivalent.

7.2.3 Accuracy Of Automatic Classification

Manual classification is an onerous procedure under normal circumstances and can only be completed viably by either a cytologist or a cyto-technician, to study the classification correctness increased detail must be recorded, increasing further this time consuming process, as such a limited number of cases were first reviewed and the results gained from this smaller study used to infer assumptions on a larger study. Five of the 141 cases were chosen at random to review the accuracy of the decision tree method for correctly grouping cell types in detail. The accuracy of classification was determined by the changes following automatic classification; either insertions or deletions completed by the

user either to or from the epithelia cell gallery (1). The mean classification correctness was found to be 82% for this small sample reviewed in detail; results are shown in **Table 7.3**. The Percentage correct original classification = (number of nuclei after edit- number of nuclei imported from other galleries) / number of nuclei before edit.

Test I	Before Edit	After Edit	Removed from Gallery 1	Imported from other Galleries	Total number of nuclei changes	Percentage correct original classification
1	1486	1136	352	2	354	76.20%
2	1479	1386	93	0	93	93.70%
3	1070	902	168	0	168	84.30%
4	1471	1213	260	2	262	82.20%
5	1420	1096	336	12	348	75.50%
Standard Deviation	178.10	176.23	110.61	5.02	113.81	7.37%
Mean	1385	1147	242	3	245	82.40%

Table 7.3 Correctness of automatic classification

The standard deviation of the number of cells before editing is shown in **Table 7.3**. The standard deviation in the number of nuclei captured by the system of 178.10 for the 5 cases, this is caused by the variation of the density of cells within the preparation differences between specimens.

The mean classification correctness was found to be 82.40% with a standard deviation of 7.37%. The majority of the incorrectness of classification was accounted for by the removal of nuclei from the Gallery rather than insertions. The deviation in accuracy of classification is a result of setting of the values boundaries used in the classification tree to fixed values which are found to best provide the highest average classification correctness. Due to biological variation for each specimen there is a variation in the characterises of nuclei within the specimen. Biological differences can also increase the number of artefacts in any specimen so the proportion of the number of artefacts to objects will increase making the probability of mis-classification higher.

Following the detailed examination and confidence gained that most of the changes arose from removal of nuclei from Gallery 1 a larger subset of 50 samples was used to measure the correctness of classification with the assumption that the only changes made were removal of cells, this is shown in **Figure 7.7** and **Table 7.4**. The reason for obtaining results on classification in this way was that as the manual re-classification has to be completed by cyto technicians it was considered overly onerous to request that such high level of detail was recorded for the classifications of all samples within the study. For most

of the cases from the larger study fell within the values expected, however there was one case where the classification correctness was very low. On checking this case it the preparation was found to contain more than the normal amount of artefacts which followed the earlier observation.

Number of Cases	Mean	Minimum	Maximum	Standard Deviation
50	81%	31%	97%	12%

Table 7.4 Number of cells remaining in Gallery 1 following classification as a percentage of the original number
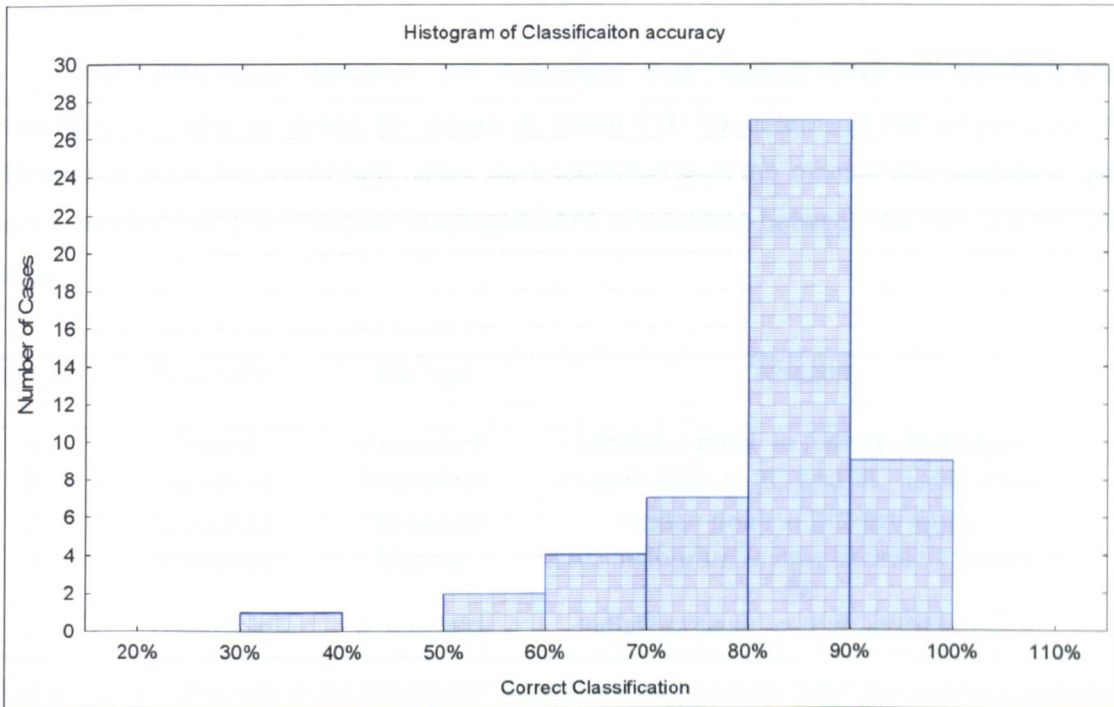
Figure 7.7 Classification correctness

7.2.4 Comparison Of DNA Ploidy Classifications

DNA Ploidy classification was made on data collected both manually and automatically. The concordance between the methods is shown in **Table 7.5**.

	Data collected manually			
Data collected automatically	Aneuploid	Diploid	Tetraploid	Total
Aneuploid	10	1	2	13
Diploid	1	88		89
Tetraploid	1		38	39
Total	12	89	40	141

Table 7.5 Concordance of histogram classification from results captured by automatic and manual DNA Ploidy systems.

The differences between the automatic and manual DNA Ploidy histogram classifications were reviewed as shown in **Table 7.6**. To determine the reasons for the differences, once the discordant cases were identified both the manual and automatic data were reloaded into the histogram draftsman and comparison between the two graphs were made.

Case No	Automatic	Manual	Reason
A	Diploid	Aneuploid	Indistinct peak in manual histogram
B	Aneuploid	Tetraploid	Hidden peak in 2C and 4C distributions
C	Aneuploid	Tetraploid	Hidden peak in 2C distribution
D	Aneuploid	Diploid	Initial histogram review showed 2 peaks in 2C
E	Tetraploid	Aneuploid	Indistinct peak in manual histogram

Table 7.6 Differences in the histogram classifications between the manual and automatic capture

The histograms for case D are shown in **Figure 7.8**. As can be seen it is possible to see two peaks within the data collected using automatic method, where it is not visible in the data collected using manual methods.
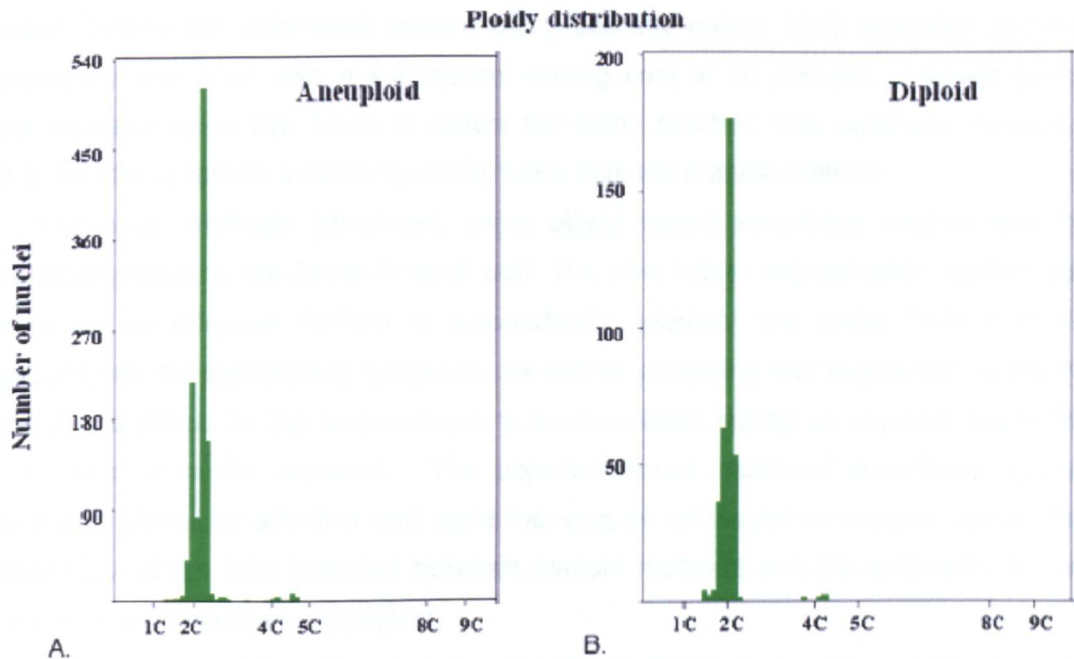
Figure 7.8 Comparative histograms

The 2C peaks are set by reference cells (not shown). A) The automatic capture shows an aneuploid population next to the 2C peak. B) In the manual capture of case D a diploid distribution is shown, the aneuploid peak is not visible.

In 136 of 141 cases (96 %), there were concordances between the DNA Ploidy histograms in automatic and manual analysis. In three of five cases the automatic system showed aneuploid histograms while the manual measures did not. It seems that an increase in sensitivity and number of nuclei captured makes it easier to define aneuploid peaks. The two remaining cases showed aneuploid, but indistinct, peaks in the manual histograms. It is believed that these uncertain peaks are not genuine, and that an automatic measure shows a more correct DNA Ploidy distribution, due to increased sensitivity and number of cells captured.

7.2.5 New Findings

In terms of elapsed time, automatic collection of data was found to be faster than manual collection on a per nuclei basis. However, more significant was the reduction in manual intervention, where the operator was only required for placement of the slide on the system. The collection time of approximately 85 minutes for manual measurement requires continual manual intervention, where as for automatic cell capture this is reduced to

approximately 20 minutes to verify the classification of the capture nuclei. Automated operation has allowed the number of cell nuclei that are collected to be dramatically increased. Where the automated system can practically collect 1500 epithelial nuclei in approximately one hour, with a subsequent editing time of 20 minutes, it would take a manual operator up to five hours to collect the same number. The automatic system is found to be 15x as fast on a nuclei by nuclei basis than the manual method.

The novel methods introduced, using object based auto-focus method and the segmentation systems are found to work well. The new hybrid segmentation system was found to be an effective method to automatically segment the nuclei from both the background and the surrounding cytoplasm. As well as producing well segmented nuclei the hybrid method allows for the segmentation to be completed rapidly as required due to the large number of nuclei captured. The objected based multilevel auto-focus system implemented allows for effective and rapid focusing of cell nuclei of multiple planes The calculated CV of the data collected between manual methods and the automatic system were found to be statistically equivalent.

The accuracy of the manual and automatic methods were also compared for the clinical tests that have been completed genealogical cancers in an early cases over the last two years at Rikshospitalet – Radiumhospitalet HF (Oslo). The CVs of the 2C peaks for the manual and automatic methods was found to be 3.33% (95% CI 3.23:3.42) and 2.93% (95 CI 2.85; 3.03) 366 case and 545 cases, respectively. An independent T-test was completed and this difference found was found to be significant ($p<0.0001$).

Using parametric extraction equations and the implemented decision tree classification system as presented, the mean accuracy of the classification of nuclei into groups used within the system was found to be 82 %.

In 136 of 141 cases (96 %), there were concordances between the DNA Ploidy histograms in automatic and manual analysis. This means that for the histograms of Integrated Optical Density (IOD) reviewed and classified by a pathologist using data collected on both systems 96% of the resulting classifications were identical.

As well as increasing the number of nuclei captured, the DNA Ploidy method would benefit if the accuracy of measurements could be increased. Future work should critically asses the image capture methods to review if further increases in accuracy can be obtained. Improvements on the system may come from improvements of the focus, segmentation of shade correction of parametric data extraction as well as refinement in the preparation and staining methodology. Any increase of the specificity will further increase the usefulness of DNA Image Ploidy in detecting DNA abnormalities.

In summary, the system presented is found to provide advantages in performing the DNA Image Ploidy procedure. Advantages are found in terms of reduction of labour burden and the ability to increase the sampling. As the speed of the computing platform increases, the elapsed time to complete the measurement is expected to decrease. The main manual burden remaining is the editing of galleries that have been captured and classified automatically; it may be possible in the future to increase the accuracy of classification. However, care will have to be taken to ensure that abnormal cells are not incorrectly classified, affecting the final Ploidy classification.

7.3   Medical Clinical Evaluation

Clinical evaluation of the DNA Image Ploidy using the system developed has been completed by users of the system. Three applications of the application and the results from these published works are introduced, illustrating how the system has been used for clinical study on Ovarian cancer; Oral cancer and in use in the refinement of the diagnosis of Hydatidiform moles. The scientific results that have been obtained by these studies is briefly explained. For these studies the author's role was to commission, setup, and calibrate the hardware and software systems. Aid was given to the end users on the use of the system, including tuning required of the rules system for the classification system.

7.3.1   Heterogeneity, Histological Features And DNA Ploidy In Oral Carcinoma

The study was completed by the Department of Oral Pathology, Guy's Hospital using the system developed and presented in this Thesis. The aim of the study was to determine if Oral squamous carcinomas were heterogeneous using DNA Image Ploidy and if there was correlation with histological parameters [150].

a) Method

6x50 µm sections were cut from each selected area, dewaxed in xylene, rehydrated and the nuclei extracted using protease type XXIV (Sigma Chemical Co., Poole, UK). Monolayers were prepared using a cytospin 4(Thermo Shandon, UK) and stained by the Feulgen-Schiff method. The nuclei were collected using the system described in this thesis. A total of 225 monolayers were analysed, from 42 carcinomas with a minimum of 300 nuclei imaged per sample. The DNA Ploidy classification method was completed using published methods [105]. The specimens were also graded histologically using a standard pathology grading system.

b) New Results

The results presented found that the DNA Ploidy status was closely related to nuclear morphology but poorly to differentiation. The results that DNA Image Ploidy can be used to analyze smaller samples than flow cytometry as smaller tissue samples can be used making it more suitable for review of the heterogeneity as the nuclei analysed can be morphologically controlled. The discussion describes that some of the samples gave false negative results, possibly due to sampling errors, and that previous work suggests that sample size has a role in the correct determination of heterogeneity. The data presents that of the 42 samples analysis 16 were found to be heterogeneous, and that in order to confidently diagnose an oral squamous cell carcinoma as diploid a minimum of 5 samples must be analyzed. The automatic system due to time efficiencies allows for the higher number of samples to be analyzed.

7.3.2 Prediction Of Long-Term Outcome For Women With Invasive Stage 1 Ovarian Cancer.

This study was completed by the department of Gynecologic Oncology and the department of Pathology at the Norwegian Radium Hospital using the developed system. The objective of the study was to determine if DNA image Ploidy was of use in predicting long-term survival of patient with early ovarian cancer. The study was completed on 284 cases with clinical follow-up information available for all patients. The paper introduces the importance of the identification of prognostic information as important as patients who suffer from relapses after surgery do so because of the presence of sub clinical metastases and the use of DNA Image Ploidy may be able to detect those patent at increased risk [151].

a) Method

Histological sections were reviewed by a Pathologist, and classification completed using World Health Organisation (WHO) criteria. The tumours were graded as well, moderate or poorly differentiated, with the exception of clear cell carcinomas and mixed tumour with clear cell elements. The specimens were prepared in a way as described in 7.3.1.1. Approximately 300 tumour nuclei were collected and stored, lymphocytes and plasma cells were included as internal controls when available. The histograms were classified by trained personnel without knowledge of the clinical outcome. Classification of the histograms where of diploid, tetraploid, polyploidy or aneuploid as previously described [105].

(A)

(B)

(C)
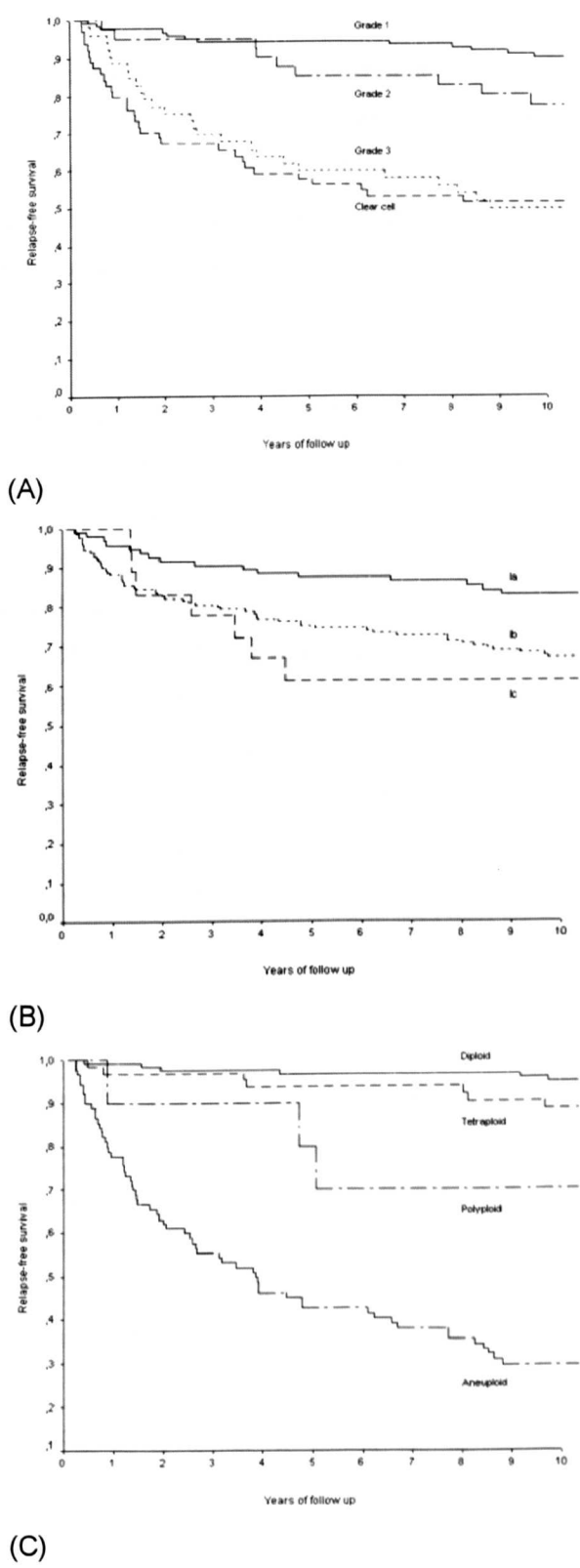
Figure 7.9 Relapse-free survival

(A) Grade of differentiation/clear cell histology; (B) FIGO Stage; (C) Relapse-free
survival according to DNA Ploidy classification by image cytometry

b) New Results

The paper reported that no difference in replase-free survival was seen with patient with clear cell tumours and poorly differentiated tumours. Patients with diploid or tertraploid tumours had a good prognosis. Patients with polyploidy or aneuploid tumours had a poor prognosis. The results from the paper are shown in **Figure 7.9** and show the clear prognostic advantage in using DNA Image Ploidy.

7.3.3 Hydatidiform Moles

This study was completed by the Academic Unit of Pathology and the Division of Genomic Medicine, at the University of Sheffield. Hydatidiform moles are abnormal gestations arising as a consequence of the fertilization of an abnormal ovum. The paper describes that the diagnosis of the Hydatidiform mole is clinically important because of the potential to give rise to future medical problems. The incidence of persistent disease is higher in patients with complete moles than partial moles. Flow cytometry is widely accepted as a rapid and easy test for Ploidy in this application area. The study looks at the comparison of using DNA image Ploidy and DNA flow Ploidy and the use of immunohistochemical techniques to refine the diagnosis. The paper describes that although with traditional manual systems for DNA Image Ploidy have been shown to have a greater specificity than flow with manual systems completion of the test is time consuming due to the manual processes required [152].

a) Method

40 cases were randomly selected and reviewed and confirmed in 38 cases, 22 cases were complete moles 16 partial moles. For flow cytometry a tissue block was selected and analysis using a flow cytometer, 10,000 cells were measured for each histogram. The specimens for DNA Image Ploidy were prepared as described[105], 1500 nuclei were captured for each specimen, taking approximately 30 minutes per sample, following automatic capture and classification manual review was completed and any further artefacts were rejected. Samples containing less than 300 nuclei were discarded. The p57^{kipp2} antibody was used for testing immunoreactivity, the preparation technique is described in full in the paper. The presence or absence of nuclear immunostaining was assessed independently by two individuals.

b) New Results

DNA Image Ploidy showed 21 of the 22 cases of complete moles had diploid histograms, triploid for 1 case. 13 of the 16 partial moles had triploid histograms 3 diploid.

The kappa scores between histological diagnosis and image cytometry was found to be k=0.78, k=0.79 between DNA image Ploidy and p57^{kipp2}. Agreement between flow and image cytometry is presented to be (Kappa score) k=0.88.

The paper concludes that in this study the Automatic DNA image Ploidy system was found to be a simple and rapid technique, more sensitive in detecting triploidy than standard flow cytometry which was confirmed in this study and had been introduced in previous papers. The automated DNA Image Ploidy technique had increased sensitivity compared to traditional manual DNA Image Ploidy systems.

This chapter has presented results and results from clinical obtained using the developed methods and systems. Objective results have been presented for the reconstruction and visualisation system. For the Ploidy system objective results have been presented comparing the developed automatic system with the traditional manual DNA image Ploidy method. Clinical studies have been introduced that have been conducted on the systems, these presented further comparison of the system and existing methods. The next chapter concludes on work completed for this study, and the progress against the aims as set out in Chapter 1, these include the development of objective and subjective microscopy systems; the development of software and image processing and visualisation for medical applications and the evaluation of developed software by experimental results. Further work that could extent the area of research is also presented in the next chapter.

Chapter 8 Conclusions And Further Work

Chapter 7 presented results that have been obtained using the systems as developed detailed in Chapter 4, 5 and 6. This chapter concludes on the work that has been completed in this study and suggests further work that could extend the area of research and suggestions for increasing acceptance for the systems presented.

8.1   Contribution

The research objectives for this study as stated in Chapter 1, Section 1.3. were 1.3.1 Development of an image capture system;1.3.2 Development of medical image algorithms for 3D reconstructions and visualisation; 1.3.3 Development of an automated DNA Image Ploidy analysis system and; 1.3.4 Evaluation of completed work using clinical tests.

Following research and review of the characteristics of the bright field microscope, its limitations and concerns related to resolution and digital image capture, an image capture system has been designed that allows for the image capture from the microscope. The system has employed third party hardware and that optionally supplied with the microscope by the manufacturer for the automation of the system, providing a flexible system for the development of qualitative and quantitative systems. A flexible software development environment has been implemented providing a framework for the development of specific applications. The framework has considered the image processing requirements for image processing required for robust analysis for clinical specimens.

A 3D reconstruction visualisation system has been designed and developed employing novel methods for both reconstruction and visualisation.

The automated DNA Image Ploidy system presented implemented novel methods for the automatic focus, segmentation and parametric extraction, providing a complete solution for the DNA Ploidy test in clinical applications.

There have been robust clinical studies completed on the systems yielding increased understanding for the subjects understudy and validating the new methods developed against existing methods. This study considered both the subjective and objective imaging needs for prognostic and diagnostic applications in microscope based systems, employing digital imaging and image processing techniques. This work has provided a good research base to consider the development of future application of advanced image processing techniques to address other clinical imaging needs.

8.1.1 Development Of An Image Capture System

The optical characteristics and issues related to digital image capture from a bright field microscope have been researched and described in detail. This has included the requirement for the selection of the correct lens type, consideration of the maximum resolutions that can be achieved and the selection of the correct imaging equipment. The hardware system implemented for image capture used generic systems for imaging, automation and processing, where the complete imaging system contains a bright field microscope, robotic stage, Piezo focusing device, and digital camera. The controlling computer is a generic personal computer running Microsoft Windows (98, 2000 or XP). All of the applications developed in this study have associated user manuals which explain in detail user operation of the system.

Image processing methods have been used and developed during this research. Algorithms for the illumination invariant analysis have been implemented. There has been consideration of the requirements for segmentation methods both for use in visualisation and as required to effectively segment objects for further analysis. The use of image texture has been used as an assessment criteria for the auto-focus system where has been used in combination with multiple linear regression to improve system speed when capturing individual object within a field, texture methods have also been used for the classification of cell types. The segmentation methods used within the automatic DNA Image Ploidy system have proved to be efficient both in terms of the results obtained and operational speed. Algorithms have been employed to perform parametric feature extraction from the segmented objects which have then been used to provide prognostic and diagnostic information as well acting as an input the classification system. The implementation of methods developed has proved to be robust with processing of hundreds of thousands of nuclei within the results presented within this report alone.

The systems developed have employed a modular design built on a generic system framework. The framework has provided generic hardware control and image processing features. The modular design that has been used has allowed for specific systems to be researched and developed effectively. The development of the systems has been completed using Visual Basic for the graphical user interface and Visual C++ for the back end functional code. While the development of the applications using these tools has undoubtedly taken longer than if there was extensive use of third party image processing libraries and 4GL development tools it has lead to increased understanding and commercial quality applications.

8.1.2 Development Of Medical Image Algorithms For 3D Reconstruction And Visualisation

Reconstruction for histological study has been studied in detail. An easy to use alignment software package has been developed that supports both manual and automatic rigid body alignment; warping and fiducial point alignment. The semi-automatic alignment method takes advantage of the Fibonacci search to allow full image cross correlation automatic search to be completed in near real time. The combined tools developed have allowed a multitude of datasets to be successfully registered by users. The results presented show increased insight in the given specific areas. While a warping function was developed it was not found to be of practical use, due to the level of objectiveness that could be inserted into the dataset by the user, and at the magnification for the datasets considered it was not obviously required.

As described within the report, when operating in manual mode there is a temptation for the user to follow structures which appear to be normal to the section, but if this is not the case then this will result in a skewed dataset. This was the case in the reconstruction of the fly ganglion, where the user had assumed prior knowledge of the structural arrangement data, a method was been developed to remove this effect in final datasets as detailed in Chapter 7.

A 3D reconstruction system has been designed and implemented as part of this study. The system, primarily a Voxel rendering package includes functions as provided in many other applications. Features developed as part of this study including depth encoded rendering systems, opacity animations and complex logical rendering system based on user selected object masks. However one if not the primary feature of the system is its ease of use, it was this reason that caused it to be selected as an OEM product and further proof is given by the independent research that has been completed using the system. Some comparative work was undertaken using surface rendering techniques; these methods show advantages for presentation of information without the advantage of movement but at the disadvantage of the loss of fine detail.

The literature describes the need for differing forms of segmentation of images; the two requirements have been met by this application with the use of histogram based segmentation techniques in the use of the opacity editor and for minimum and maximum point rendering modes. The requirements for region based segmentation have been met through the introduction of an object generation and masking system, that allows for user defined specification of objects leading to precise control of dataset visualisation characterises of the dataset. An opacity animation system has been designed which extends the requirements for imaging systems as found in the literature in that it uses the time element for the introduction of clarity of rendered objects where a distinct setting of an

intensity threshold is not possible. Opacity animation proves to be an effective tool for the study of areas of interest, while keeping the area under review in the full dataset in context. It offers a tool that can be used even for the most complex datasets where human interpretation of results is required, and effective segmentation cannot be achieved. Results arising from the study of different datasets are presented that have allowed for increased insight to be gained. Due the requirement to section prepare and image a large number of slides, future work is required to automate the process or find alternative imaging solutions, one possible solution may be provided by the development of new microscopy systems as discussed in 8.2.2

8.1.3   Development Of An Automatic DNA Image Ploidy Analysis System

An automated DNA Image Ploidy system has been designed, developed, tested and validated. The system has dramatically reduced the manual burden for the completion of this test.   Detail has been presented on the object capture, focusing, and parametric extraction and classification methods developed.   Specifically this included research and implementation of a novel focus method, segmentation system and parametric extraction methods.

Clinical study has tested the systems performance in terms of speed, image capture performance, and classification accuracy. The system was found to dramatically reduce the manual capture speed on per nuclei basis with the automatic system being approximately 4 times quicker while reducing manual burden to 1/15th of that when using a manual system. The image collection time is found to vary dependent on the density of the preparation of the cell nuclei. The image capture quality was found to be statistically equal between the automatic and manual system. Classification and rejection of artefacts was found to be 80% accurate.   Three clinical applications of the system have been introduced comparing the DNA Ploidy Image system with these existing methods of flow cytometry and exploring its use in allowing a more complete review of clinical cases.

The evaluations found the classification of the nuclei into correct cell type galleries, still required manual interaction. It is this area that if improved would be the highest impact in reducing the user amount of interaction required. It is considered that there are several methods that could be considered in order to increase the accuracy of the system. The methods can be seen as two fold, firstly to develop parametric descriptors that can identify more accurately the difference between valid nuclei and artefacts.   The main types of artefacts seen to be present are cut nuclei and objects which are comprised of two over lapping nuclei. It is possible that it may be possible to correct the overlapping nuclei by the use of the watershed segmentation technique.   The second part of system improvement

that would increase the classification accuracy would be to improve the setup of the classification method used. This could be achieved by giving the user more sophisticated tools to select the classification bounds or to change the method used to determine the cell groups away from the decision tree method currently employed. The tools that could help the user to select the parametric thresholds more efficiently include the integration of discriminate analysis and graphic display of the distribution of cell groups and artefacts. Early in application development a system was developed that allowed the weighting of calculated parameters, and a fuzzy logic selection of the correct gallery for each nuclei. It however was not possible for the user to setup the correct parameters. It is considered that concentrated development in this area may be able to produce a system that allows a semi automated selection of parameters from a training set. What ever method is developed in the future care has to be taken not to increase the overall accuracy of the system while decreasing the detection rate of abnormal nuclei. As well as increasing the number of nuclei captured, DNA Ploidy measurement would benefit if the accuracy of measurements could be increased. Future work should critically asses the image capture methods and specimen preparation to review if further increases in accuracy can be obtained. Improvements on the system may come from specimen preparation, auto-focus and segmentation methods and extraction of parametric data. Any increase of the specificity will further increase the usefulness of DNA Image Ploidy in detecting minor DNA abnormalities.

8.1.4   Image Processing And Quantification For Medical Images

The use of image processing for the quantification of medical images is diverse area with many differing potential applications. The considerations for machine vision and image processing differ from that optimal for human review. Machine vision can provide highly objective and repeatable quantification of images but requires normalisation of images and efficient segmentation of images to allow for processing to occur. The human reviewer can provide subjective and semi quantitative information and is tolerant of illumination effects and other distortions.

The work that has been completed on Automatic DNA Ploidy system is of most interest in the consideration of image processing and requirements for the quantification of medical images. The established use and requirement as detailed in the literature, for the use of a specific narrow band pass filter in the imaging the Feulgen stain has addressed and important criteria in reducing the effect of that differing illumination colour has on the eventual captured image removing the need for colour correction in this case. However the requirement for intensity normalisation for both segmentation and measurement remained. In the developed systems this has been tackled in two ways, firstly a reference background

image has been used to correct global issues, constant artefacts within the microscope such as dust on the optics, illumination differences across the field of view caused by uneven illumination. Local measurement of background intensity counters the effect that residual cytoplasm would have had on accurate Integrated Optical Density (IOD) measurement. Although image analysis methods can be developed to allow robust quantification it is also important to consider the method of preparation for the sample, in this case it can be seen that the cytoplasum would have effected the accuracy of IOD calculation had it not been accounted for..

The segmentation systems required in microscopy are highly specimen specific, and have ranging considerations. The DNA Ploidy system described uses a preparation method that separates cell nuclei from each other and the surrounding connective tissue and other components of the cell that are not of interest to the measurement method (cytoplasum and membrane), this while leaving significant challenges aided the segmentation challenge. Significant challenges still exist if for example individual sub cellular components (nuclei, cytoplasum and membrane) are to be distinguished from each other through segmentation techniques for further quantification. It is considered that the design of image processing systems benefits greatly from collaboration with medical scientists, where many methods can be used to aid in the quantitification of images, processing specimens so that the subject understudy is more suitable for image analysis. One example has been shown here with the use of the monolayer techniques and the Feulgen stain, another example is the ability to select the intensity and colour of the chromogen as used when employing Immunohistochemical (IHC) techniques.

Parametric extraction methods have been presented that describe individual cell nuclei in terms of its shape, texture, intensity and general morphology. These have allowed different type of nuclei to be grouped and the identification of artefacts. The algorithms presented are useful for objects that have been individually identified. It may not always be possible, or advantageous to accurately separate individual objects from each other and new parametric extraction methods would be required to be applied to regionally segmented areas.

Quantification of images from medical specimens requires consideration of sampling concerns. It is extremely rare in the case of quantification of microscopic images for the analysis not to take place on a sample of the original specimen. Considering the pathology review case, the original specimen is prepared and a selected area is taken and embedded in a paraffin block representing a sampling step, from this paraffin block a thin section is cut and placed on a slide representing a second sampling step selected areas are then reviewed. As such it not necessary to measure the whole area of the slide as this in no case

will represent the quantification of the specimen as a whole. There is concern however to measure a sufficient number of cells or to quantify sufficient tissue in order that minor relevant events can be detected. The requirement to measure a large enough representation also presents an issue in many manual method in medicine where manual counting of events is required, such as applications include where biomarkers are used to identify certain cells, which are then simply counted by hand to provide a prognostic score this requires a significant number of objects to be counted to ensure the robustness of the test. It is the combination of advanced image processing methods and the increased sampling that allows results compared to manual methods to have increased objectiveness, even for simple methods will prove to be extremely advantageous.

8.2   Further Work

Following the studies that have been completed, questions still remain as to the other systems that can be developed employing advanced image processing methods for clinical use and specific application areas that can be developed. Future work in this section in terms of clinical studying, advanced image processing and real time applications, telemedicine and distributed healthcare and other more generic concerns.

8.2.1   Clinical Studying

Clinical studying has proved to be a vital part of this study and will continue to be in any other developments in this area. It has provided two important factors for consideration in the development of systems, firstly that involvement of bio-medical scientist in the development of systems has produced systems that can find application upon completion that are suitable for the designed purpose. The second important element is that by user involvements during development the users have a clearer understanding of the developed system and are more able to continue independent research.

There are many other areas where employing advanced image processing methods could give rise to important developments using machine vision in clinical imaging. Both the technical research elements of future study need to be addressed and consideration given to the methods of validation and study required for new methods to gain acceptance in the medical community. This future research should not only consider the technical elements but consider the economic environment in which these applications are to be developed.

8.2.2 Advanced Imaging Processing And Real-Time Applications

While the bright field microscope has proved to be a good hardware base for the studies in this thesis is still not an optimum platform for high throughput use as required for clinical purposes. The microscope as detailed has been fitted with robotic stage and focus units that allow for initial automation to be completed. The acquisition elements of the system would benefit from slide loading automation. The aim would be to allow for many slides 50+ to be placed on the system and for all these samples to be scanned without human interaction. Existing commercial slide loaders are available such as the SL50 (Vision BioSystems Inc) allowing for 50 slides to be paced in the loader, and supports interfacing to existing microscopes. The use of such systems could further greatly reduce the manual burden and increase the capacity of the systems presented here. For the automatic Image Ploidy system, slides could be left to be captured overnight. For the 3D reconstruction studies the large number of slides that have to be imaged for each dataset could be completed in a couple of days.

Full slide loading automation presents additional challenges with regard to the correct positioning of the slide, accurate slide identification systems and robust failure mechanisms. The failure mechanisms are particularly important as there will remain circumstances where the system will be unable to automatically image specimens, and will require user intervention. These samples must be identified during the automated process and the system must allow for a semi automatic methods to be used to rescan failed slides. Also of consideration is the optical track in the traditional microscope, if a system is to be used for purely automated review there is no need for a human optical interface and considerations as to the optimum machine vision requirements can be revisited.

Developments of a new class of microscope is underway, these instruments provide integrated slide loading, stage and imaging systems. The optical/human interfaces have been removed. Such as system is one called Nanozoomer developed by Hamamatsu, Japan. The author has worked on aspects of software development of this system, particularly object identification, automatic focus system and storage of the large images that it produces (greater than 100,000 by 100,000 pixels). The system allows for 210 slides to be automatically scanned, and uses a line scan technique to complete this rapidly with a resolution up to 0.23 μm per pixel. While these dedicated systems will provide increased automation possibilities, many challenges are still present with concerns to the focusing systems and image normalisation. The concerns as to the optical considerations and system requirements discussed in this thesis remain the same, for these new systems as for standard microscopes.

The software environment used for development has been Visual basic and Visual C++ which at the time of development was the best choice in terms of low level flexibility and graphical user interface design. The Microsoft .Net environment now presents a more efficient development platform, future work should consider switching. As initial design separated the low level functional code from the user interface this is a practical proposition as functional code is able to remain in tact. Future work on the application development, particularly in consideration of the use of dedicated slide scanning systems, could be biased towards operation the internet using web browsers for visualisation and data review. It would be possible to consider this development for both DNA Ploidy and 3D reconstruction; the DNA Ploidy system is more suited.

There is pressure to produce results from research activities, and with the available 4GL development tools such as Matlab, it is certainly faster to complete research and development work required produce initial results. However 4GL development tools while increasing development speed are not necessarily the best option for implementation of systems where speed or usability are primary concerns, faster program operation may be achieved if dedicated image processing libraries are used or key elements of the application are optimised using low level code.

8.2.3 Telemedicine And Distributed Healthcare

As was found in the literature, there is increasing acceptance of the use of imaging within clinical applications using a variety of image capture methods and image processing techniques to improve subjective information. Since imaging systems are now being used in many situations local to the patient, it is only operational speed which prevents these applications being used for distributed healthcare solutions [153].

There are advantages of distributed healthcare solutions in that improved patent care can be offered while reducing travelling time, as it may be possible to visit a local centre rather than to travel to see a specialised consultant. There are potential improvements in patient care in that specific conditions can be referred to specialists where economics would previously have prohibited this. Speed of diagnosis may reduce and healthcare professional's time may be more optimally used. Second options may be more expediently be obtained, and thus allowing multiple opinions for more situations as standard. Telepathology may help with retention of staff in smaller institutions, where specialisation would be more easily possible due to the ability to route cases to the best person rather then those only immediately local.

Multi disciplinary meetings are considered to be of increasing importance for determination of most appropriate patent care. The use of telemedicine allows for the

various members of the patient treatment team (surgeons, oncologists, pathologists and radiologist) to meet virtually and to discuss cases, presenting findings and options visually as well as providing cross disciplinary education.

Digital imaging is used for medical application in many areas, image quality is considered acceptable and image collection methods efficient. For microscopy the image quality is acceptable but the speed of image collection and review even for local situations is still slower when compared with traditional methods, restricting it the introduction of image based systems. For other areas such as haematology rapid imaging systems are yet to be developed that provide the resolution required, as such technical developments are still required.

For applications where image quality and data collection methods are to an accepted level the challenges for the practical delivery of images remotely are those of speed, quality and economics. Quality is the first concern the must be met, an image not of diagnostic quality cannot be used, different compression standards are suitable for different imaging. Speed is a two fold concern, both the speed in which system can be used to reach a diagnosis and the elapsed time from data collection to when a response is required to determine future patent treatment. The consideration of both these speed requirements will determine the how a system should be designed and used, and the mode of operation best suited to the requirement. Non urgent applications for example can use store and forward methods to transfer data at night for optimal review speeds the next day.

The cost of domestic Internet connections are now extremely cost effective, however there are concerns and restrictions regarding patient confidentially when operating telemedicine over public networks, so the encryption methods need to be addressed and sanctioned by the National Health Service Information Authority (NHS IA) to take advantage of this. However like the advantages that have been gained by employing the advances in computing power driven by economic domestic and business needs it is likely that telemedicine networks in healthcare will benefit if methods are found to leverage the cost advantage in using public networks and the security issues are addressed.

Interoperability for telemedicine systems remains a major problem, the multiple providers of telemedicine systems have different standards, and hospital information systems are not standardised, as a result different institutions adopting systems from different providers reduces some of the advantages of telemedicine.

8.2.4   Others

Potential further application of the developed DNA Ploidy system is to determine rare events, directing the human observer to cells nuclei that require further evaluation.

Traditional DNA Image Ploidy is concerned with the characterisation of a nuclei population. There is an extension on this method that would allow not just the population to be studied but for abnormal nuclei (rare events) to be found within a normal population. It is thought that this type of system would find application in cervical screening. The method as yet remains unproven and technical advances have only recently been made that make such a system a feasible possibility, such advances are in the speed of the automation hardware and speed of camera system. A recent presentation at the ESACP conference Amsterdam, 2003 presents the background of the system as shown in Appendix B. The design of the system represents considerable speed and image processing challenges. For the system to find effective clinical use, it will have to be proven scientifically that this novel method can be used to accurately and robustly locate rare events of abnormal cases from within large normal cell population between 50,000 and 100,000 cells within a time frame of between 5-10 minutes. Consideration as to if the quality of the images required and can be compromised to achieve the required speed system, as the images are to be used for identification rather than objective measurement the requirements of image quality can be relaxed.

Appendix A Publication List

This appendix lists journal publications, submitted papers, conference presentations and patent publications.

Journal Publications and Submitted Papers

1. J.R. Maddison, M. E. Pretorius, W. Kildal, N.F. Clinch, G.Y. Tian and H. E. Danielsen; Automated image cytometry system for image capture, segmentation, classification and analysis for DNA Ploidy; Submitted Image and Vision Computing Aug 2005.

2. J.R. Maddison, V.M. Abeler, B. Risberg, A.Wotherspoon, P.Knudsen, N.Clinch, H.E. Danielsen; Diagnostic Accuracy in Telepathology; Submitted Journal of Human Pathology; Aug 2005.

3. E.C. Paish, J.R. Maddison, D. Macmillan, T. Kurien, A.R. Green, G.Y.Tian and I.O.Ellis; 3D reconstruction of breast tumour metastases within human axillary lymph nodes; Submitted J Pathol; Aug 2005.

4. J.R. Maddison, E.C Paish, T. Kurien, R.D. Macmillian, A.R. Green, G.Y. Tian and I.O. Ellis. 3D reconstruction and visualisation for exploration of human axillary lymph nodes. Medical Information Visualisation (Medi05-VIS) IEEE Computer society; pp55-59; July 2005;

5. J.R. Maddison, T. Kurien, E.C. Paish, A.R. Green, I.O.Ellis, G.Y. Tian; Practical application of Voxel based 3D visualisation in histology- Submitted image and vision computing; Jan 2005.

6. T Kurien, R W G Boyce, E C Paish, J Ronan, J Maddison, E A Rakha, A R Green and I O Ellis; Three-dimensional reconstruction of a human breast carcinoma using routine laboratory equipment and immunohistochemistry; Journal of Clinical Pathology, 58:968-972, Sept 2005.

7. C.J. Daly, A. McGee, E . Vila, A. Briones, S M. Arribas, S. Pagakis, J. Adler, A. Merle, J. Maddison, J. Pedersen, J.C. McGrath. Analysing the 3D structure of blood vessels using confocal microscopy. *Microscopy & Analysis* , 92, pp5-8. Nov 2002.

8. C.J. Daly, E.Vila, S.M. Arribas, S. Pagakis, B. Thébault, J. Maddison, J. Pedersen and J.C. McGrath. 3-dimensional analysis of vascular structure, function & receptor distribution using confocal laser scanning microscopy. *Pharmacol. Toxicol.,* 87 Suppl II, pp10; Sept 2000

9. N.M. Tyrer, J.R. Maddison, D. Shepherd, D.W. Williams; Confocal quality imaging of afferent neurons from semi-thin sections of Drosophila ganglia. Neurosci Lett; 22;296(2-3):pp93-6; Dec 2000.

Conference Presentations And Posters

1. J. Maddison; Presentation of 3D reconstruction visualisation for exploration of human Axillary lymph nodes; MediVis 05; July 2005.

2. J. Maddison; Presentation on the application of virtual microscopy; European Histology Forum; May 2005.

3. R. Bradshaw, P. Dosanjh, J. Bell, J. Maddison and C. Murray, J. Bell, Quantitative Assessment of Phospho Marker Expression, Poster presentation European histology Forum, May 2005.

4. R. Bradshaw, P. Dosanjh, J. Bell, J. Maddison and C. Murray; Comparison of ICC methods for phosphor- market detection; Poster presentation European histology Forum; May 2005.

5. J.S. Ploem and J. Maddison; Detection of rare nuclei showing DNA-heterogeneity in populations of 50.000 cervical cells, using a high speed hyper threaded scanning and cell-analysis program (HTSA); Heidelberg Cytometry Symposium; Oct 2003.

6. P. Knudsen, J. Maddison, H.E. Danielsen.; Norwegian Radium hospital; Poster presentation ESACP; Heidelberg; July1999.

1. N. Clinch, J. Maddison. Telemicroscopy, Virtual microscopy; Published, April 2000; Granted 4 May 05 European (EP 0 994 433)

2. N. Clinch, J. Maddison. Telemicroscopy, Virtual microscopy; Published, Jan 2005; Granted 25 Jan 05 US (US 6 847 729)

3. J. Maddison. Method for Providing Quantitative Data and Images for Use in Pathology Analysis; TelePloidy; Published, Oct 2004 (GB 2 400 205)

4. J. Maddison. Method for Providing Quantitative Data and Images for Use in Pathology Analysis; TelePloidy; Published, Oct 2004 (EP 1 455 305)

5. J. Maddison. Microscope System and Method Navigation of microscope slides; Published, Aug 2004; Granted 1 Jun 05 (GB 2 398 196B)

6. J. Maddison. Microscope System and Method Navigation of microscope slides; Published, Aug 2004 (EP1 447 699)

7. J. Maddison. Microscope System and Method Navigation of microscope slides; Published, Sept 2004 (US2004/0184678)

8. J. Maddison; Microscopy Imaging System and Method; Continuous Scanning, Published, July 2001 (GB 2 838 487)

9. J. Maddison; Microscopy Imaging System and Method; Continuous Scanning, Published, July 2003 (EP 1 324 097)

10. J. Maddison; Microscopy Imaging System and Method; 3D virtual microscope, Published, Aug 2003; Granted, 7 Jan 04 (GB 2 385 481)

11. J. Maddison; Microscopy Imaging System and Method; 3D virtual microscope, Published, Aug 2003 (EP 1 336 888)

12. J. Maddison; Microscopy Imaging System and Method; 3D virtual microscope, Published, Nov 2003 (US 2003/214706)

Appendix B Automated DNA Ploidy System For Rare Event Detection

The DNA Ploidy system that is described in this report has been used for quantitative assessment of the DNA within cell nuclei. It is possible to use the system that has been developed for rare event detection as the following conference abstract describes.

Title: *Detection of rare nuclei showing DNA-heterogeneity in populations of 50.000 cervical cells, using a high speed hyper threaded scanning and cell-analysis program (HTSA)*

Authors:
J.S. Ploem* and J. Maddison**
* Leiden University, J.S.Ploem@Umail.Leidenuniv.nl
** Fairfield Imaging Ltd j.maddison@fairfield-imaging.co.uk

The purpose of this study is to describe an instrumental strategy to detect rare (frequency below 0.01%) suspect cells which may be missed by visual evaluation in e.g. ASCUS specimens in cervical cytology. Modern high speed PC processors using hyperthreading techniques can now facilitate applications that have to handle simultaneous piezo-electric focusing, image acquisition by CCD, cell segmentation and classification. Nuclear DNA analysis with this method is not used primarily for diagnostic or prognostic purposes, but only as a screening method to be followed by colposcopy and histopathology for further diagnostic evaluation. Increased DNA content is one of the most robust cellular parameters in cytometry for cytology screening. In large previous studies (1,2) it was found that cervical specimens from healthy woman very rarely showed high nuclear DNA values. These investigations were performed with earlier instruments such as the MIAC system from LEICA and the DISCOVERY system from BECTON and DICKINSON .The screening of nuclei with increased DNA-content took about 45 minutes per specimen. For practical application in a routine cytology laboratory this was not a cost effective procedure. Fairfield Imaging Ltd (Nottingham, England) has now developed an instrument that can analyse a sufficient number of cells in approximately 10 minutes using HSCA of liquid cytology slides with well flattened nuclei (these specimens require only few focusing steps). The clinical importance of the detection of rare nuclei with abnormal DNA content in cervical ASCUS

cases has been shown by Bertino (3). In a significant number of specimens a few nuclei with suspect DNA values were found among 50.000 nuclei present on a Feulgen stained ASCUS slide.

(1) van Driel-Kulker et al., Cytometry 1985;6:268

(2) Strohmeier et al., Cytopathology 1993; 4: 139

(3) Bertino et al. 2001:http://rex.iutcaen.unicaen.fr/7esacp/abstracts/A012.html

Appendix C VTK Isosurface Generation

It is possible to complete isosurface generate and visualisation using a relatively small amount of code and standard libaries the following is a the TCL script used to generate and then display the iso-surface as shown in **Figure 7.5**.

```
package require vtk
package require vtkinteraction

#
# This example reads a volume dataset, extracts the
#lymph node surface
#and contours the metastatic region
#

# Create the renderer, the render window, and the
#interactor. The renderer
# draws into the render window, the interactor #enables
mouse- and
# keyboard-based interaction with the scene.

vtkRenderer aRenderer
vtkRenderWindow renWin
  renWin AddRenderer aRenderer
vtkRenderWindowInteractor iren
  iren SetRenderWindow renWin

# The following reader is used to read a series of 2D
#slices (images) that compose the volume. The slice
#dimensions are set, and the  pixel spacing. The data
#Endianness must also be specified. The reader
# usese the FilePrefix in combination with the slice
#number to construct  filenames using the format
#FilePrefix.%d. (In this case the FilePrefix
# is the root name of the file: quarter.)

vtkTIFFReader v16
        v16 SetFilePrefix
"C:\\images\\datasets\\C_paish_ax_nodes\\01100292
2AX1 ALIGNED\\sm\\slide"
        v16 SetFilePattern "%s%03i.tif"
        v16 SetDataExtent 5 152 5 145 1 30
        v16 SetDataSpacing 1 1 1
        v16 SetDataByteOrderToLittleEndian

# An isosurface, or contour value of 30  is known to
#correspond to the
# lymph node surface. Once generated, a
#vtkPolyDataNormals filter is
# is used to create normals for smooth surface #shading
during rendering.
# The triangle stripper is used to create triangle strips
#from the
# isosurface these render much faster on may #systems.

vtkContourFilter skinExtractor
  skinExtractor SetInput  [v16 GetOutput]
  skinExtractor SetValue 0 30

vtkDecimatePro skindecimate
skindecimate SetInput [skinExtractor GetOutput]
skindecimate SetTargetReduction 999999999999
skindecimate PreserveTopologyOn
skindecimate BoundaryVertexDeletionOn

vtkWindowedSincPolyDataFilter skinsmooth
    skinsmooth SetInput [skindecimate GetOutput]
    skinsmooth SetNumberOfIterations 50
    skinsmooth BoundarySmoothingOn
    skinsmooth SetFeatureAngle 180
    skinsmooth SetEdgeAngle 90
    skinsmooth SetPassBand 0.1

vtkPolyDataNormals skinNormals
  skinNormals SetInput [skinsmooth GetOutput]
  skinNormals SetFeatureAngle 30.0

vtkStripper skinStripper
  skinStripper SetInput [skinNormals GetOutput]

vtkPolyDataMapper skinMapper
  skinMapper SetInput [skinStripper GetOutput]
  skinMapper ScalarVisibilityOff

vtkActor skin
  skin SetMapper skinMapper
  [skin GetProperty]  SetDiffuseColor 0 0 1
  [skin GetProperty] SetSpecular .3
  [skin GetProperty] SetSpecularPower 20
        [skin GetProperty] SetOpacity 0.7

# An isosurface, or contour value of 50 – 255  is #known
to correspond to the
# metastatic region. Once generated, a
#vtkPolyDataNormals filter is
# is used to create normals for smooth surface #shading
during rendering.
# The triangle stripper is used to create triangle strips
f#rom the
# isosurface these render much faster on may #systems.

vtkContourFilter boneExtractor
  boneExtractor SetInput  [v16 GetOutput]
boneExtractor GenerateValues 25 50 255

vtkDecimatePro bonedecimate
bonedecimate SetInput [boneExtractor GetOutput]
bonedecimate SetTargetReduction 99999999999
bonedecimate PreserveTopologyOn
bonedecimate BoundaryVertexDeletionOn

vtkWindowedSincPolyDataFilter boneSmooth
    boneSmooth SetInput [bonedecimate GetOutput]
    boneSmooth SetNumberOfIterations 50
    boneSmooth BoundarySmoothingOn
    boneSmooth SetFeatureAngle 180
    boneSmooth SetEdgeAngle 90
    boneSmooth SetPassBand 0.1

vtkPolyDataNormals boneNormals
  boneNormals SetInput [boneSmooth GetOutput]
  boneNormals SetFeatureAngle 65.0
vtkStripper boneStripper
  boneStripper SetInput [boneNormals GetOutput]
vtkPolyDataMapper boneMapper
  boneMapper SetInput [boneStripper GetOutput]
  boneMapper ScalarVisibilityOff
vtkActor bone
  bone SetMapper boneMapper
  [bone GetProperty] SetDiffuseColor 1 0 1
[bone GetProperty] SetOpacity 0.2
```

```
# An outline provides context around the data.        # vrml SetSpeed 5.5
#                                                      # vrml Write
vtkOutlineFilter outlineData
  outlineData SetInput  [v16 GetOutput]
vtkPolyDataMapper mapOutline
  mapOutline SetInput [outlineData GetOutput]
vtkActor outline
  outline SetMapper mapOutline
  [outline GetProperty] SetColor 0 0 0

# It is convenient to create an initial view of the data. #The
FocalPoint
# and Position form a vector direction. Later on
#(ResetCamera() method)
# this vector is used to position the camera to look at #the
data in
# this direction.

vtkCamera aCamera
  aCamera SetViewUp  0 0 -1
  aCamera SetPosition  0 1 0
  aCamera SetFocalPoint  0 0 0
  aCamera ComputeViewPlaneNormal

# Actors are added to the renderer. An initial camera
#view is created.
# The Dolly() method moves the camera towards the
#FocalPoint,
# thereby enlarging the image.

aRenderer AddActor outline
aRenderer AddActor skin
aRenderer AddActor bone
aRenderer SetActiveCamera aCamera
aRenderer ResetCamera
aCamera Dolly 1.5

# Set a background color for the renderer and set the
#size of the
# render window (expressed in pixels).

aRenderer SetBackground 1 1 1
renWin SetSize 640 480

# Note that when camera movement occurs (as it #does
in the Dolly()
# method), the clipping planes often need adjusting.
#Clipping planes
# consist of two planes: near and far along the view
#direction. The
# near plane clips out objects in front of the plane the far
plane
# clips out objects behind the plane. This way only #what
is drawn
# between the planes is actually rendered.
aRenderer ResetCameraClippingRange

# Set up a callback (using command/observer) to #bring
up the Tcl
# command GUI when the keypress-u (UserEvent) #key
is pressed.

iren AddObserver UserEvent (wm deiconify .vtkInteract)

# Interact with data. The Tcl/Tk event loop is started
#automatically.

iren Initialize
wm withdraw .

#optional VRML output

#vtkVRMLExporter vrml
#  vrml SetInput renWin
#  vrml SetFileName
```

Appendix D Contents Pages From User Manuals

The software systems described in this thesis have complete manuals, however as it is not practical to include them a cover page and contents page is shown in this Appendix Which shows the scope and the coverage of the documents Full software manuals are included on the attached CD.

FiRender User Manual

Version 2.0

Fairfield Imaging Ltd.

TABLE OF CONTENTS

FiAlign Manual

Version 1.4

Fairfield Imaging Ltd

CONTENTS

DNA PLOIDY CELL CAPTURE PROGRAM

USER MANUAL
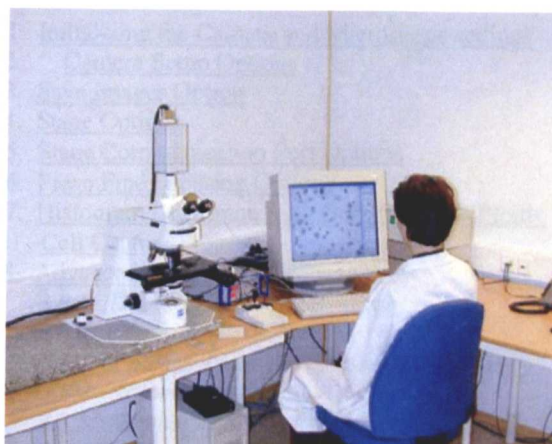
Fairfield DNA Ploidy System

FAIRFIELD IMAGING Ltd.

TABLE OF CONTENTS

HISTOGRAM DRAFTSMAN

USER MANUAL

VERSION 1.3

FAIRFIELD IMAGING Ltd.

TABLE OF CONTENTS

References

[1]   H. Muller, N. Michoux, D. Bandon, and A. Geissbuhler, "A Review of content-based image retrieval system in medical applications-clinical benefits and future directions," *International Journal of Medical Informatics*, vol. 73, pp. 1-23, July2004.

[2]   D. Mutter, G. Bouras, and J. Marescaux, "Digital technologies and quality improvement in cancer surgery," *European Journal of Surgical Oncology*, vol. 31, no. 6, pp. 689-694, Aug.2005.

[3]   "Why use a confocal microscope?, " *University of Washington*, http://depts.washington.edu/keck/intro.htm, 2004.

[4]   C. J. Daly, E. Vila, S. M. Arribas, S. M. Pagakis, B. Thebault, J. Maddison, J. Pedersen, and J. McGrath, "3-dimensional analysis of vascular structure, function & receptor distribution using confocal laser scanning microscopy," *Phatmacol. Toxicol*, vol. 87, no. Suppl II, p. 10, 2004.

[5]   A. Mitulescu, W. Skalli, D. Mitton, and J. A. De Guise, "Three-dimensional surface rendering reconstruction of scoliotic vertebrae using a non stereo-corresponding points technique," *Eur Spine J*, vol. 11, no. 4, pp. 344-352, Aug.2002.

[6]   P. Mitchell, I. D. Wilkinson, P. D. Griffiths, K. Linsley, and J. Jakubowski, "A stereoscope for image-guided surgery," *Br. J Neurosurg.*, vol. 16, no. 3, pp. 261-266, June2002.

[7]   S. Bradbury and Royal Microscopical Society, "An introduction to the optical microscope," Oxford: Oxford University Press, 1984.

[8]   B. H. Williams, I. S. Hong, F. G. Mullick, D. R. Butler, R. F. Herring, and T. J. O'Leary, "Image quality issues in a static image-based telepathology consultation practice," *Hum. Pathol*, vol. 34, no. 12, pp. 1228-1234, Dec.2003.

[9]   S. S. Cross, J. L. Burton, A. K. Dube, K. M. Feeley, P. D. Lumb, T. J. Stephenson, and R. D. Start, "Offline telepathology diagnosis of colorectal polyps: a study of interobserver agreement and comparison with glass slide diagnoses," *J Clin. Pathol*, vol. 55, no. 4, pp. 305-308, Apr.2002.

[10] M. Picardi and T. Jan, "Recent advances in computer vision, " *The industrial physicist*, http://www.aip.org/tip/INPHFA/vol-9/iss-1/p18.html, 2004.

[11] G. Klancar, M. Kristan, S. Kovacic, and O. Orqueda, "Robust and efficient vision system for group of cooperating mobile robots with application to soccer robots," *ISA Trans.*, vol. 43, no. 3, pp. 329-342, July2004.

[12] A. M. Marchevsky and P. H. Bartels, *Image analysis a primer for pathologists*. New York: Raven Press, 1994.

[13] R. Peretti-Renucci, C. Feuerstein, M. Manier, P. Lorimier, M. Savasta, J. Thibault, N. Mons, and M. Geffard, "Quantitative image analysis with densitometry for immunohistochemistry and autoradiography of receptor binding sites--methodological considerations," *J Neurosci. Res.*, vol. 28, no. 4, pp. 583-600, Apr.1991.

[14] E. K. Fishman, D. Magid, R. A. Drebin, A. F. Brooker, Jr., W. J. Scott, Jr., and L. H. Riley, Jr., "Advanced three-dimensional evaluation of acetabular trauma: volumetric image processing," *J Trauma*, vol. 29, no. 2, pp. 214-218, Feb.1989.

[15] S. S. Yoo, C. U. Lee, B. G. Choi, and P. Saiviroonporn, "Interactive 3-dimensional segmentation of MRI data in personal computer environment," *J Neurosci. Methods*, vol. 112, no. 1, pp. 75-82, Nov.2001.

[16] M. Picardi and T. Jan, "Recent advances in computer vision," *The industrial physicist*, 2004.

[17] R. Shekhar, V. Zagrodsky, C. R. Castro-Pareja, V. Walimbe, and J. M. Jagadeesh, "High-speed registration of three- and four-dimensional medical images by using voxel similarity," *Radiographics*, vol. 23, no. 6, pp. 1673-1681, Nov.2003.

[18] N. Jimenez-Lozano, M. Chagoyen, J. Cuenca-Alba, and J. M. Carazo, "FEMME database: topologic and geometric information of macromolecules," *J Struct. Biol.*, vol. 144, no. 1-2, pp. 104-113, Oct.2003.

[19] W. Abramovits and L. C. Stevenson, "Changing paradigms in dermatology: new ways to examine the skin using noninvasive imaging methods," *Clinics in Dermatology*, vol. 21, no. 5, pp. 353-358, 2003.

[20] K. A. Miles, "Diagnostic imaging in undergraduate medical education: an expanding role," *Clinical Radiology*, vol. 60, no. 7, pp. 742-745, July2005.

[21] A. O. Bilska-Wolak, J. Floyd, J. Y. Lo, and J. A. Baker, "Computer Aid for Decision to Biopsy Breast Masses on Mammography: Validation on New Cases1," *Academic Radiology*, vol. 12, no. 6, pp. 671-680, June2005.

[22] F. M. Vanhoenacker, A. M. De Schepper, J. L. Gielen, and P. M. Parizel, "MR imaging in the diagnosis and management of inheritable musculoskeletal disorders," *Clinical Radiology*, vol. 60, no. 2, pp. 160-170, Feb.2005.

[23] M. K. Hong, G. S. Mintz, C. W. Lee, B. K. Lee, T. H. Yang, Y. H. Kim, J. M. Song, K. H. Han, D. H. Kang, and S. S. Cheong, "The Site of Plaque Rupture in Native Coronary Arteries: A Three-Vessel Intravascular Ultrasound Analysis," *Journal of the American College of Cardiology*, vol. 46, no. 2, pp. 261-265, July2005.

[24] F. Davignon, J. F. Deprez, and O. Basset, "A parametric imaging approach for the segmentation of ultrasound data," *Ultrasonics*, vol. In Press, Uncorrected Proof.

[25] A. Elliott, "Medical imaging," *Nuclear Instruments and Methods in Physics Research Section A: Accelerators, Spectrometers, Detectors and Associated Equipment*, vol. 546, no. 1-2, pp. 1-13, July2005.

[26] N. Kamiyama, "Update of ultrasound contrast imaging," *International Congress Series*, vol. 1274, pp. 53-56, Oct.2004.

[27] E. H. Hopman, L. Rozendaal, R. H. M. Verheijen, P. Kenemans, and T. J. M. Helmerhorst, "Digital color imaging colposcopy: A matter of choice," *European Journal of Obstetrics & Gynecology and Reproductive Biology*, vol. 77, no. 2, pp. 229-234, Apr.1998.

[28] Z. Ai, F. Dech, M. Rasmussen, and J. C. Silverstein, "Radiological tele-immersion for next generation networks," *Stud. Health Technol. Inform*, vol. 70, pp. 4-9, 2000.

[29] G. S. Bova, G. Parmigiani, J. I. Epstein, T. Wheeler, N. R. Mucci, and M. A. Rubin, "Web-based tissue microarray image data analysis: initial validation testing through prostate cancer Gleason grading," *Hum. Pathol*, vol. 32, no. 4, pp. 417-427, Apr.2001.

[30] S. Bruins, M. C. de Jong, K. Heeres, M. H. Wilkinson, M. F. Jonkman, and J. B. van der Meer, "Fluorescence overlay antigen mapping of the epidermal basement membrane zone: I. Geometric errors," *J Histochem. Cytochem.*, vol. 42, no. 4, pp. 555-560, Apr.1994.

[31] C. K. Govind and R. G. Chiang, "Correlation between presynaptic dense bodies and transmitter output at lobster neuromuscular terminals by serial section electron microscopy," *Brain Res.*, vol. 161, no. 3, pp. 377-388, Feb.1979.

[32] K. Yogesan, T. Jorgensen, F. Albregtsen, K. J. Tveter, and H. E. Danielsen, "Entropy-based texture analysis of chromatin structure in advanced prostate cancer," *Cytometry*, vol. 24, no. 3, pp. 268-276, July1996.

[33] N. Takahashi, M. Iwasaki, T. Kunieda, Y. Wakita, and N. Day, "Image retrieval using spatial intensity features," *Signal Processing: Image Communication*, vol. 16, no. 1-2, pp. 45-57, Sept.2000.

[34] T. Jorgensen, K. Yogesan, K. J. Tveter, F. Skjorten, and H. E. Danielsen, "Nuclear texture analysis: a new prognostic tool in metastatic prostate cancer," *Cytometry*, vol. 24, no. 3, pp. 277-283, July1996.

[35] B. Nielsen, F. Albregtsen, W. Kildal, and H. E. Danielsen, "Prognostic classification of early ovarian cancer based on very low dimensionality adaptive texture feature vectors from cell nuclei from monolayers and histological sections," *Anal. Cell Pathol*, vol. 23, no. 2, pp. 75-88, 2001.

[36] T. Jorgensen, Y. Kanagasingam, O. Kaalhus, K. J. Tveter, M. Bryne, F. Skjorten, A. Berner, and H. E. Danielsen, "Prognostic factors in patients with metastatic (stage D2) prostate cancer: experience from the Scandinavian Prostatic Cancer Group Study-2," *J Urol.*, vol. 158, no. 1, pp. 164-170, July1997.

[37] S. Baheerathan, F. Albregtsen, and H. E. Danielsen, "Registration of serial sections of mouse liver cell nuclei," *J Microsc.*, vol. 192 (Pt 1), pp. 37-53, Oct.1998.

[38] B. Nielsen, F. Albregtsen, and H. E. Danielsen, "The use of fractal features from the periphery of cell nuclei as a classification tool," *Anal. Cell Pathol*, vol. 19, no. 1, pp. 21-37, 1999.

[39] K. Yogesan, H. Schulerud, F. Albregtsen, and H. E. Danielsen, "Ultrastructural texture analysis as a diagnostic tool in mouse liver carcinogenesis," *Ultrastruct. Pathol*, vol. 22, no. 1, pp. 27-37, Jan.1998.

[40] T. Wurflinger, J. Stockhausen, D. Meyer-Ebrecht, and A. Bocking, "Robust automatic coregistration, segmentation, and classification of cell nuclei in multimodal cytopathological microscopic images," *Comput. Med Imaging Graph.*, vol. 28, no. 1-2, pp. 87-98, Jan.2004.

[41] A. S. Frangakis and R. Hegerl, "Segmentation of two- and three-dimensional data from electron microscopy using eigenvector analysis," *J Struct. Biol.*, vol. 138, no. 1-2, pp. 105-113, Apr.2002.

[42] H. Penzkofer, B. J. Wintersperger, A. Knez, J. Weber, and M. Reiser, "Assessment of myocardial perfusion using multisection first-pass MRI and color-coded parameter maps:: A comparison to 99mTc Sesta MIBI SPECT and systolic myocardial wall thickening analysis," *Magnetic Resonance Imaging*, vol. 17, no. 2, pp. 161-170, Feb.1999.

[43] D. C. Durairaj, M. C. Krishna, and R. Murugesan, "Integration of color and boundary information for improved region of interest identification in electron magnetic resonance images," *Computerized Medical Imaging and Graphics*, vol. 28, no. 8, pp. 445-452, Dec.2004.

[44] J. R. Maddison, E. C. Paish, T. Kurien, R. D. Macmillian, A. R. Green, G. Y. Tian, and I. O. Ellis, "3D reconstruction and visualisation for exploration of human axillary lymph nodes," *Medical Information Visualisation (Medi05-VIS) IEEE Computer society;* pp. 55-59, July2005.

[45] G. Finlayson and G. Yun Tian, "Color normalization for color object recognition," *Pattern Recognition and Artificial Intelligence*, vol. 13, no. 8, pp. 1271-1285, Dec.1999.

[46] J. Johansson, "Stereoscopy," *ParrelComputing and Visualization Workshops 2005*, May2006.

[47] K. Idrissi, G. Lavoue, J. Ricard, and A. Baskurt, "Object of interest-based visual navigation, retrieval, and semantic content identification system," *Computer Vision and Image Understanding*, vol. 94, no. 1-3, pp. 271-294, 2004.

[48] B. G. Khang and Q. Zaidi, "Cues and strategies for color constancy: perceptual scission, image junctions and transformational color matching," *Vision Research*, vol. 42, no. 2, pp. 211-226, Jan.2002.

[49] I. M. Shih and R. J. Kurman, "Ki-67 labeling index in the differential diagnosis of exaggerated placental site, placental site trophoblastic tumor, and choriocarcinoma: a double immunohistochemical staining technique using Ki-67 and Mel-CAM antibodies," *Hum. Pathol*, vol. 29, no. 1, pp. 27-33, Jan.1998.

[50] T. W. King, E. M. Brey, A. A. Youssef, C. Johnston, and C. W. Patrick, Jr., "Quantification of vascular density using a semiautomated technique for immunostained specimens," *Anal. Quant. Cytol. Histol.*, vol. 24, no. 1, pp. 39-48, Feb.2002.

[51] M. A. Webster, G. Malkoc, A. C. Bilson, and S. M. Webster, "Color contrast and contextual influences on color appearance," *J Vis.*, vol. 2, no. 6, pp. 505-519, 2002.

[52] D. I. MacLeod, "New dimensions in color perception," *Trends Cogn Sci.*, vol. 7, no. 3, pp. 97-99, Mar.2003.

[53] H. Y. Vander, J. M. Naeyaert, I. Lemahieu, and W. Philips, "An imaging system with calibrated color image acquisition for use in dermatology," *IEEE Trans. Med Imaging*, vol. 19, no. 7, pp. 722-730, July2000.

[54] A. Oliva and P. G. Schyns, "Diagnostic colors mediate scene recognition," *Cognit. Psychol.*, vol. 41, no. 2, pp. 176-210, Sept.2000.

[55] Guyton and Hall, *Medical Physiology*, 11 ed. Philadelphi: Elsvevier Saunders, 2006, pp. 632-633.

[56] G. Rougeron and B. Peroche, "Color Fidelity in Computer Graphics: a Survey," *Computer Graphics Forum*, vol. 17, no. 1, pp. 3-15, 1998.

[57] M. Garcia-Esteban, D. Ansorena, O. Gimeno, and I. Astiasaran, "Optimization of instrumental colour analysis in dry-cured ham," *Meat Science*, vol. 63, no. 3, pp. 287-292, Mar.2003.

[58] I. Philipp and T. Rath, "Improving plant discrimination in image processing by use of different colour space transformations," *Computers and Electronics in Agriculture*, vol. 35, no. 1, pp. 1-15, July2002.

[59] A. P. Gonzales, L. Burin, and M. d. P. Buera, "Color changes during storage of honeys in relation to their composition and initial color," *Food Research International*, vol. 32, no. 3, pp. 185-191, Apr.1999.

[60] D. Berwick and S. W. Lee, "Spectral gradients for color-based object recognition and indexing," *Computer Vision and Image Understanding*, vol. 94, no. 1-3, pp. 28-43, June2004.

[61] T. Gevers and A. W.M.Smeulders, "Color-based Object Recognition," *Pattern Recognition*, vol. 32, no. 3, pp. 453-464, Mar.1999.

[62] G. Finlayson, S. Hordley, G. Schaefer, and G. Yun Tian, "Illuminant and device invariant colour using histogram equalisation," *Pattern Recognition*, vol. 38, no. 2, pp. 179-190, Feb.2005.

[63] S. G.Kong, J. Heo, B. R.Abidi, J. Paik, and Mongi A.Abidi, "Recent advances in visual and infrared face recognition—a review • ARTICLE," *Computer Vision and Image Understanding*, May2004.

[64] G. Haroske, J. P. Baak, H. Danielsen, F. Giroud, A. Gschwendtner, M. Oberholzer, A. Reith, P. Spieler, and A. Bocking, "Fourth updated ESACP consensus report on diagnostic DNA image cytometry," *Anal. Cell Pathol*, vol. 23, no. 2, pp. 89-95, 2001.

[65] S. Li and J. Shawe-Taylor, "Comparison and fusion of multiresolution features for texture classification," *Pattern Recognition Letters*, vol. 26, no. 5, pp. 633-638, Apr.2005.

[66] X. Wang and A. R. Hanson, "Surface Texture and Microstructure Extraction from Multiple Aerial Images," *Computer Vision and Image Understanding*, vol. 83, no. 1, pp. 1-37, July2001.

[67] A. Samal, J. R. Brandle, and D. Zhang, "Texture as the basis for individual tree identification," *Information Sciences*, vol. In Press, Corrected Proof.

[68] M. Hall-Beyer, "GLCM Texture: A Tutorial, " http://www.cas. sc.edu/geog/rslab/Rscc/mod6/6-5/texture/tutorial. html, 2000.

[69] K. Faulkner and B. M. Moores, "Analysis of x-ray computed tomography images using the noise power spectrum and autocorrelation function," *Phys. Med. Biol.*, vol. 29, pp. 1343-1352, 1984.

[70] D. M. Healy, Jr., J. Lu, and J. B. Weaver, "Two applications of wavelets and related techniques in medical imaging," *Ann. Biomed. Eng*, vol. 23, no. 5, pp. 637-665, Sept.1995.

[71] J. Sinkkonen, H. Tiitinen, and R. Naatanen, "Gabor filters: an informative way for analysing event-related brain activity," *J Neurosci. Methods*, vol. 56, no. 1, pp. 99-104, Jan.1995.

[72] M. Sharma, M. Markou, and S. Singh, "Evaluation of texture methods for image analysis," *Pattern recognistion letters*, 2004.

[73] J. C. Fu, S. K. Lee, S. T. C. Wong, J. Y. Yeh, A. H. Wang, and H. K. Wu, "Image segmentation feature selection and pattern classification for mammographic microcalcifications," *Computerized Medical Imaging and Graphics*, vol. In Press, Corrected Proof.

[74] M. Sharma, M. Markou, and S. Singh, "Evaluation of texture methods for image analysis," *Pattern recognistion letters*, 2004.

[75] F.Idris and S.Panchanathan, "Review of image and video indexing techniques," *Journal of Visual Communications and image representation*, vol. 8, no. 2, pp. 146-166, June1997.

[76] J.M.Dischler and D.Ghazanfarpou, "A survey of 3D texturing," *Computer and graphics*, vol. 25, no. 1, pp. 135-151, Feb.2001.

[77] A. Robles-Kelly and E. R. E. Hancock, "A probabilistic spectral framework for grouping and segmentation," *Pattern Recognition*, vol. 37, no. 7, pp. 1387-1405, July2004.

[78] M. Nadir Kurnaz, Z. Dokur, and T. Olmez, "Segmentation of remote-sensing images by incremental neural network," *Pattern Recognition Letters*, vol. In Press, Corrected Proof.

[79] E. Navon, O. Miller, and A. Averbuch, "Color image segmentation based on adaptive local thresholds," *Image and Vision Computing*, vol. 23, no. 1, pp. 69-85, Jan.2005.

[80] T. Zouagui, H. oit-Cattin, and C. Odet, "Image segmentation functional model," *Pattern Recognition*, vol. 37, no. 9, pp. 1785-1795, Sept.2004.

[81] de Bruijne M., B. van Ginneken, M. A. Viergever, and W. J. Niessen, "Interactive segmentation of abdominal aortic aneurysms in CTA images," *Med Image Anal.*, vol. 8, no. 2, pp. 127-138, June2004.

[82] D. J. Halazonetis, "What does the histogram of an image show?," *Am. J Orthod. Dentofacial Orthop.*, vol. 125, no. 2, pp. 220-222, Feb.2004.

[83] T. R. Reed and J. M. H. Dubuf, "A Review of Recent Texture Segmentation and Feature Extraction Techniques," *CVGIP: Image Understanding*, vol. 57, no. 3, pp. 359-372, May1993.

[84] S. Liapis, E. Sifakis, and G. Tziritas, "Colour and texture segmentation using wavelet frame analysis, deterministic relaxation, and fast marching algorithms," *Journal of Visual Communication and Image Representation*, vol. 15, no. 1, pp. 1-26, Mar.2004.

[85] K. M. Chen and S. Y. Chen, "Color texture segmentation using feature distributions," *Pattern Recognition Letters*, vol. 23, no. 7, pp. 755-771, May2002.

[86] Y.Yemez and F.Schmitt, "3D reconstruction of real objects with high resolution shape and texture," *Image and Vision Computing*, vol. 19, no. 14, pp. 1-17, July2004.

[87] W. E. Loresen and H. E. Cline, "Marchnig Cubes: a high resolution 3D surface reconstruction algorithm," *Computer Graphics*, vol. 21, no. 4, pp. 163-169, 1987.

[88] S. Seitz and C. Dyer, "Photorealistic Scene Reconstruction by Voxel Coloring," *International Journal of Computer Vision*, vol. 25, no. 3, pp. 1067-1073, Nov.1999.

[89] A. Losch, F. Eckstein, M. Haubner, and K. H. Englmeier, "A non-invasive technique for 3-dimensional assessment of articular cartilage thickness based on MRI. Part 1: Development of a computational method," *Magn Reson. Imaging*, vol. 15, no. 7, pp. 795-804, 1997.

[90] G. R. Ferretti, F. Thony, J. L. Bosson, C. Pison, F. Arbib, and M. Coulomb, "Benign abnormalities and carcinoid tumors of the central airways: diagnostic impact of CT bronchography," *AJR Am. J Roentgenol.*, vol. 174, no. 5, pp. 1307-1313, May2000.

[91] G. R. Davis and F. S. L. Wong, "X-ray microtomography of bones and teeth," *Physiological Measurement*, vol. 17, pp. 121-146, Aug.1996.

[92] I. K. Chun, M. H. Cho, S. C. Lee, M. H. Cho, and S. Y. Lee, "X-ray micro-tomography system for small-animal imaging with zoom-in imaging capability," *Physics in Medicine and Biology*, no. 17, pp. 3889-3902, 2004.

[93] M. Heuschmid, O. Luz, J. F. Schaefer, D. Stuecker, R. Vonthein, W. Luboldt, C. D. Claussen, and M. D. Seemann, "Comparison of volume-rendered and surface-rendered MR colonography," *Technol. Cancer Res. Treat.*, vol. 2, no. 1, pp. 13-18, Feb.2003.

[94] K. D. Hopper, A. T. Iyriboz, S. W. Wise, J. D. Neuman, D. T. Mauger, and C. J. Kasales, "Mucosal detail at CT virtual reality: surface versus volume rendering," *Radiology*, vol. 214, no. 2, pp. 517-522, Feb.2000.

[95] B. S. Duerstock, C. L. Bajaj, and R. B. Borgens, "A comparative study of the quantitative accuracy of three-dimensional reconstructions of spinal cord from serial histological sections," *J Microsc.*, vol. 210, no. Pt 2, pp. 138-148, May2003.

[96] J. Holman, M. Cookson, and E. Dykes, "Applications of a microcomputer-based reconstruction system to produce realistic three-dimensional shaded images from serial sections," *Med Inform (Lond)*, vol. 14, no. 2, pp. 173-184, Apr.1989.

[97] K. Denk and H. Horstmann, "Serial Block-Face Scanning Electron Microscopy to Reconstruct Three-Dimensional Tissue Nanostructure," *PLoS Biology*, vol. 2, no. 11, pp. 1900-1909, Nov.2004.

[98] M. Vuillemin and et al, "A Two step alignment method for 3D computer-aided reconstruction based on fiducial markets and applied to mouse embryonic hearts," *Eur j Morphol*, vol. 30, no. 3, pp. 181-193, 1992.

[99] O. Bossert, "A robust method for alignment of histological images," *Computer Methods and Programs in Biomedicine*, vol. 78, no. 1, pp. 35-38, Apr.2005.

[100] Y. H. Xu, G. Lahvis, H. Edwards, and H. C. Pitot, "Three-dimensional reconstruction from serial sections in PC-Windows platform by using 3D_Viewer," *Computer Methods and Programs in Biomedicine*, vol. 76, no. 2, pp. 143-154, Nov.2004.

[101] K. Bloom and D. Harrington, "Enhanced accuracy and reliability of HER-2/neu immunohistochemical scoring using digital microscopy," *Am J Clin Pathol*, vol. 121, no. 5, pp. 620-630, May2004.

[102] K. Denk and H. Horstmann, "Serial Block-Face Scanning Electron Microscopy to Reconstruct Three-Dimensional Tissue Nanostructure," *PLoS Biology*, vol. 2, no. 11, pp. 1900-1909, Nov.2004.

[103] H. Danielsen, T. Lindmo, and A. Reith, "A method for determining ploidy distributions in liver tissue by stereological analysis of nuclear size calibrated by flow cytometric DNA analysis," *Cytometry*, vol. 7, no. 5, pp. 475-480, Sept.1986.

[104] J. A. Sudbo, M. Bryne, A. Johannessen, and H. E. Danielsen, "Abnormal DNA content predicts the occurrence of carcinomas in non-dysplastic oral white patches," *Oral Oncol*, vol. 37, no. 7, pp. 558-565, 2001.

[105] J. Sudbo, W. Kildal, B. Risberg, H. S. Koppang, H. E. Danielsen, and A. Reith, "DNA content as a prognostic marker in patients with oral leukoplakia," *N-Engl-J-Med*, vol. 344(17); pp. 1270-1278, 2001.

[106] W. Kildal, J. Kærn, S. M. Kraggerud, V. M. Abeler, J. Sudbø, C. G. Tropè, R. A. Lothe, and H. E. Danielsen, "Evaluation of genomic changes in a large series of malignant ovarian germ cell tumors – relation to clinopathological variables," *Cancer Genetics and Cytogenetic*, vol. 155, pp. 25-32, 2004.

[107] J. Sudbo, W. Kildal, A. C. Johannesen, H. S. Koppany, A. Sudbo, H. E. Danielsen, B. Risberg, and A. Reith, "Gross genomic aberrations in precancer: clinical implications of a long-term follow-up study in oral erythroplakias," *Journal of Clinical Oncology*, vol. 20, no. 2, pp. 456-462, 2002.

[108] G. B. Kristensen, KildalW, V. M. Abler, E. O. Pettersen, C. Trope, and H. E. Danielsen, "Large scale genomic instability predicts long-term outcome of women with early ovarian Cancer," *Annuals of Oncology*, 2004.

[109] J.Sudbo, S.M Lippman, J.J.Lee, L Mao, W Kildal, A Sudbo, Simone Sagen, M Bryne, Adel El-Nagar, B Risberg, J.F.Evensen, and A.Reith, "The influence of Resection and Aneuploidy on Mortality in Oral Leukoplakia," 2004.

[110] B. Bertino, W. A. Knape, M. Pytlinska, K. Strauss, and J. C. Hammou, "A comparative study of DNA content as measured by flow cytometry and image analysis in 1864 specimens," *Anal. Cell Pathol*, vol. 6, no. 4, pp. 377-394, May1994.

[111] H. Motherby, N. Pomjanski, M. Kube, A. Boros, T. Heiden, B. Tribukait, and A. Bocking, "Diagnostic DNA-flow- vs. -image-cytometry in effusion cytology," *Anal Cell Pathol*, vol. 24, no. 1, pp. 5-15, 2002.

[112] A. W. Welsh, K. Humphries, D. O. Cosgrove, M. J. Taylor, and N. M. Fisk, "Development of three-dimensional power Doppler ultrasound imaging of fetoplacental vasculature," *Ultrasound Med Biol.*, vol. 27, no. 9, pp. 1161-1170, Sept.2001.

[113] Y. Sugawara, H. Kamioka, T. Honjo, K. i. Tezuka, and T. Takano-Yamamoto, "Three-dimensional reconstruction of chick calvarial osteocytes and their cell processes using confocal microscopy," *Bone*, vol. 36, no. 5, pp. 877-883, May2005.

[114] A. C. Andreasson, M. Abt, and A. C. Jonsson-Rylander, "Confocal scanning laser microscopy measurments of atherosclerotic lesions in mice aorta: A fast evaluation method for volume determinations," *Atherosclerosis*, vol. 179, no. 1, pp. 35-42, Mar.2005.

[115] J. Gellermann, W. Wlodarczyk, H. Ganter, J. Nadobny, H. Fahling, M. Seebass, R. Felix, and P. Wust, "A practical approach to thermography in a hyperthermia/magnetic resonance hybrid system: Validation in a heterogeneous phantom," *International Journal of Radiation Oncology*, vol. 61, no. 1, pp. 267-277, Jan.2005.

[116] J. A. Perkins, M. Sidhu, S. C. Manning, V. Ghioni, and R. Sze, "Three-dimensional CT angiography imaging of vascular tumors of the head and neck," *International Journal of Pediatric Otorhinolaryngology*, vol. 69, no. 3, pp. 319-325, Mar.2005.

[117] H. Greess, A. Nomayr, B. Tomandl, M. Blank, M. Lell, M. Lenz, and W. A. Bautz, "2D and 3D visualisation of head and neck tumours from spiral-CT data," *European Journal of Radiology*, vol. 33, no. 3, pp. 170-177, Mar.2000.

[118] A. Rawlinson, C. Elcock, A. Cheung, A. Al-Buhairi, S. Khanna, T. F. Walsh, and R. P. Ellwood, "An in-vitro and in-vivo methodology study of alveolar bone measurement using extra-oral radiographic alignment apparatus, Image Pro-Plus(R) software and a subtraction programme," *Journal of Dentistry*, vol. In Press, Corrected Proof.

[119] C. L. Liner, "Geophysics and NIH Image," *Computers & Geosciences*, vol. 25, no. 4, pp. 403-414, May1999.

[120] H. E. Brown, M. M. Garcia, and R. E. Harlan, "A two focal plane method for digital quantification of nuclear immunoreactivity in large brain areas using NIH-image software," *Brain Research Protocols*, vol. 2, no. 4, pp. 264-272, June1998.

[121] X. Lin, A. Liu, Y. Li, and P. Wu, "A MATLAB programming for simulation of X-ray capillaries," *Applied Mathematics and Computation*, vol. In Press, Corrected Proof 2005.

[122] "Microsopy resource centre, " *Olympus*, http://www.olympusmicro.com/primer/index.html, 2004.

[123] "Conjugate planes in Optical Microscopy, " *Nikon*, http://www.microscopyu.com/articles/formulas/formulasconjugate.html, 2004.

[124] "Stage specifications, " *Prior Scientific*, http://www.prior.com/downloads/user_files/en/H101ADatasheet.pdf, Feb.2006.

[125] "Microscope Slides and Cover Slips, " *SPI*, http://www.2spi.com/catalog/ltmic/quartz.shtml, Feb.2006.

[126] T. J. Holmes, "Blind deconvolution of quantum-limited incoherent imagery: maximum-likelihood approach," 9 ed 1982, pp. 1052-1062.

[127] P. W. Shaw, "The point-spread function of a confocal microscope: its measurement and use in deconvolution of 3D data," 163 ed 1991, pp. 151-165.

[128] T.Hollinger, "Histological Stains, " *University of Florida*, http://medinfo.ufl.edu/dental/denhisto/stains.html, 2002.

[129] T. Kurien, E. C. Paish, J. Rowe, J. Maddison, E. A. Rakha, A. R. Green, and I. O. Ellis, "Three-dimensional reconstruction of human breast carcinoma using routine laboratory equipment and immunohistochemistry which is comparable to confocal imaging," *J Clin. Pathol*, vol. 58, pp. 968-972, Sept.2005.

[130] E. C. Paish, J. R. Maddison, D. Macmillian, T. Kurien, A. J. Green, G. Y. Tian, and I. O. Ellis, "3D reconstruction of breast tumour metastases within human Axillary lymph nodes," *Submitted - J Pathol*, 2006.

[131] N. M. Tyrer, J. R. Maddison, D. Shepherd, and D. W. Williams, "Confocal quality imaging of afferent neurons from semi-thin sections of Drosophila ganglia.," *Neurosci Lett*, vol. 22, no. 296(2-3), pp. 93-96, Dec.2000.

[132] "Lead tools, " *Lead Technologies*, www.leadtools.com, 2004.

[133] C. J. Daly, A. McGee, A. Vila, A. Briones, S. M. Arribas, S. Pagakis, J. Adler, A. Merle, J. Maddison, J. Pedersen, and J. C. McGrath, "Analysing the 3D structure of blood vessels using confocal microscopy," *Microscopy & Analysis*, no. 92, pp. 5-8, Nov.2002.

[134] K. Mueller, "Histogram equalisation, " *State University of New York*, http://www.cs.sunysb.edu/~mueller/, 2004.

[135] J. F. Brinkley and C. Rosse, "The Digital Anatomist Distributed Framework and Its Applications to Knowledge-based Medical Imaging,", 4 ed 1997, pp. 165-183.

[136] K. H. Hoffmann and P. Salamon, "The optimal simulated annealing schedule for a simple model," *Journal of Physics A: Mathematical and General*, no. 15, pp. 3511-3523, 1990.

[137] N. Ng Kuang Chern, P. A. Neow, and H. A. J. Marclo, "Practical issues in pixel-based autofocusing for machine vision," 2001.

[138] W. Heidrich, M. McCool, and J. Stevens, "Interactive Maximum Projection Volume Rendering," *Proceedings of the 6th conference on Visualization '95*, p. 11, 1995.

[139] A. Kumar, "Neural network based detection of local textile defects," *Pattern Recognition*, vol. 36, no. 7, pp. 1645-1659, July2003.

[140] S. Y. Kim, B. Y. Moon, D. E. Kim, and S. C. Shin, "Automation of hull plates classification in ship design system using neural network method," *Mechanical Systems and Signal Processing*, vol. In Press, Corrected Proof.

[141] G. Brown, J. Wyatt, R. Harris, and X. Yao, "Diversity creation methods: a survey and categorisation," *Information Fusion*, vol. 6, no. 1, pp. 5-20, Mar.2005.

[142] R. aiz-Rodriguez, A. Guerrero-Curieses, and J. Cid-Sueiro, "Minimax classifiers based on neural networks," *Pattern Recognition*, vol. 38, no. 1, pp. 29-39, Jan.2005.

[143] R. Srinivasan, C. Wang, W. K. Ho, and K. W. Lim, "Neural network systems for multi-dimensional temporal pattern classification," *Computers & Chemical Engineering*, vol. In Press, Corrected Proof.

[144] D. R. Carvalho and A. A. Freitas, "A hybrid decision tree/genetic algorithm method for data mining," *Information Sciences*, vol. 163, no. 1-3, pp. 13-35, June2004.

[145] F. Berzal, J. C. Cubero, N. Marin, and D. Sanchez, "Building multi-way decision trees with numerical attributes," *Information Sciences*, vol. 165, no. 1-2, pp. 73-90, Sept.2004.

[146] R. Miglio and G. Soffritti, "The comparison between classification trees through proximity measures," *Computational Statistics & Data Analysis*, vol. 45, no. 3, pp. 577-593, Apr.2004.

[147] J. R. Maddison, M. E. Pretorius, W. Kildal, N. F. Clinch, G. Y. Tian, and H. E. Danielsen, "Automated image cytometry system for image capture, segmentation, classification and analysis for DNA Ploidy," *summited Image and Vision Computing*, Aug.2005.

[148] J. R. Maddison, E. C. Paish, T. Kurien, R. D. Macmillian, A. R. Green, G. Y. Tian, and I. O. Ellis, "3D reconstruction and visualisation for exploration of human axillary lymph nodes," *Medical Information Visualisation (Medi05-VIS) IEEE Computer society;* pp. 55-59, July2005.

[149] N. M. Tyrer, "Celloidin-wax sandwich microtomy: a novel and rapid method for producing serial semithin sections," *J. Microsc.*, vol. 196 (Pt 3), pp. 273-278, Dec.1999.

[150] N. Diwakar, M. Sherriff, A. Brown, and E. W. Odell, "Heterogeneity,histological features and DNA ploidy in oral carcinoma by image-based analysis," *Oral Oncology*, vol. 41, no. 416, p. 422, 2005.

[151] G. B. Kristensen, W. Kildal, V. M. Abeler, J. Kaern, I. Vergote, C. G. Trope, and H. E. Danielsen, "Large-scale genomic instability predicts long-term outcome for women with invasive stage I ovarian cancer," *Ann. Oncol*, vol. 14, pp. 1494-2500, 2003.

[152] H. Crisp, J. L. Burton, R. Stewart, and M. Wells, "Refining the diagnosis of hydatidiform mole: image ploidy analysis and p57KIP2 immunohistochemistry," *Histopathology*, vol. 43, no. 4, pp. 363-373, 2003.

[153] J. R. Maddison, V. M. Abeler, B. Risberg, A. Wotherspoon, and H. E. Danielsen, "Diagnostic Accuracy in Telepathology," *Submitted - Human Pathology*, Aug.2005.